APPLICATION OF SEMI CONDUCTOR FILMS OVER GLASS/CERAMIC SURFACES AND THEIR LOW TEMPERATURE PHOTOCATALYTIC ACTIVITY

A THESIS SUBMITTED TO
THE GRADUATE SCHOOL OF NATURAL AND APPLIED SCIENCES
OF
MIDDLE EAST TECHNICAL UNIVERSITY

BY

TUĞÇE İRFAN ERSÖZ

IN PARTIAL FULFILLMENT OF THE REQUIREMENTS
FOR
THE DEGREE OF MASTER OF SCIENCE
IN
CHEMICAL ENGINEERING

FEBRUARY 2009

Approval of the thesis:

APPLICATION OF SEMI CONDUCTOR FILMS OVER GLASS/CERAMIC SURFACES AND THEIR LOW TEMPERATURE PHOTOCATALYTIC ACTIVITY

submitted by **TUĞÇE İRFAN ERSÖZ** in partial fulfillment of the requirements for the degree of **Master of Science in Chemical Engineering Department, Middle East Technical University by,**

Prof. Dr. Canan Özgen
Dean, Graduate School of **Natural and Applied Sciences** _____

Prof. Dr. Gürkan Karakaş
Head of Department, **Chemical Engineering** _____

Prof. Dr. Gürkan Karakaş
Supervisor, **Chemical Engineering Dept., METU** _____

Examining Committee Members:

Prof. Dr. Deniz Üner
Chemical Engineering Dept., METU _____

Prof. Dr. Gürkan Karakaş
Chemical Engineering Dept., METU _____

Assoc. Prof. Dr. Halil Kalıpçılar
Chemical Engineering Dept., METU _____

Assoc. Prof. Dr. Naime Aslı Sezgi
Chemical Engineering Dept., METU _____

Assist. Prof. Dr. Meltem Doğan
Chemical Engineering Dept., Gazi University _____

Date: 06.02.2009

I hereby declare that all information in this document has been obtained and presented in accordance with academic rules and ethical conduct. I also declare that, as required by these rules and conduct, I have fully cited and referenced all material and results that are not original to this work.

Name, Last Name: Tuğçe İrfan Ersöz

Signature:

ABSTRACT

APPLICATION OF SEMI CONDUCTOR FILMS OVER GLASS/CERAMIC SURFACES AND THEIR LOW TEMPERATURE PHOTOCATALYTIC ACTIVITY

Ersöz, Tuğçe İrfan

M.S., Department of Chemical Engineering

Supervisor: Prof. Dr. Gürkan Karakaş

February 2009, 130 pages

Semiconductor metal oxides can be induced by light with proper wavelength resulting in oxidation and reduction reactions for the transformation of water and oxygen molecules into active radicals. With this method, it is possible to obtain self-cleaning surfaces and products having antimicrobial properties.

The aim of this study is to develop semiconductor metal oxide thin films for multifunctional glass products and the characterization of photocatalytic self cleaning and antimicrobial properties. As semiconductor metal oxides; titanium dioxide (TiO_2), tin oxide (SnO_2) and their binary mixtures (TiO_2-SnO_2) are selected because of their abundancy, non toxic properties, stability and the ability of absorbing light close to visible range. Also the effect of metal dopants such as praseodymium (Pr), palladium (Pd), silver (Ag) and iron (Fe) was examined with these metal oxides.

The colloidal solutions were synthesized by using sol-gel method in order to apply the developed method to industrial usage as applying on large surfaces.

The glass substrates were coated with the colloidal solutions by dip coating and the dried samples were calcined under air flow. The best calcination condition for pure TiO_2 coated thin film was determined as 400^oC for 45 minutes. Surface characterization studies were performed by using UV-Visible Spectrophotometer for band gap measurement, CAM for contact angle measurement, SEM for surface morphology and tophology. The methylene blue adsorption tests were carried out and the effective surface area of the samples were predicted by the Langmuir adsorption isotherm of samples. The photocatalytic activities of the coated thin films were measured with the degradation of organic materials as red wine and methylene blue, and with the antimicrobial activity tests as counting the number of viable *E.coli* cells. 61.2% deactivation of methylene blue stain was achieved over SnO_2 coated thin films while this was 22.1% over TiO_2 coated thin films after irradiation for 180 minutes. The superior photocatalytic activity was observed with TiO_2 samples doped with Pd and Ag ions. The TiO_2-SnO_2 coated samples performed limited photocatalytic activity which is less than the activity of SnO_2 coated samples which was confirmed with surface area measurements as SnO_2 coated samples had higher surface area (9.81 cm^2/cm^2) than TiO_2-SnO_2 coated samples. Surface area increased with increasing the amount of SnO_2 and it was in the following order: SnO_2 > 80% SnO_2 + 20% TiO_2 > 50% SnO_2 + 50%TiO_2 > 35% SnO_2 + 65%TiO_2 > 20% SnO_2 + 80% TiO_2 > TiO_2.

Keywords: Semiconductor, self-cleaning, antimicrobial, photocatalysis, thin films, TiO_2, SnO_2, sol-gel, photocatalytic activity

ÖZ

CAM/SERAMİK YÜZEYLERE YARI İLETKEN FİLM UYGULAMALARI VE BU FİLMLERİN DÜŞÜK SICAKLIKTA FOTOKATALİTİK AKTİVİTESİ

Ersöz, Tuğçe İrfan

Yüksek Lisans, Kimya Mühendisliği Bölümü

Tez Yöneticisi: Prof. Dr. Gürkan Karakaş

Şubat 2009, 130 sayfa

Yarı iletken metal oksit maddeler uygun dalga boylarında ışıkla uyarıldığında su ve oksijen moleküllerinin aktif radikallere dönüşümünü sağlayan yükseltgenme ve indirgenme tepkimeleri meydana gelir. Bu yöntemle anti-bakteriyel özellikli kendini temizleyen yüzey ve ürünler elde edilebilir.

Bu çalışmanın amacı, fotokatalitik olarak kendini temizleyen ve anti-bakteriyel özelliğe sahip, çok fonksiyonlu, cam ürünler için yarı iletken metal oksit tabanlı ince filmler üretmek ve üretim teknikleri geliştirmektir. Yarıiletken metal oksit olarak, çok bulunmaları, zehirsiz oluşları, kararlılıkları ve gün ışığına yakın aralıktaki ışıkları soğurmaları nedeniyle titanyum dioksit (TiO_2) kalay oksit (SnO_2), ve bunların ikili karışımları seçilmiştir. Saf TiO_2 ve SnO_2'nin fotokatalitik aktiviteleri güneş ışığı altında sınırlı olup katkı maddeleri olarak praseodimiyum (Pr), paladyum (Pd), gümüş (Ag) ve demirin (Fe) etkileri de incelenmiştir.

Geliştirilen yöntemlerin geniş yüzeylere endüstriyel boyutta uygulanabilmesini sağlamak amacıyla, kolloidal çözeltiler, sol-jel tekniği ile hazırlanmıştır. Cam yüzeyler ise, daldırma yöntemi kullanılarak, bu çözeltiler ile kaplanmış ve

kurutulduktan sonra kalsine edilmiştir. Saf TiO_2 için, en iyi kalsinasyon şekli 400^oC'de 45 dakika olarak belirlenmiştir. Yüzey özelliklerinin belirlenmesinde, bant genişliği ölçümü için UV-Vis Spektrofotometre, temas açısı ölçümü içim CAM, yüzey morfolojisi ve topolojisi için ise SEM kullanılmıştır. Kaplanan yüzeylerin fotokatalitik özellikleri kırmızı şarap ve metilen mavisi gibi organik maddelerin degredasyonu ve *E.coli* sayma gibi organik yöntemler yardımı ile ölçülmüştür. Metilen mavisi konsantrasyonu 180 dakikalık bekleme sonrasında SnO_2 ile kaplanmış yüzeylerde %61.2 oranında azalmış olup, TiO_2 kaplı yüzeylerde ise bu oran %22.1'dir. En iyi fotokatalitik özellik ise Pd ve Ag eklenmiş TiO_2 ile kaplanmış yüzeylerde gözlemlenmiştir. TiO_2-SnO_2 karışımı ile kaplanmış yüzeyler SnO_2 kaplı yüzeylerden daha düşük fotokatalitik aktivite göstermiş olup, bu durum, SnO_2 kaplı yüzeylerde yüzey alanının daha düşük olması (9.81 cm^2/cm^2) ile açıklanbilecek bir durumdur. Yüzey alanı SnO_2 miktarı arttıkça artmakta olup sıralama su şekildedir: SnO_2 > 80% SnO_2 + 20% TiO_2 > 50% SnO_2 + 50%TiO_2 > 35% SnO_2 + 65%TiO_2 > 20% SnO_2 + 80% TiO_2 > TiO_2.

Anahtar Kelimeler: Yarı iletken, kendini temizleyen ürünler, antimikrobiyal, fotokataliz, ince filmler, TiO_2, SnO_2, sol-gel, fotokatalitik aktivite

To my beloved mother,

ACKNOWLEDGEMENTS

First and foremost, I would like to express my deepest gratitude to my thesis supervisor, Prof. Dr. Gürkan Karakaş for introducing me to this research subject, for his invaluable advice and guidance throughout this study.

I would like to thank all my friends in Environmental Catalysis Laboratory. I am especially grateful to Ahmet Onur Yurtsever for his invaluable friendship and helpful contributions throughout this study.

I also wish to give my special thanks to my friends Güzide Aydın for her endless cordiality and Saltuk Pirgalıoğlu for his friendship and support.

I am, also, very grateful to the staff and technicians in Chemical Engineering Department.

Financial support of The Scientific and Technological Research Council of Turkey (TÜBİTAK) to the project, 106M168, is also acknowledged. Additionally, I would like to thank my colleagues at Engineering Research Grant Committee, TÜBİTAK. I am especially grateful to Fatih Babuçcu for his contribution and cordiality while writing this thesis.

Last but certainly not least, I would like to express my deepest gratitude to my family for their love, support, encouragement and patience throughout my life. I have always felt the privilege of having such a family.

TABLE OF CONTENTS

LIST OF TABLES

LIST OF FIGURES

NOMENCLATURE

Symbols

c	Speed of light
h	Planck's constant
E_g	Photon energy
n_e	Carrier density of electrons
n_h	Carrier density of holes
e	Electron charge
MO	Metal oxide
h^+	Hole
e^-	Electron
L_D	Depletion layer
L_C	Characteristic length of the particle
E_C	Conduction band
E_V	Valence band
E_F	Fermi level
M	Metal
h	Coating thickness
U	Withdrawal speed
A	Surface porosity factor
UP	Ultra pure
C_E	Equilibrium concentration of methylene blue remaining in the solution
X/m	Quantity of methylene blue adsorbed per unit weight of adsorbent
X_m	Adsorption capacity
k	Bonding energy constant
S	Specific surface area
A	Cross-sectional area of methylene blue adsorbed on the surface
L	Avogadro's number
N	Coverage factor

Greek Letters

σ	Conductivity
μ_e	Mobility of electron
μ_h	Mobility of hole
ν	Frequency of photon
η	Viscosity
γ_{LV}	Specific surface energy of liquid-vapor interface, liquid-vapor surface tension
γ_{SV}	Specific surface energy of solid-vapor interface
γ_{SL}	Specific surface energy of solid-liquid interface
θ	Contact angle

Abbreviations

CAM	Contact Angle Meter
SEM	Scanning Electron Microscope
LPD	Liquid Phase Deposition
XRD	X-Ray Diffraction
TCO	Transparent Conducting Oxide
BET	Brunauer Emmett Teller

CHAPTER 1

INTRODUCTION

Ceramic and glass products are widely used because of their environmentally friendly nature, easy cleaning, durability, easy maintenance, durability and maintaining their shape, color and stability for a long time. Glass and ceramic industry has special importance with current high capacity and raw materiald. On the other hand, due to the increasing energy cost and immense competition, these industries can not satisfy the demanded profit resulting in the low export income. By taking this situation into consideration, products having speciality and extraordinary properties having higher value add, might have a viable market chance to overcome these difficulties. With their physical and chemical properties, semiconductor metal oxides are suitable materials in order to develop multifunctional high qualified products. Their transparency on the visible light region, and absorption of energy in IR and UV ranges, limited electrical conductivity, and the release of electrons as a result of UV adsorption yield many products such as thermal and UV filters, antistatic coatings, gas sensors, touch screen LCD panels, and photocatalytic materials where electron and hole pairs are utilized in a designed manner. By using electron and hole pairs to activate water and oxygen molecules, which are available in ambient, might be used to produce surfaces with photocatalytic properties. Such multifunctional surfaces having photocatalytic activity can be utilized as self cleaning surfaces, super hydrophilic surfaces, super hydrophobic surfaces, antimicrobial surfaces as well as their original structural properties such as floor tiles or window glasses, bottles, etc.

In recent studies, due to the chemical, electrical and optical properties, titanium dioxide (TiO_2) has caught special attention because of its wide band gap resulting in high transmittancy along the wide range of wavelength spectru,

availability, low cost and non-toxic properties. Among different conducting materials, TiO_2 is used widely due to its predominant photocatalytic properties. Besides that, it is chemically and physically stable and does not have any side reaction during photocatalytic reactions take place. TiO_2 surfaces exhibit hydrophilic surfaces where hydrophilicity allows water to split completely instead of remaining as droplets resulting in the clear surfaces that can be easily washed [Popielarski, 1998]. Hydrophilic TiO_2 films can be used for practical applications like door mirrors for cars, coatings for buildings, etc.

Other semiconductor metal oxide used widely is tin oxide (SnO_2). SnO_2 is an n-type semiconductor having wide band gap where band gap energy is around 3.6 eV. Using these metal oxides for their photocatalytic properties has a disadvantage as the surfaces should be irradiated in order to obtain photocatalytically active surfaces since band gap energies of TiO_2 and SnO_2 are around 3.2 eV and 3.6 eV, respectively [Trapalis et al., 2003]. For increasing the photocatalytic activity by decreasing the band gap energy of semiconductor metal oxides, metal ions have been widely used. The mostly used metal catalysts for this purpose are palladium (Pd), silver (Ag), iron (Fe), gold (Au), cobalt (Co) and copper (Cu).

In this study, semiconductor metal oxides having large band gap were applied to the surfaces of glasses as thin films, and photocatalytic, hydrophilic and antimicrobial surface properties were characterized. For this purpose, TiO_2, SnO_2 and their binary mixtures (TiO_2-SnO_2) were the selected semiconductor metal oxides having large band gap because of being easily prepared, their chemical stabilities, high photocatalytic activities, resistance to corrosion and low cost [Yang et al., 2006]. Furthermore, photocatalytic activities of TiO_2 and SnO_2 thin films doped with metal ions having catalytic properties was examined with doping Pr, Pd, Ag and Fe ions having high oxygen transfer ability, charge separation sites and their unique catalytic properties.

The coated thin films were characterized by using CAM, SEM and UV-Visible Spectrophotometer. For surface area measurements, Langmuir isotherms of the samples with methylene blue were used and photocatalytic activities of the films

were measured with the degradation of organic materials when subjected to artificial solar light irradiation and with antimicrobial activity tests as counting viable *E.coli* cells after irradiation.

CHAPTER 2

LITERATURE SURVEY

In health facilities, laboratories and swimming pools; hygiene of ceramic and glass products is very important issue as sterilization of microorganisms. It is known that, health problems, because of the microorganisms, have started to appear due to the reproduction of microorganisms under optimum conditions of temperature and moisture for their reproducibility. One way of disinfection is the using chemicals including chlorinated organic compounds which is named as manual disinfection and has been the most applied method for disinfection of these microorganisms for several years. On the other hand, it should be noted that chlorinated organic compounds cause contaminations on the applied surfaces because of the following reasons:

- Toxicity
- Causing environmental pollution
- Not establishing long-time protection

The alternative way of disinfection is the photochemical method with utilizing light source at UV-C wavelength (100 nm-280 nm). By considering the drawbacks of using chlorine, the studies about photocatalytic reactions, for the purpose of solving the problems of environmental interest, have been fastened during last ten years in spite of knowing that sufficient activation energy for the reactions can be acquired by using photocatalysis and light sources after 1970s. However, photochemical disinfection method is hazardous for the living organisms and causes degradation on polimeric materials and dye stuffs. So, it can be used for technical and medical applications by satisfying the requirements of controlled environment.

The application of photochemical disinfection with photons having energy closer to visible region and solar spectrum with proper density of UV-A (315 nm-400 nm) is possible only with the use of photocatalysts. On the other hand, besides the antimicrobial properties of photocatalytic materials, they have different hydrophilicities and self-cleaning propeties that increase the usage area of photocatalytic materials.

Hydrogen production by photocatalytic water splitting [Cunningham et al., 1981; Nam and Han, 2007], destruction of microorganisms by oxidation of them in water [Hoffmann et al., 1995; Sivakumar and Shanthi, 2000], self-cleaning hydrophilic surfaces [Guan, 2005; Wang et al., 2008; Euvananont et al., 2008] and degradation of organic pollutants [Evans and Sheel, 2007] are the most studied fields in the literature for the purpose of searching photocatalysis and photocatalytic reactions.

By considering the drawbacks of using chlorine, the studies about photocatalytic reactions, for the purpose of solving the problems of environmental interest, have been fastened during last ten years in spite of knowing that sufficient activation energy for the reactions can be acquired by using photocatalysis and light sources after 1970s. Hydrogen production by photocatalytic water splitting [Cunningham et al., 1981; Nam and Han, 2007], destruction of microorganisms by oxidation of them in water [Hoffmann et al., 1995; Sivakumar and Shanthi, 2000], self-cleaning hydrophilic surfaces [Guan, 2005; Wang et al., 2008; Euvananont et al., 2008] and degradation of organic pollutants [Evans and Sheel, 2007] are the most studied fields in the literature for the purpose of searching photocatalysis and photocatalytic reactions.

Titanium dioxide (TiO_2), tin oxide (SnO_2) and zinc oxide (ZnO) are the most studied photocatalysts due to their large band gap and optical absorbance energies [Diebold, 2003; Hsiunga et al., 2006; Zhang et al., 2006]. Being non-toxic and having resistance to environmental factors, like corrosion and moisture, due to their chemical stability make these photocatalysts more preferable than chlorine. In literature, these semiconductor photocatalysts have been studied and practically used in two ways; powder, which is applied directly, and liquid for thin film coatings.

2.1. Definition and General Properties of Semiconductors

Solids have two energy bands which are conduction band and valence band. According to the band theory of solids, at absolute zero temperature, valence band is the lower energy band filled with electrons while conduction band is the upper energy band being empty. The energy difference between the top of the valence band and the bottom of the conduction band is called the band gap and by gaining enough thermal energy, electrons are able to jump from valence band to conduction band by creating electron and hole pairs [Grove, 1967].

At the temperatures different from absolute zero, electrical conductivity of solids depends on the magnitude of the band gap and according to the magnitude of the band; the type of the solid, whether it is conductor, semiconductor or insulator, can easily be understood. As shown in Figure 2.1, insulators have a large band gap, also called forbidden band gap, which results in difficulties for electrons to jump from one band to another. On the other hand, metals do not have band gap, in other words, valence band and conduction band overlaps, so, as a conductor, it is easy for electrons to move from one band to another [Reddya et al., 2002].

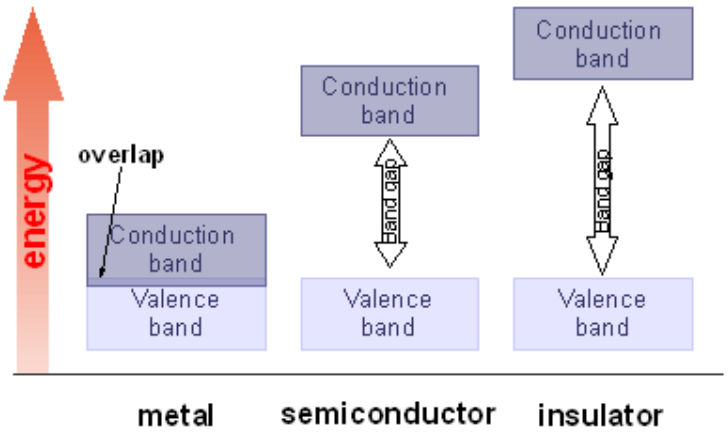

Figure 2.1 Band gaps of metal, semiconductor and insulator

A solid having electrical conductivity between an insulator and conductor is called a semiconductor and semiconductors have a narrow band gap when compared with the band gap of insulators. Because of the presence of band gap, conductivity of semiconductors is lower than the conductivity of metals and doping the semiconductor is considered to be the way of increasing the conductivity of the solid by increasing the number of electrons in the conduction band.

Intrinsic semiconductors are undoped and very poor semiconductors having certain amount of electron and holes at room temperature. In order to change the concentration of electrons and achieve extrinsic semiconductors, impurities which are different than the intrinsic semiconductors, are introduced to the semiconductors. These impurities are called dopants which can be either donors or acceptors. Donors, which is named as *n-type dopants*, increase electron concentration by donating electrons to semiconductor's conduction band while acceptors, which is named as *p-type dopants*, increase hole concentration by accepting electrons from semiconductor's valence band or provide holes to semiconductor's valence band. The semiconductors doped with n-type dopants are called n-type semiconductors and the ones doped with p-type dopants are called p-type semiconductors as shown in Figure 2.2. The semiconductors used in this study, titanium dioxide and tin oxide, are n-type semiconductors.

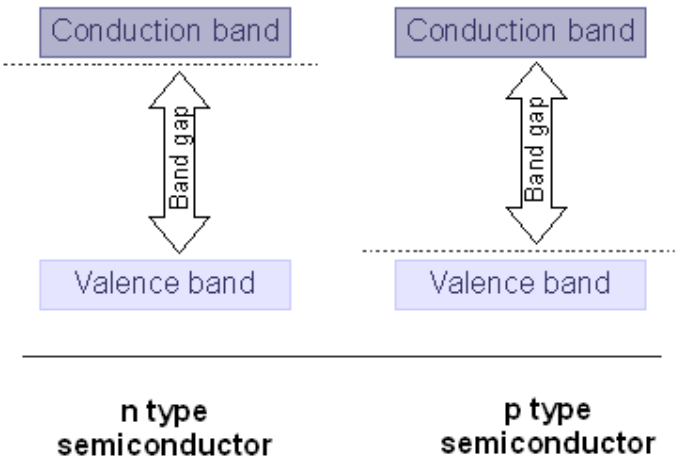

Figure 2.2 Band gaps of extrinsic semiconductors; n-type semiconductor, p-type semiconductor

2.1.1 Optical Band Gap of Semiconductors

Band gap and band gap energy of semiconductors can be determined by using absorbance spectrum in the UV-Visible range as shown in Figure 2.3. Having an İdea about the photon energy corresponding to the band gap allows for an experimental method in determining band gap of semiconductors.

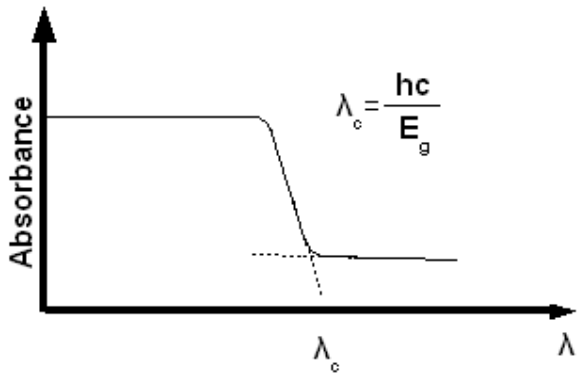

Figure 2.3 Relation between photon energy and band gap of semiconductors

The photon energy is [Diebold, 2003]:

$$E_g = \frac{hc}{\lambda_c} \tag{2.1}$$

where

E_g : Photon energy, J

H : Planck's constant, 6.626×10^{-34} kg.m^2/s

C : Speed of light, 3×10^8 m/s

λ_c : Wavelength, m.

2.1.2 Electrical Conductivity of Semiconductors

As explained in section 2.1.1, electrical conductivity depends on the magnitude of the band gap and the mobility of electrons moving from the valence band to the conduction band. The electrical conductivity can be expressed by equation 2.2.

$$\sigma = n_e e \mu_e + n_h e \mu_h \qquad (2.2)$$

n-type p-type

where

σ : Conductivity, $\Omega^{-1}.m^{-1}$

n : Carrier density of electrons (e) and holes (h), electrons/m^3

e : Electron charge, $1.6x10^{19}$ C

μ : Mobility of electrons (e) and holes (h), $m^2/V.s$

Mobility of electrons and holes is defined by:

- Lattice defects like self interstitial and vacancies at low temperatures,
- Lattice vibrations (phonon) at high temperatures.

The carrier density and mobility of electrons and holes change due to the property of solids whether being metals or semiconductors. The carrier density of metals is much greater than carrier density of semiconductors while mobility of semiconductors is greater than the mobility of metals.

By increasing temperature, conductivity of metals decreases due to the fact that lattice vibrations gain energy and causes more scattering of electrons with their larger amplitudes which reduces the mobility of electrons and holes [Mirkelamoglu, 2002]. On the other hand, increasing temperature results in increased conductivity for semiconductors since number of electrons is increased in the conduction band.

2.2 Photocatalysis

2.2.1 Definition and Mechanism of Photocatalysis

The word photocatalysis is the composite name of *photo* and *catalysis*: *photo* stands for light while *catalysis* is the process where a substance is used in order to increase the rate of a thermodynamically possible reaction by reducing the activation energy in which the reactant known to be catalyst is not consumed [Chanon, 1997]. The most important feature that makes this type of reactions advantageous is that; at room temperature and atmospheric pressure, photocatalytic reactions can take place without any need for heat supply for activation. The studies about photocatalytic reactions have been increasing since sun light can be utilized as a light source [Grätzel, 1983; Tseng and Huang, 1991].

Photocatalysis is classified as homogeneous and heterogeneous photocatalysis. Homogeneous photocatalysis is mostly implied with organic reactions which are accelerated by organo metallics, metal ions, etc. and is out of focus of this study. So, only the heterogeneous photocatalysis and related literature is considered in this is study.

For heterogeneous catalytic reaction mechanism, factors affecting rate of catalytic reaction can be classified as factors inside and outside the catalyst particles. Transfer steps outside the catalyst particle are shown in Figure 2.4 and listed as follows:

1. Transfer of reactives to the external surface of the catalyst
2. Adsorption of at least one reactive
3. Reaction of the reactive at the surface and formation of product on the surface
4. Desorption of the product from the external surface of the catalyst
5. Transfer of the product to the bulk medium

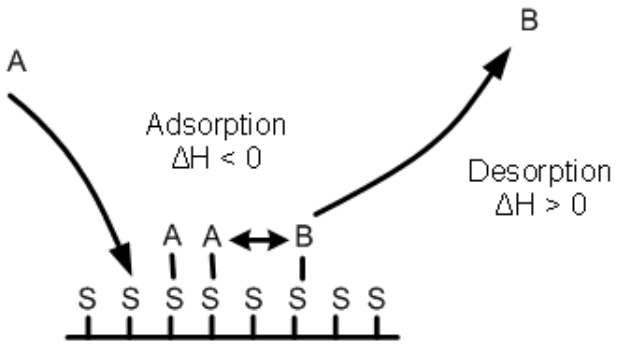

Figure 2.4 Adsorption, reaction and desorption steps on the external surface of heterogeneous catalyst

Adsorption step is an important step for determining the amount of reactives on the external surface of the catalyst. Heterogeneous photocatalysts present in solid phase, increases the formation rate of free radicals as a result of absorption of photons existing in the reaction medium which is either liquid phase or gaseous phase. Heterogeneous photocatalysts are metal oxide semiconductors since they can absorb photons in the wavelength range of UV or visible light.

Photocatalytic reaction is a series of chain reactions taking place on the surface of metal oxide semiconductors, in which an emitted photon in the appropriate wavelength, a catalyst surface and an oxidizing-reducing agent (mostly oxygen is utilized for this purpose) have to be present for the reactions to take place [Lasa et al., 2005]. The chain reactions can be classified as below:

- Charge carrier formation
- Charge carrier adsorption
- Charge carrier recombination
- Photocatalytic degradation

Absorption of photon is the first step of photocatalytic reaction and the reaction starts when a photon having energy greater than the band gap energy of the photocatalyst reaches to the surface of the photocatalyst [Jaeger, 1979; Prairie,

1993; Lasa et al., 2005]. With the absorption of photon, electrons present in the valence band are excited to the conduction band having higher energy. This excitation results in the formation of electron and hole pairs (e^-/h^+) inside the semiconductor photocatalyst which is metal oxide (MO) as shown in Figure 2.5 (equation 2.3).

$$MO + h\nu \Rightarrow MO\ (h+ - e-) \qquad (2.3)$$

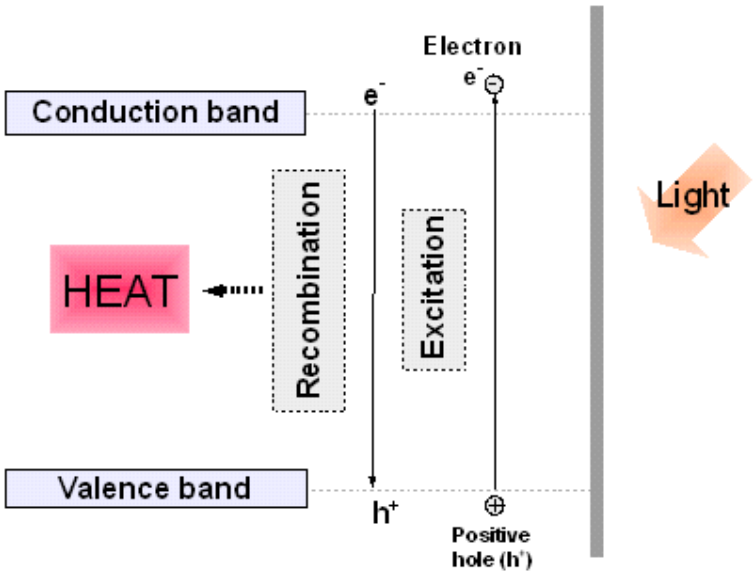

Figure 2.5 Formation of electron and hole pairs

In Table 2.1, semiconductors used frequently, their band gaps and wavelengths are given. In order to use the semiconductor metal oxide efficiently, it should give reaction with photons having energy greater than the band gap energy of semiconductor.

Table 2.1 Semiconductors, their band gaps and wavelengths

Semiconductor (MO)	Band Gap (eV)	Wavelength (λ-nm)
TiO_2 (anatase)	3.2	388
TiO_2 (rutile)	3.0	413
SnO_2	3.6	338
ZnO	3.4	363
Fe_2O_3	2.3	539

Most of the photocatalytic applications are aimed to take place under sun light. UV light is classified as; UV-A for 315 nm-400 nm, UV-B for 280 nm-315 nm and UV-C for 100 nm-280 nm, and after being filtered by atmospheric layers, small portion of UV reaches to earth. Due to the fact that the existence of photocatalytic reaction, the flux of sun light is almost 0.1 % of the flux of light consisting of visible and infrared lights which is 1300 W/m^2, shifting band gaps of semiconductor metal oxides to the visible region (red shift) has great importance for the improvement of quantum efficiency.

For metals, electrons and holes can recombine at very short time intervals since there is continuity between valence band and conduction band. On the other hand, semiconductor photocatalyst has broader band gap when compared with band gap energies of conductors or metals. So, in semiconductors, formed electrons and holes after the absorption of photons, are transferred to the external surface of the catalyst particle with diffusion and they are adsorbed by having interaction with absorbed water (H_2O) and oxygen (O_2) molecules which are in their equilibrium concentrations with the bulk. Holes at the external surface are adsorbed by water (H_2O) and hydroxyl (-OH) group which are absorbed on the surface resulting in hydroxyl radical (•OH) group formation (equations 2.4 and 2.5) [Legrini et al., 1993; Hoffman et al., 1995]. Hydroxyl radicals appearing at the end of this reactions are very active and can give several reactions with the chemicals absorbed on the surface (see Figure 2.6).

$$H_2O + h^+ \Rightarrow \bullet OH + H^+ \quad (2.4)$$

$$-OH + h^+ \Rightarrow \bullet OH \quad (2.5)$$

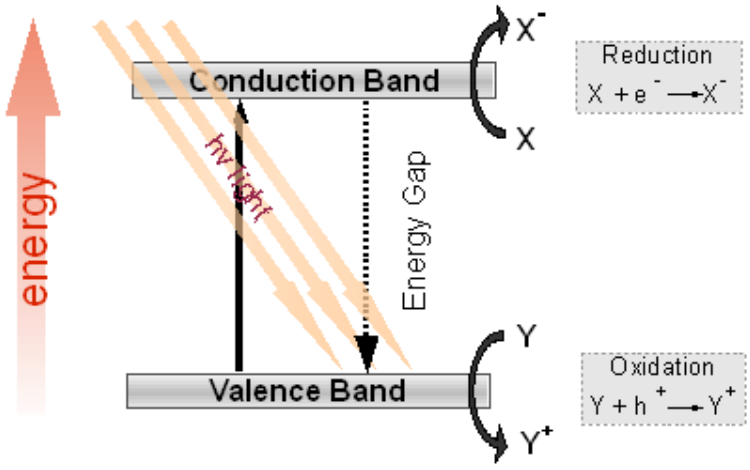

Figure 2.6 Mechanism of photocatalysis

Molecular oxygen being free in the bulk medium (either liquid phase or gaseous phase) acts as an acceptor for the electrons that reached to the external surface of the catalyst by diffusion and with this reaction, super oxygen radicals ($\bullet O_2^-$) are formed as given in equation 2.6. Protons (H+) formed by adsorption of water with holes (equation 2.4) give reaction with electrons and the products of this reaction are peroxy radical ($HO_2\bullet$) and hydrogen peroxide (H_2O_2) (equations 2.7 and 2.8) [Carp, 2004].

$$O_2 + e^- \rightarrow \bullet O_2^- \quad (2.6)$$

$$H^+ + O_2^-\bullet \rightarrow HO_2\bullet \quad (2.7)$$

$$2\ HO_2\bullet \rightarrow H_2O_2 + O_2 \quad (2.8)$$

The products of equations 2.7 and 2.8 ($HO_2\bullet$ and H_2O_2) have very high oxidation potentials and, as given in equations from 2.9 to 2.12, several reactions take place with these products resulting in the formation of hydroxy and peroxy radicals [Garcia and Takashima, 2003].

$$\bullet O_2^- + HO_2\bullet \rightarrow HO_2^- + O_2 \quad (2.9)$$

$$HO_2^- + H^+ \rightarrow H_2O_2 \quad (2.10)$$

$$H_2O_2 + e^- \rightarrow \bullet OH + -OH \quad (2.11)$$

$$H_2O_2 + \bullet O_2^- \rightarrow OH + -OH + O_2 \quad (2.12)$$

2.2.2 Quantum Efficiency

As explained in section 2.2.1, the chain reactions for photocatalysis to take place are finalized with the formation of super oxygen ($\bullet O_2^-$), hydroxy ($\bullet OH$) and peroxy ($HO_2\bullet$) radicals at the end of the adsorption reactions of electrons (e^-) and holes (h^+) with water (H_2O) and oxygen (O_2) molecules on the surface. On the other hand, little portion of photons absorbed by the crystallite can pass these steps since some of the electrons and holes recombine and lose their activities by transforming energy taken from photons to heat as shown in equation 2.13. This recombination of electron and holes (charge recombination) resulting in losing activities can occur during the adsorption on the surface of the crystallite as well as inside the crystallite [Hoffmann et al., 1995]. Rate of the termination reaction (equation 2.13) is high since particle size is much greater than the minority charge carrier length. The distance effective in the transfer of electron and hole pairs to the external surface of the catalyst particle, are closely related to the particle size. In artificially produced semiconductor materials having porosity, absorption of photon takes place faster and greater photocatalytic activity is achieved since greater surface area per unit volume exists [Kamat, 2002; Bard, 1979]. Similarly, for nano structured materials, in case the distance between charge carriers is greater than the particle size, the possibility of the termination reaction (equation 2.13) to take place decreases and the efficiency increases. Other studies in order to use the catalyst particle more efficiently and increases the reaction turnover are; using photons having higher wavelength (red shift) and preventing recombination of charge carriers.

$$MO\ (h^+ - e^-) \Rightarrow MO + heat \quad (2.13)$$

The adsorption of electrons and holes by the absorbed water and oxygen molecules on the surface and very slow reactions for the formation of free radicals are the main reasons of losing activity. The ratio of formed free radicals to the absorbed photons is very low due to the reasons listed above as electron and hole pair formation is very fast while free radical formation reaction is very slow and little portion of absorbed photons can take place in free radical formation reaction [Hoffmann et al., 1995; Grela et al., 1996; Harbour and Hair, 1986; Sun and Bolton, 1996]. This ratio is called as quantum efficiency and given in equation 2.14.

$$Quantum \quad Efficiency = \frac{Number \quad of \quad produced \quad reac\tan ts}{Number \quad of \quad adsorbed \quad photons} \tag{2.14}$$

Two parameters that affect quantum efficiency are degree of losing charge carriers with recombination and degree of adsorption of charge carriers by absorbed molecules on the surface. In the absence of electron acceptor or donor (water, oxygen, etc.) on the surface, the rate of recombination of charge carriers is the main factor affecting quantum efficiency and it is very low since the rate of charge recombination reactions is high when compared with other reaction rates. Considering this effect, quantum efficiency can be increased by increasing the rate of reactions on the surface resulting in the formation of free radicals [Carp et al., 2004]. The maximum quantum efficiency reached with this way is 12 % [Serpone et al., 1993].

One of the method listed below can be used in order to increase the quantum efficiency:

- Having nanoparticles which offers shorter path for diffusion into surface
- Higher porosity and higher crystallinity
- Metal doping

Light is an electromagnetic wave and is called as UV between 200 nm and 400 nm while it is called as visible light between 400 nm and 720 nm. Since activation energy needed for the formation of electron and hole pairs in the semiconductor is high, photons in UV region and having high energy are used.

On the other hand, photons having higher wavelength are transformed into heat by absorption. The minimum energy needed for the formation of electron and hole pairs is the energy equivalent to the band gap of the semiconductor.

Studies about shifting the band gaps of semiconductors to the visible region by decreasing the particle size are available in literature. Most of these studies are related with synthesizing modified metal oxides having smaller particle size [Kumar et al., 2000; Cho et al., 2005; Yu et al., 2006; Ostomel and Stucky 2004; Erdural et al., 2008]; doping with metals having different crystal structures [Sonawane and Dongare, 2006; Sharma et al., 2006; Lee et al., 2006; Erkan et al., 2006; Sakthivel et al., 2004; Sun et al., 2003]; doping with metal oxides [Gärtner et al., 2005; Ohno et al., 2009] or with ions [Hong et al., 2005; Serpone, 2006].

2.2.3 Photocatalytic Activity

For a photocatalytic reaction to take place, it is necessary that the electron and hole pairs reaching to the surface of the semiconductor metal oxide should not lose their activity after recombination reactions. In other words, to increase quantum efficiency, transferring adequate amount of water and hydrogen molecules to the surface is expected for the adsorption of charge carriers. As explained in section 2.2.1, adsorption of charge carriers by OH^-, H_2O and O_2 and formation of free radicals depends on the amount of water and oxygen molecules absorbed on the surface. In literature, the density of hydroxy molecules on the surface is estimated as 5-15 OH molecules/nm^2 for titanium dioxide [Legrini et al., 1993; Hoffmann et al., 1995]. Since the density of hydroxy and oxygen molecules is the limiting agent for the adsorption of electron and hole pairs, in order to increase the photocatalytic activity by increasing the surface density of these molecules, following techniques can be applied:

- Synthesizing porous catalyst particles having larger surface area.
- Having more acidic medium resulting in the increase of hydroxy molecule density and crystallinity. For that purpose, micro porous or meso porous semiconductors can be synthesized.

- Creating charge separation centers by doping metallic catalysts such as Pd, Pt, Au, Ag, Fe, etc.

Particles having larger surface area have higher quantum efficiency and highly porous surface structure offers huge amount of catalytic sites when compared with the dense ones which results in higher photocatalytic activity [Guo et al., 2005]. Besides that, surface area has more effect on the photocatalytic activity when depletion layer thickness is decreased below 10 nm and this decrease in the crystallite size improves optical efficiency. Depletion layer is an electric double layer formed at the surface of contact between a metal and a semiconductor having different work functions since the mobile charge carrier density is insufficient to neutralize the fixed charge density of donors and acceptors [Tahiri et al., 1996; Carraway et al., 1994; Zhang et al., 1998]. With decreasing the crystallite size, faster adsorption of charge carriers is achieved by decreasing the minority charge carrier length and the possibility of charge recombination reactions to take place decreases.

The percent of atoms on the surface increases with the decrease in the particle size. So, semiconductor materials having high porosity, surface area and crystallinity have higher surface area in unit volume and this causes faster adsorption of photons resulting in improved photocatalytic activity [Negishi and Tageuchi, 1999; Jiang et al., 2004; Sopyan, 2007].

Nano structured materials have high free surface energy since most of the atoms are at the surface. Having high surface energy means that nano structured material surfaces have high chemical potential and strong interaction with the molecules around. So, on the surface of nano structured materials, the amount of hydroxy and oxygen molecules are greater when compared with that of molecules having increased particle size. The adsorption of charge carriers to the surface takes place in short times and the possibility of charge recombination decreases for this type of materials. Electron energy levels for nano and micro-macro structured materials after photocatalytic reaction are given in Figure 2.7.

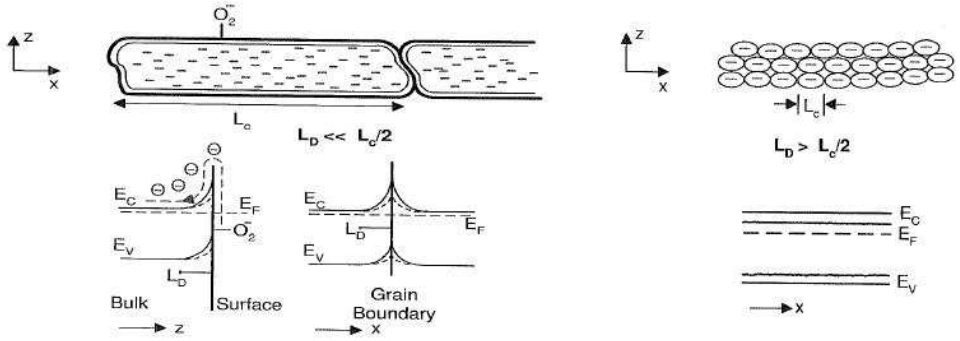

(a) (b)

Figure 2.7 Electron energy levels of (a) micro-macro and (b) nano structured materials

where

L_D : The depletion layer which is also known as barrier layer; blocking layer; space-charge layer

L_C : Characteristic length of the particle

E_C : Conduction band

E_V : Valence band

E_F : Fermi level

The advantage of having high surface energy for improvement of the photocatalytic activity has a kind of drawback that high surface energy causes instability of particles. For instance, structure of nano particles can be damaged because of the environmental factors such as temperature, pressure, existence of fluids, etc. It is very hard to separate nano structured materials in gas and liquid phases. So, for practical applications, nano structured materials needed to be adsorbed on the surface, transformed into thin films or used in order to form materials having higher particle size by agglomeration.

As explained above, high surface area and high crystallinity are desired for good photocatalytic activity. But a problem exists at that point as when the temperature is increased, crystallinity also increases. On the other hand, the

surface area decreases by increasing temperature, which causes in the limitation of substrates. Ma and Goh studied on this issue as *anatase films were deposited at 50^{o}C and 200^{o}C by LPD (liquid phase deposition) to determine if the higher crystallinity attained by the 200^{o}C process produces greater photocatalytic activity without the need for post deposition heat treatments* [Ma et al., 2006]. From SEM micrographs of cross sections of films grown at different temperatures, it was observed that, the film could be separated into two regions for both of the deposition temperatures: densely packed crystallites occur in the region which is closer to the interface of film and substrate while columnar like crystallites occur in the region which is closer to film surface and the columnar structures are porous as pores are formed at the junction of neighboring crystallites [Goh et al., 2004]. So it can be concluded that, the films at 200^{o}C are more porous than the films at 50^{o}C.

In order to see the effect of deposition temperature on crystallinity, the crystallinity of the precipitated powders are determined by X-ray diffraction (XRD) and Rietveld structure refinements. From the experiment, it was observed that maximum crystallinity of the powder was 90% and 75% at 200^{o}C and 50^{o}C, respectively. It could also be concluded that crystallinity increases with increase in the deposition time.

As a general idea, higher growth temperatures increase the rate of hydrolysis reaction, which results in the higher crystallinity. On the other hand, Goh and co-workers indicated that even if the hydrolysis and dehydration reactions are complete, the formed material couldn't be crystalline [Goh et al., 2005]. The reason is that crystalline anatase TiO_2 is formed when the octahedral titanium complexes repeatedly connect through shared edges in a periodic fashion to form skewed chains via dehydration reactions between the OH ligands of the octahedral complexes [Zheng et al., 2001].

Besides the effect of structural properties as crystallinity and particle size, metal doping has also effect on improving photocatalytic activity. Metal ions such as Au^{3+}, Ag^{+1}, Nb^{3+}, V^{2+}, Pt^{4+}, and Pd^{2+}, etc. decreases the possibility of charge recombination [Trapalis et al., 2003; Erkan et al., 2006; Sharma et al., 2006; Sonawane and Dongare, 2006; Lee et al., 2006; Sakthivel et al., 2004; Sun et

al., 2003]. By doping Au^{3+} and Pd^{2+} ions to titanium dioxide, shifting of band gap to the visible region which results in quantum efficiency increase, has been observed [Erkan, 2005]. On the other hand, metal doping can cause photocatalytic activity to disappear in the case of having metal particles with great particle size, since in this situation; metal particles become charge adsorption centers. For this reason, it is expected for metal particles to be dispersed on the surface excellently.

2.3 Semiconductor Photocatalysts

2.3.1 Titanium Dioxide

Titanium dioxide is one of the most studied photocatalyst because of being inert, easily prepared, its chemical stability, high photocatalytic activity, resistance to corrosion and its low cost [Yang et al., 2006]. As it can be seen from Table 2.1, band gap of titanium dioxide is closer to visible light when compared with the band gaps of other semiconductor metal oxides [Pascual, 1978]. The fields that TiO_2 is used as photocatalyst, are mainly, antibacterial coatings, self-cleaning (decomposition of organic pollutants) [Rao et al., 1980; Tanaka et al., 1997]. On the other hand, only 5% of UV radiation reaching to the earth can be transformed into free radicals photocatalytically by titanium dioxide.

Titanium dioxide is a powder having variable color depending on its purity. When ilmenite is treated with sulfuric acid, titanium sulfate is obtained and if it is further processed; the product will be in anatase form of titanium dioxide [Diebold, 2003; Mahanty et al., 2003; Lasa et al., 2005].

Crystalline titanium dioxide exists in three phases as anatase, rutile and brookite. Anatase and rutile phases have tetragonal structure while brookite phase has orthorhombic structure. When these three phases are compared;

- Anatase phase is more photocatalytically active than rutile and brookite phases.
- Rutile phase is the most stable phase.

- Brookite phase does not have any photocatalytic activity [Ma et al., 2006].

Despite the fact that, anatase phase is the most photocatalytically active phase, there are studies in literature that show rutile phase has also considerable photocatalytic activity [Mahanty et al., 2003].

By calcination, amorphous phase of titanium dioxide can be transformed into crystalline anatase phase and it can be, further, transformed into rutile phase [Rivera et al., 1993].

Formation of phases of titanium dioxide depends on:

- Starting material
- Deposition method
- Calcination temperature

As shown in Figure 2.8, anatase and rutile phases of titanium dioxide are similar materials in such a way that both of them are formed from TiO_6 octahedral basic structures and have the same tetragonal crystalline structure. The distortion along the octahedron structures which effects the alignment of octahedrons is the property that results in difference between rutile and anatase phases. Each Ti^{4+} ion in the structure is surrounded by six O^{2-} ions which exist in octahedron. In rutile phase, octahedrons are not regular and slightly show distortion to orthorhombic structure, while octahedrons in anatase phase show distortion at high amount and anatase phase gives less symmetric structure when compared with the structure of rutile phase [Linsebigler et al., 1995; Diebold, 2003]. This difference between the crystal structures of anatase and rutile phases causes to have differences in electron densities and band structures. Anatase phase shows higher photocatalytic activity than rutile phase in most of the reactions in spite of having higher band energy [Tsai and Cheng, 1997; Ohno et al., 2001; Sun et al., 2003].

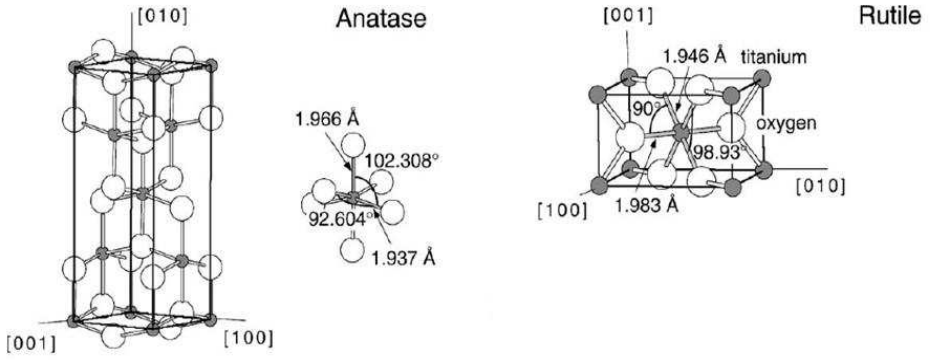

Figure 2.8 Octahedral crystal structures of anatase and rutile phases [Diebold, 2003]

2.3.2 Tin Oxide

There are three application fields of tin oxide: transparent conducting oxide (TCO), oxidation catalyst and solid state gas sensing material [Batzill and Diebold, 2005]. When the literature studies about the surface structure of titanium dioxide are taken into account, it is observed that the surface structure of tin oxide is comparatively unexplored because of the reasons that tin oxide does not have single crystal structure and there are no specific methods for producing well-defined thin films like the ones established for titanium dioxide [Diebold, 2003].

There are two main oxide forms of tin as stannic oxide (SnO_2) and stannous oxide (SnO) where stannous oxide has a band gap in the range of 2.5-3 eV being smaller than the band gap of stannic oxide which is 3.6 eV as given in Table 2.1. On the other hand, form the literature studies, it can be derived that stannic oxide is more characterized than stannous oxide due to the lack of single crystals facilitating studies about stannous oxide. Stannic oxide is the mostly found form of tin oxide and it is important for the applications of oxidation catalysts and gas sensing. From the structural point of view, stannic oxide exhibits rutile structure which is the most stable phase as explained in section

2.3.1 and at high temperatures, orthorhombic structure exists which is more dense [Batzill and Diebold, 2005].

Tin oxide is also a semiconductor being photocatalytically active. Even if, it has antibacterial properties, the antibacterial activity of titanium dioxide is higher than that of tin oxide [Erkan, 2005].

2.4 Synthesis Methods of Semiconductors

Thin films have meso and micro porous structures that can enable chemical reactions where nano structured crystallites are continuous. Since thin films have low mechanical strength, they are applied to the surfaces of glasses, ceramic tiles, etc. in order to use their properties efficiently. On the other hand, the coated surfaces gain new properties as a result of the chemical and physical properties of thin films and there are optic filters, conducting glass surfaces and sensors that have gained new properties from the coated materials.

There are several chemical and physical methods in literature for producing thin films. The mostly used methods are emulsion method, gas condensation, sputtering, liquid phase deposition, spray pyrolysis, solid-state reaction method and sol-gel. Since these methods, different than sol-gel method, need expensive materials and conditions like high vacuum, magnetic waves, it is not feasible to use these methods for the application of thin films on large surfaces. Sol-gel method is a way of producing high quality glasses and ceramic tiles having large surfaces [Kaya, 2002]. Furthermore, it is one of the most successful methods for producing photocatalytically active nano structured metal oxide materials [Sonawane et al., 2006].

2.4.1 Sol-Gel Process

Sol-gel method is one of the mostly used methods for the formation of thin films and it is colloidal route used to synthesize ceramics with an intermediate stage including a sol or/and a gel state [Pierre, 1998].

Basic steps followed during the production of metal oxides with sol-gel method are hydration of metal alkoxides with water; condensation of metal alkoxides; drying and calcination after aging [Scwartz et al., 1995; Brinker et al., 1992].

The mostly used technique for the production of metal oxides with sol-gel method is calcination of nano structured gel colloidal solutions obtained after the hydrolysis and condensation reactions of metal alkoxides (see Figure 2.9). First step for the sol-gel synthesis is choosing the starting material called *precursor* which determines whether reaction leads towards the formation of polymeric gels or colloidal particles. Metal alkoxides are the mostly used precursors in sol-gel synthesis which are composed of alcohol molecules attached to metal (M) atom. The mostly used metal alkoxides in the sol-gel synthesis are ethyl, propyl and butyl alkoxides of metals. For instance, in the formation of TiO_2, titanium alkoxides, $Ti(OR)_n$ is used to form oxopolymers [Su et al., 2004].

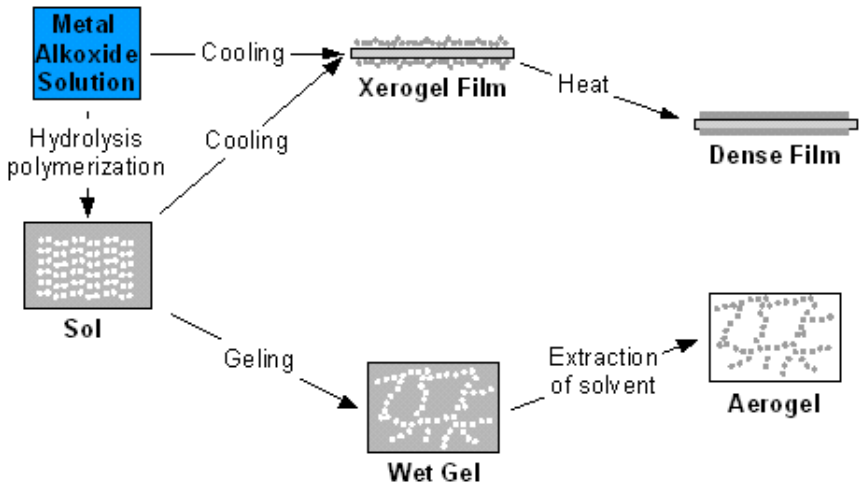

Figure 2.9 Sol-gel process for dense film and aerogel formation

After choosing the precursor, the next step is hydrolysis reaction of metal alkoxide solution with water as given in equation 2.15. During the hydrolysis reaction, alcohol molecules in the structure of metal alkoxides are eliminated with the replacement of water.

$$M(OR)_n + H_2O \rightarrow M(OR)_{n-1}(OH) + ROH \quad (2.15)$$

Hydrolysis reactions and condensation reactions, given in equations 2.16 and 2.17, take place at the same time. So, metal alkoxide compounds are not completely hydrolyzed and form polymeric chains. On the other hand, the reaction rate decreases because hydrolysis of polymeric alkoxy groups formed by condensation reactions is limited with mass transfer. In the condensation reactions (equation 2.16), alcohol is eliminated directly while in dehydration condensation (*oxolation*) reactions (equation 2.17), water is eliminated and the product metal oxide is obtained at the end of condensation reactions.

$$M(OR)_n + M(OR)_{n-1}(HO) \rightarrow M_2O(OR)_{2n-2} + ROH \quad (2.16)$$

$$2M(OR)_{n-1}(OH) \rightarrow M_2O(OR)_{2n-2} + H_2O \quad (2.17)$$

On the other hand, there are some kinds of side reactions occurring in addition to the above reactions during sol-gel synthesis. The most important side reactions are *olation* reactions where two hydroxyl-metal groups take place.

$$M\text{-}OH + M\text{-}OH \rightarrow M\text{-}(OH)\text{-}M + H_2O \quad (2.18)$$

$$M\text{-}OH + M\text{-}OH \rightarrow M\text{-}(OH)_2\text{-}M + H_2O \quad (2.19)$$

The overall reaction for sol-gel synthesis is given in equation 2.20.

$$M(OR)_n + \frac{n}{2} H_2O \rightarrow MO_{n/2} + n\ ROH \quad (2.20)$$

Polymerization can be continued with equivalent reaction rates by increasing the hydrolysis reaction rate catalytically. For that purpose, acidic catalysts like HCl, H_2SO_4, etc. can be used instead of basic catalysts. Because of this reason, in order to finish hydrolysis reaction, acidic catalysts and water, more than stoichiometric amount, are used.

When the equations above are analyzed, it can be seen that amount of water added to the mixture at the beginning, is very effective on the relative rates of reactions. In case of low amount of water in the starting mixture, reaction system

is governed by alkoxides and since, coordination number of titanium is four in Ti-O-Ti chains, closely packed three dimensional crystallite structures of Ti-O-Ti derivatives are formed at the end of condensation and oxolation reactions. On the other hand, by increasing the amount of water to the stoichiometric amount, reaction system is governed by hydrolysis reaction and the rate of oxolation reaction is very low resulting in the formation of derivatives of $Ti(OH)_4$. Furthermore, by adding more water, rate of oxolation reaction is increased which prevents formation of Ti-O-Ti derivatives and the resultant product would be Ti-OH derivatives having low density, being not three dimensional and not closely packed [Su et al., 2004]. By further increasing the amount of water, formation of $Ti(OH)_4O^+H_2$ derivatives and Ti-O-Ti chain having high density is another mechanism for sol-gel synthesis. As explained above, water has great importance on the structure and photocatalytic activity of crystal during the production of nano structured metal oxides by sol-gel method.

In the application of thin films on glasses and ceramic tiles, the physical properties should be considered in such a way that application should not cause any change on the color, optical properties of the substrate strong adhesion to the surface should be achieved. On the other hand, semiconductor thin films are not bright and have low adhesion strength because of having highly porous surface and high surface area in order to increase photocatalytic activity. For that reason, parameters during the production titanium dioxide and tin oxide having different morphologies should de analyzed separately. Also, it should be noted that, calcination step has more effect on the crystal structure, porosity and surface area of the product [Brinker et al., 1992; Uhlmann et al., 1997].

Even if there are several methods for producing thin films, sol-gel method is the mostly used one since it has many advantages over other methods as given below:

- Reactions take place at low temperatures which allows saving energy, reducing losses due to evaporation and other advantage is that, at low processing temperatures, kinetics of the chemical reactions can be easily controlled.
- Simple equipments are needed during sol-gel synthesis.

- By controlling nucleation and growth of the colloidal particles, desired particle size and shape can be achieved.
- The process occurs in liquid medium avoiding pollution arises from the dispersion of dust particles.
- It is possible to use different kind of substrates with different sizes and so, sol-gel process can be used in order to produce hybrid organic-inorganic materials which do not exist naturally.
- The final product has high homogeneity and high purity.

Besides the advantages, there are some disadvantages as given below:

- Used precursors are expensive.
- There is a possibility of residual carbon or hydroxyl existence on thin films.
- Materials used during sol-gel synthesis are health hazardous.
- There is a lot of lost in material during process because of the long processing time.

2.5 Coating Types for Sol-Gel Process

Coating type of the thin films is a parameter affecting the properties of the final product. There are mainly two coating types for sol-gel process: dip coating and spin coating.

2.5.1 Dip Coating

Dip coating is the mostly used and easy way in order to produce transparent layers by depositing sol-gel film on the substrate which can be flat panels, cylinders or in complex geometry [Erkan, 2005]. During dip coating, substrate is immersed in liquid and withdrawn with a defined speed under controlled conditions of temperature and pressure.

Advantages of dip-coating process [Turhan, 2000]:

- Coating thickness can be easily controlled.
- Multi-layered coatings can be obtained.
- Coating having high homogeneity can be achieved.

Batch dip coating process is divided into five stages: immersion, start-up, deposition, drainage and evaporation (Figure 2.10) [Scriven et al., 1988]. In the existence of volatile solvents like alcohol, evaporation accompanies the start-up, deposition and drainage steps. When the moving substrate is immersed into the substrate, boundary layer, consisting of sol, exists on the coating layer. During the deposition and drainage steps, boundary layer splits into two as the inner and outer layers. The outer layer returns to the sol while the inner layer moves upward with the substrates [Brinker and Scherer, 1990].

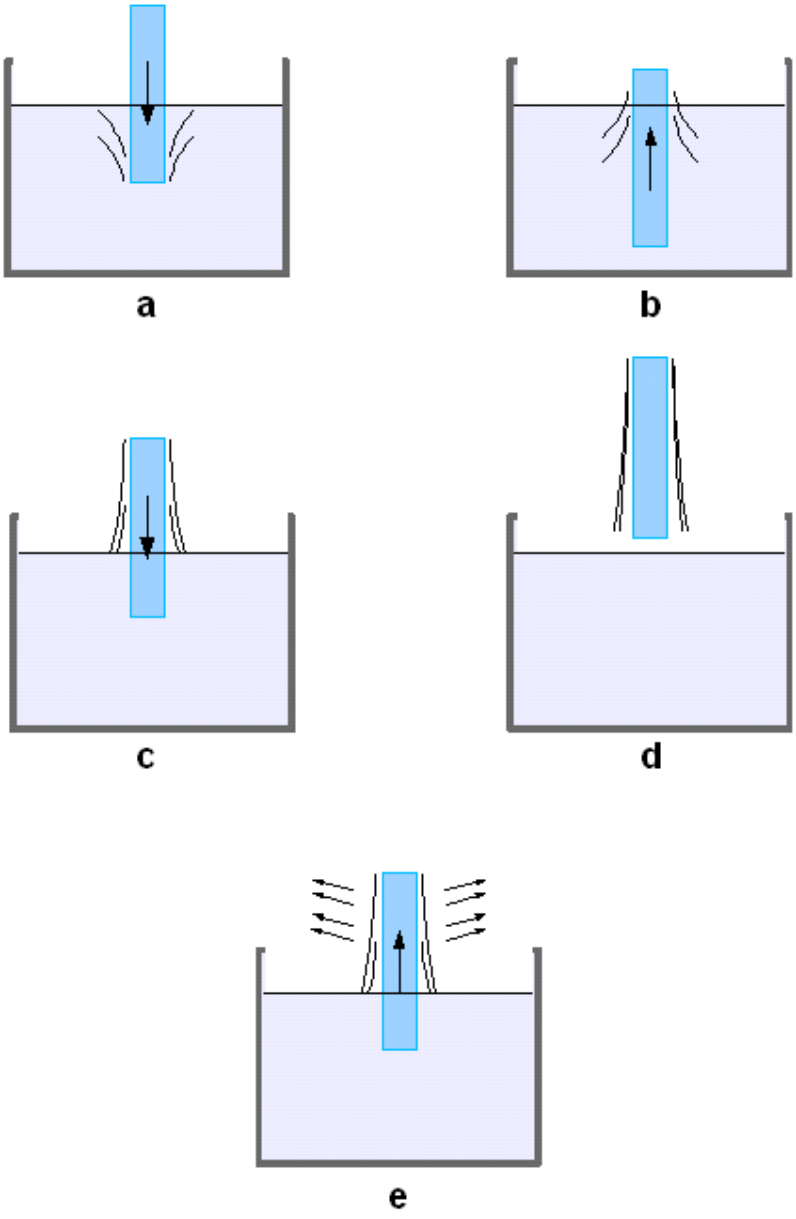

Figure 2.10 Dip-coating process steps; (a): immersion, (b): start-up, (c): deposition & drainage, (d): drainage, (e): evaporation

The main forces that affect the thickness of the film are listed as [Scriven et al., 1988]:

- Moving substrate's viscous drag upward on the liquid
- Gravitational force
- Surface tension of sol resulting in the concavely curved meniscus
- Boundary layer liquid's inertial force arriving at the deposition region
- Surface tension gradient (It is important to have coating thickness less than 1 μm)

As indicated above, the coating thickness is determined by a defined withdrawal speed, solid content and liquid viscosity. When the liquid viscosity and the withdrawal speed are not high in order to keep system in the Newtonian regime, the coating thickness can be calculated by using Landau and Levich equation (equation 2.21) [Landau and Levich, 1942].

$$h = 0.94 \frac{(\eta U)^{2/3}}{\gamma_{LV}^{1/6} (\rho g)^{1/2}} \tag{2.21}$$

where

h : Coating thickness

η : Viscosity

U : Withdrawal speed

γ_{LV} : Liquid-vapor surface tension

ρ : Density

g : Gravity

The applicability of Landau and Levich equation for the calculation of coating thickness is found to be limited since the equation above assumes Newtonian regime for the system and ignores parameters affecting the thickness like pH, viscosity derivation, evaporation during dip coating process [Kaya, 2002].

2.5.2 Spin Coating

Spin coating is a way of depositing thin films on hard surfaces and inclined substrates**.** During spin coating, the substrate spins around an axis being perpendicular to the coating area. Spin-coating is divided into four stages: deposition, spin-up, spin-off and evaporation (Figure 2.11) [Bornside et al., 1987].

The first stage is the deposition stage and excess amount of liquid is applied to the substrate surface. During the spin-up stage, liquid tends to go outward radially because of the centrifugal forces. At the end of spin-off stage, excess amount of liquid leaves the surface as droplets. In case of a decrease in the film thickness, amount of leaving liquid also decreases. The reason of this situation is that by decreasing film thickness, resistance to flow increases [Brinker and Scherer, 1990]. There can be differences for the coating thickness depending on surface tension, rotational rate and liquid viscosity. On the other hand, by keeping the system in the Newtonian regime and by keeping initial coating thickness uniform, a uniform coating thickness can be achieved at any time during the spin coating process and this is an advantage for spin-coating [Scriven et al., 1988]. The last stage is the evaporation stage which is the most important stage for thinning the coatings.

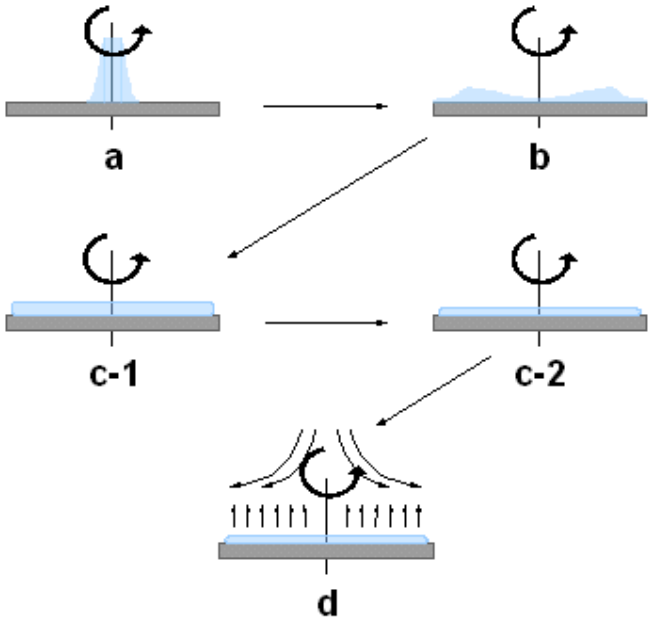

Figure 2.11 Spin-coating process steps; (a): deposition, (b): spin-up, (c-1) and (c-2): spin-off, (d): evaporation

The final thickness of the coating depends on several parameters like angular velocity, viscosity and solvent evaporation rate. Meyerhofer described this dependence by separating spin-off and evaporation stages in order to calculate coating thickness (equations 2.22 and 2.23) [Mennig et al., 1998]. On the other hand, the model developed by Meyerhofer is limited since it is only applicable for the systems in the Newtonian regime.

$$h_{final} = (1 \quad \rho_{0_A} / \rho_A) \left(\frac{3\eta m}{2\rho_{0_A} w^2} \right)^{1/3} \tag{2.22}$$

and

$$t_{final} = t_{spin\ \ off} + h_{spin\ \ off} \rho_{0_A} / m\rho_A \tag{2.23}$$

where

ρ_A : Mass of volatile solvent per unit volume

$\rho_{Å}$: Initial mass of volatile solvent per unit volume

h_{final}: Final thickness

η : Viscosity

w : Angular speed

m : Evaporation rate of the solvent depending on the mass transfer coefficient

For both coating types, equations given in order to calculate coating thickness are applicable for single component liquids and they are not applicable for multicomponent liquids since molecules in the coating liquid evaporate and after evaporation, liquid viscosity changes due to the condensation of resultant coating liquid [Ozmen, 2006].

2.6 Physical and Chemical Properties of Thin Films

2.6.1 Surface Free Energy

Liquid being on the surface has two interfaces as solid-liquid and liquid-vapor. The specific energies (J/m^2) of solid-vapor interface, γ_{SV}, and solid-liquid interface, γ_{SL}, give idea about wetting of the surface in such a way that if γ_{SV} is greater than γ_{SL}, the liquid dropped will flow over the surface [Brinker and Scherer, 1990]. Change in energy, ΔE, in the case of dropping liquid on the surface is:

$$\Delta E = \gamma_{SL} + \gamma_{LV} - \gamma_{SV} \quad (2.24)$$

where

γ_{SL} : Specific surface energy of solid-liquid interface

γ_{LV} : Specific surface energy of liquid-vapor interface

γ_{SV} : Specific surface energy of solid-vapor interface

For the situations that $\Delta E \geq 0$, solid-liquid-vapor interface is characterized by contact angle, θ, which is used in order to measure the wetting of the surface by liquid. As shown in Figure 2.12, contact angle is the angle formed where three phases have thermodynamic equilibrium and at equilibrium, the chemical potentials of three phases are equal. Contact angle is an important parameter in order to have an idea about the surface structures of photocatalytic metal oxides since it is directly related with surface energy of a metal oxide. The shape of liquid droplet on the surface is determined with thermodynamically minimum energy of it after the interactions between the surface and the liquid having different surface energies. The contact angle is determined by the Young's equation and, when θ is equal to zero, then the surface is *super hydrophilic* and the liquid is said to be *spreading liquid* since it covers the surface.

$$\gamma_{SV}=\gamma_{SL} + \gamma_{LV} \cos \theta \qquad (2.25)$$

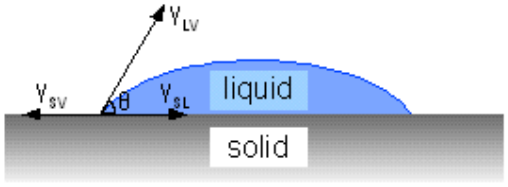

Figure 2.12 Contact angle determinations by Young's equation

Contact angle and specific surface energy of liquid are measurable properties. Contact angle of the surface, surface roughness, disorderness of crystals on the surface are related with homogeneity of the surface. The Young's equation assumes a perfectly flat surface by ignoring surface roughness and in order to reduce deviations, correction factor is added to the equation for surfaces having roughness and impurities. The relation between contact angle of water and surface porosity is determined by Wenzel equation:

$$\cos \theta_W = r\,(\gamma_{SV}=\gamma_{SL})/\,\gamma_{LV} = A \cos \theta \qquad (2.26)$$

where

A : Surface porosity factor, actual surface area/apparent surface area

θ_W : Contact angle of water on the surface

From Wetzel equation, the chemically homogeneous surface being porous has higher contact angle of water than that of the rough surface. On the other hand, this condition is not applicable for nano structured surfaces since surface porosity is lower than 0.5 nm and this amount does not have any effect on specific surface energy. According to Cassie law, chemical composition has an important effect on the specific surface energies of thin films as metal thin films have lower specific surface energy than metal oxides and pure metals [Mellott et al., 2006; Tsuge et al., 2008; Wu et al., 2006]. Due to these facts, the hydrophilicity or hydrophobicity of the surfaces of thin films depend on chemical composition in addition to surface porosity. Even if there is limited information about the relation between contact angle and chemical composition for photocatalytic materials like titanium dioxide, contact angle of semiconductor metal oxides having photocatalytic properties depends on many factors like chemical composition, size, morphology of the surfaces and the amount of –OH in the thin films [Wu et al., 2006; Guo et al., 2005].

2.6.1.1 Hydrophilicity

Hydrophilic materials can be easily wetted by polar liquids like water. This type of surfaces is covered with a liquid film. Similarly, surfaces that can be completely wetted by water are called super hydrophilic materials and contact angle is 0^o at ideal conditions. Hydrophilic materials are classified as advanced materials since they can be easily wetted by water and can be easily cleaned. They can transiently bond with water through hydrogen bonding.

Hydrophilic materials have various advantages:

- defogging glasses,
- enabling oil spots to be swept away easily with water

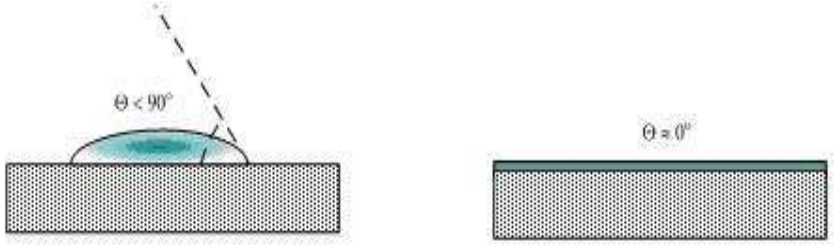

(a) (b)

Figure 2.13 Schematic representations of contact angles for (a) hydrophilic and (b) super hydrophilic surfaces

2.6.1.2 Hydrophobicity

Opposite to hydrophilic materials, hydrophobic materials repel water from their surface. Water on hydrophobic surfaces exhibits a high contact angle and forms spherical shape in order to minimize contact with the hydrophobic surface. Hydrophobic materials can be wetted by nonpolar liquids like oil, benzene, etc. Plastic materials like teflon are super hydrophobic materials having contact angle 180^{o}C at ideal conditions. These types of surfaces are not easily spoilt since they are not wetted.

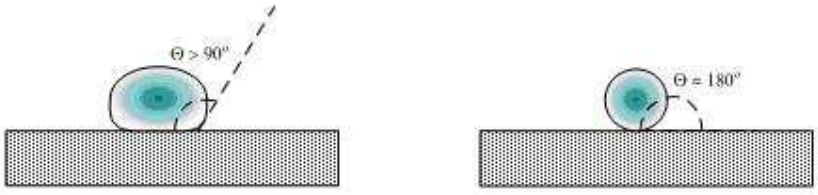

(a) (b)

Figure 2.14 Schematic representations of contact angles for (a) hydrophobic and (b) super hydrophobic surfaces

From the chemical compositions and functional groups forming the surface, the material having flat surface can be determined whether it is hydrophilic or hydrophobic. Methyl (CH_3) functional groups represent hydrophobic structure while functional groups like hydroxy (-OH) and carboxy (–COOH) represent hydrophilic structure [Beganskiene et al., 2007].

Metal oxides exhibit different contact angles when they are coated as thin films. In other words, wettability of the surfaces differs from each other according to the coating properties in such a way that, surface coated with micro structured semiconductor metal oxide can be super hydrophobic due to the air-filled pores between the particles. This is known as *Lotus effect* where coating having micro structured air-filled pores has contact angle corresponding to super hydrophobic materials. For this type of surfaces, dimensions of air-filled pores are very important. Similarly, super hydrophilicity can be achieved from micro or meso porous metal oxide coatings having smaller particles and air-filled pores. So, super hydrophobic or super hydrophilic materials can be obtained by changing the properties of metal oxide coatings like surface morphology, coating density, coating thickness and particle size.

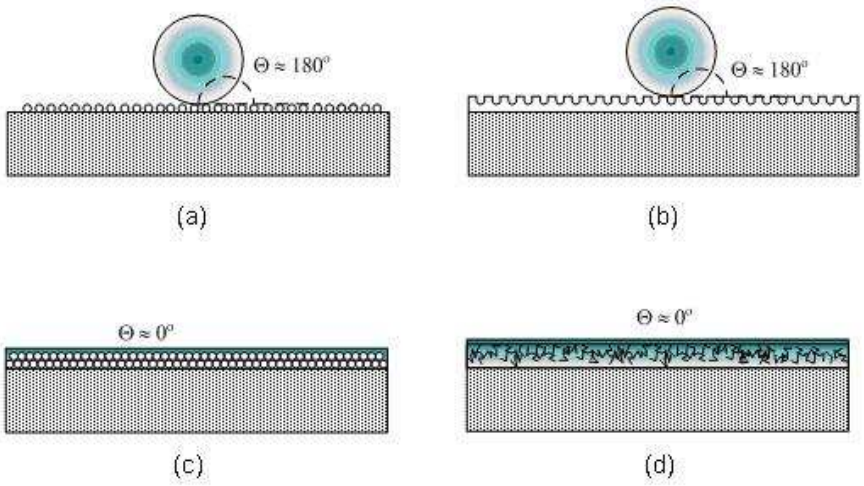

Figure 2.15 Schematic representations of contact angles for (a) super hydrophobic surfaces, (b) Lotus effect, (c) micro-meso porous super hydrophilic surfaces and (d) micro-meso porous surfaces

Furthermore, there is a relation between hydrophilicity and photocatalytic activity. Despite of having different mechanisms, hydrophilicity and photocatalysis can take place together, at the same time, on the same surface and this type of film has self-cleaning property [Fujishima et al., 2000]. According to the self-cleaning mechanism (Figure 2.16), adsorbed pollutants are removed by water since chemisorbed layer of H_2O can adsorb additional H_2O layer that results in close contact between the surface and adsorbed pollutants [Guan, 2005].

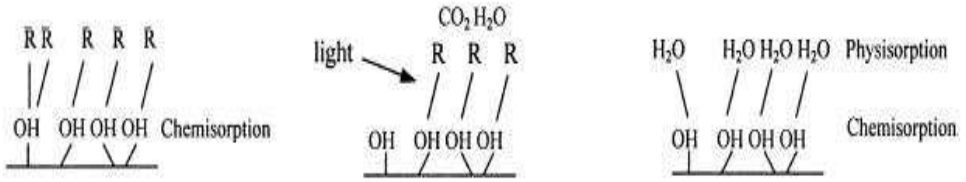

(1) (2) (3)

Figure 2.16 Steps of self-cleaning mechanism for hydrophilic thin films [Guan, 2005]

In literature, there are several studies about improving hydrophilicity and photocatalytic activity. One way is to dope tin oxide into titanium dioxide and by doping tin oxide; hydrophilicity can be improved in such a way that the composite thin film doped with 1-5 mol% tin oxide shows super hydrophilic properties [Liu et al., 2002]. The hydrophilicity is improved because of the increased amount of hydroxyl group on the surface of the composite thin film. On the other hand, in order to improve hydrophilicity, there should be an optimum doping amount since having higher amount of tin oxide results in increased contact angle. From the studies, with doping 1 mol% - 5 mol% tin oxide, super hydrophilicity was achieved while contact angle was 13.5^o by increasing the amount of tin oxide to 30 mol%.

Semiconductor metal oxides are multifunctional materials and they change their contact angles according to the conditions of medium. After the irradiation of semiconductor metal oxide by UV light, water vapor present in the medium gives

reaction on the outer surface and increases hydroxy (-OH) functional groups present on the coated surface. As a result of this property, contact angle of semiconductor metal oxide coated surfaces can be decreased with irradiation by sun light or UV sources and super hydrophilic materials can be obtained. When titanium dioxide is observed, it is found that contact angle of water on the surface is almost zero during UV irradiation and it starts to increase when the material is taken to the dark place [Guan, 2005].

2.7 Thermal Treatment

Thermal treatment is the last stage of the process in order to obtain thin films. It is divided into two stages as drying and calcination to form the ceramic phase [Erkan, 2005]. Thermal treatment affects the crystal structure, particle size and film cracking of the coated substrate.

2.7.1 Drying Between Coating Layers

When the substrates are coated with the sol-gel solution, the solution is not stable on the surface of the substrate. In order to achieve stability, substrates are dried. Drying stage can be divided into several stages. At the first stage, the coated substrate shrinks with respect to the evaporated liquid and liquid-vapor interface remains at the exterior surface of the coated substrate. Then, at the second stage, further shrinkage of the coated substrate is observed since condensation reactions take place and the coated substrate becomes stiff enough that prevents further shrinkage. Evaporation, also, continues and liquid becomes isolated in the pores at the end of condensation and evaporation steps. Furthermore, drying can continue by evaporation of the liquid within the coated substrate and diffusion of vapor to the outside [Brinker and Scherer, 1990].

At the end of drying stage, thin film is obtained in amorphous phase with having cracks on it. Cracks are formed because of the shrinkage caused by the pressure gradient in the liquid phase of a gel. To avoid cracking, drying may be

carried out at several conditions as supercritical drying, freeze-drying and drying in the presence of various drying control chemicals [Lawn and Wilshaw, 1975].

2.7.2 Calcination After Coating

Aim of the calcination stage after coating is to transform the dried thin film to ceramic oxide. During the calcination stage, these processes take place: Polycondensation reactions, pyrolysis of organic compounds and groups left in the film which is in the carbon, carbon oxidation, removal of increased amount of –OH and –OR groups due to the slowly densified thin films [Erkan, 2005; Ozmen, 2006].

2.7.2.1 Effect of Calcination Temperature

Amorphous phase of titanium dioxide can be transformed into crystalline anatase phase and it can be, further, transformed into rutile phase by calcination as indicated in section 2.3.1 [Rivera, 1993].

Kim and co-workers studied on this issue in order to observe the effect of calcination temperature on structural and optical properties of titanium dioxide [Kim et al., 2002]. At the end of the study, it is found that titanium dioxide thin films are in amorphous phase when calcined at 300 ^{o}C while they are in anatase phase after being calcined at 400^{o}C and rutile phase formation occurs at the calcination temperature of 1000^{o}C. It was observed that crystallite size of titanium dioxide thin films calcined for one hour at different temperatures increases with the increase in calcination temperature. For 400^{o}C calcination temperature, only anatase phase took place with 9.6 nm crystallite size while at 1100^{o}C, crystallite size was 43.8 nm for the rutile phase.

Furthermore, film thickness and porosity decreases by increasing calcination temperature. As observed from SEM micrographs, decrease in porosity is caused by the densification of thin film with increase in the calcination temperature.

CHAPTER 3

EXPERIMENTAL

3.1 General

In the experimental studies, pretreated glass substrates were coated with colloidal solutions synthesized by sol-gel method followed by heat treatment. Then, the surface properties and photocatalytic activities of the samples were characterized. In these studies, the colloidal solutions of TiO_2, SnO_2 and their binary mixtures were prepared and the effect of metal dopant were also investigated. The surface characterization of the samples were performed by using CAM (Contact Angle Meter) for hydrophilicity, SEM for surface morphology and UV/Visible Spectrophotometer for absorption edge energy. The photocatalytic activity of the samples were measured by the methylene blue degradation and antimicrobial activity tests. Also, surface area was analyzed by using Langmuir isotherms.

3.2 Preparation of Thin Film Samples

3.2.1 Materials

The precursors and chemicals used for the synthesis of sol-gel solutions and the preparation of thin films are listed as:

- Titanium n-butoxide [Titanium(IV) n-butoxide, $C_{16}H_{36}O_4Ti$, 99%], by Acros Organics (CAS number: 5593-70-4)
- Tin tetrachloride pentahydrate [Tin(IV) chloride pentahydrate, $SnCl_4.5H_2O$, 98%], by Acros Organics (CAS number: 10026-06-9)

- Ethanol [C_2H_5OH, 99.9%, density=0.790 kg/lt], by Merck (CAS number: 64-17-5)
- Chloroform [$CHCl_3$, 99%], by LAB-SCAN Analytical Sciences (CAS number: 67-66-3)
- Potassium hydroxide pellets [KOH, >84%] by Merck (CAS number: 1310-58-3)
- Palladium(II) acetate [$(CH_3CO_2)_2Pd$, 98%], by Aldrich (CAS number: 3375-31-3)
- Silver nitrate[$AgNO_3$, 99.9%] by Aldrich (CAS number: 7761-88-8)
- Iron(III) nitrate nonahydrate [$Fe(NO_3)_3.9H_2O$, 99.0-101.0%], by Merck (CAS number: 7782-61-8)
- Praseodymium(III) acetylacetone hydrate [$Pr(C_5H_7O_2)_3 \cdot xH_2O$, 99.9+%] by Aldrich (CAS number: 28105-87-5)

3.2.2 Pretreatment of Glass Substrates

Microscope slides, having dimensions 25mm x 75 mm x 1 mm, were used as soda-lime glass substrates. The microscope slides were supplied by Industrial Quality. Before the application of colloidal solutions to the substrates, the surfaces of the substrates were pretreated in order to improve wetting properties. In literature, the use of concentrated NaOH solution had been reported for the pretreatment process [Erkan, 2005; Lin et al., 1998]. However, KOH solution was utilized for cleaning and etching instead of NaOH solution in order to prevent the possible poisoning of thin film photocatalyst with residual Na^+ ions. The soda-lime glass substrates were, first, washed with distilled water and, then immersed in 1.0 N KOH solution for 6 hours in order to have enough hydroxylation and etching. After rinsing with distilled water, glass substrates were ultrasonicated in ethanol-chloroform solution (prepared 1:1 by volume) and in distilled water. Duration of each ultrasonication was 10 minutes. The glass substrates were, then, rinsed with distilled water and, finally dried over night at 120^oC.

3.2.3 Synthesis of Sol-Gel Solutions

Different sol-gel methods were applied for the preparation of TiO_2, SnO_2 and their binary mixed oxides. The colloidal solutions were aged for 1 day in the desiccators before the application of the solutions to the glass substrates, so that further hydrolysis was minimized and stable colloidal solutions were achieved.

3.2.3.1 Synthesis of Titanium Dioxide Colloidal Solutions

Titanium dioxide colloidal solution was prepared with the experimental method illustrated in Figure 3.1. In the preparation, 8.6 ml titanium n-butoxide ($(C_4H_9O)_4Ti$) was added into 119.5 ml ethanol and stirred for 30 minutes at room temperature by using magnetic stirrer. 65% (volume:volume) solution of HNO_3 was added dropwise to the preparation adjusting the pH value to 3.5. Hydrolysis reaction was carried out by the dropwise addition of 1.35 ml distilled water at room temperature while stirring the solution. To complete the hydrolysis reaction, solution was stirred for 5 hours at room temperature.

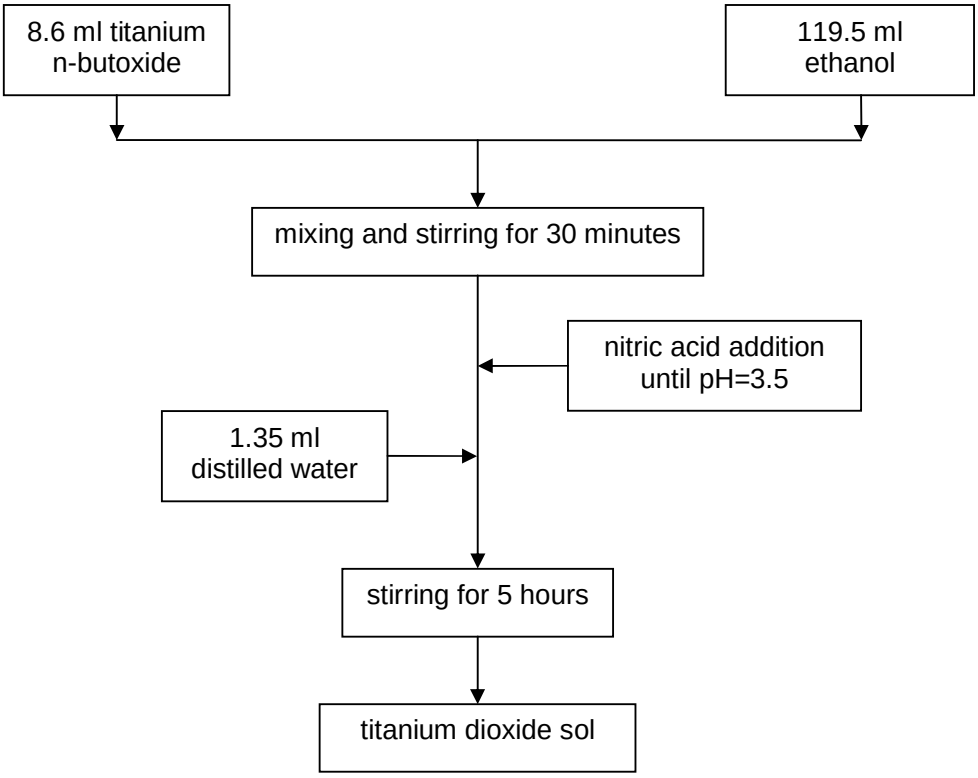

Figure 3.1 Flow chart for the preparation of titanium dioxide colloidal solution

3.2.3.2 Synthesis of Tin Oxide Colloidal Solutions

13.024 gr tin tetrachloride pentahydrate ($SnCl_4.5H_2O$) was dissolved in 192.4 ml ethanol. By using magnetic stirrer, the solution was stirred for 2 hours in the water bath at 70^{o}C. Temperature of the water bath was adjusted according to the boiling point of ethanol in order to prevent undesired vaporization of the solution. The hydrolysis reaction was carried out by adding 2.7 ml distilled water to the solution and stirring for 24 hours to achieve complete hydrolysis. The experimental procedure is illustrated schematically in Figure 3.2.

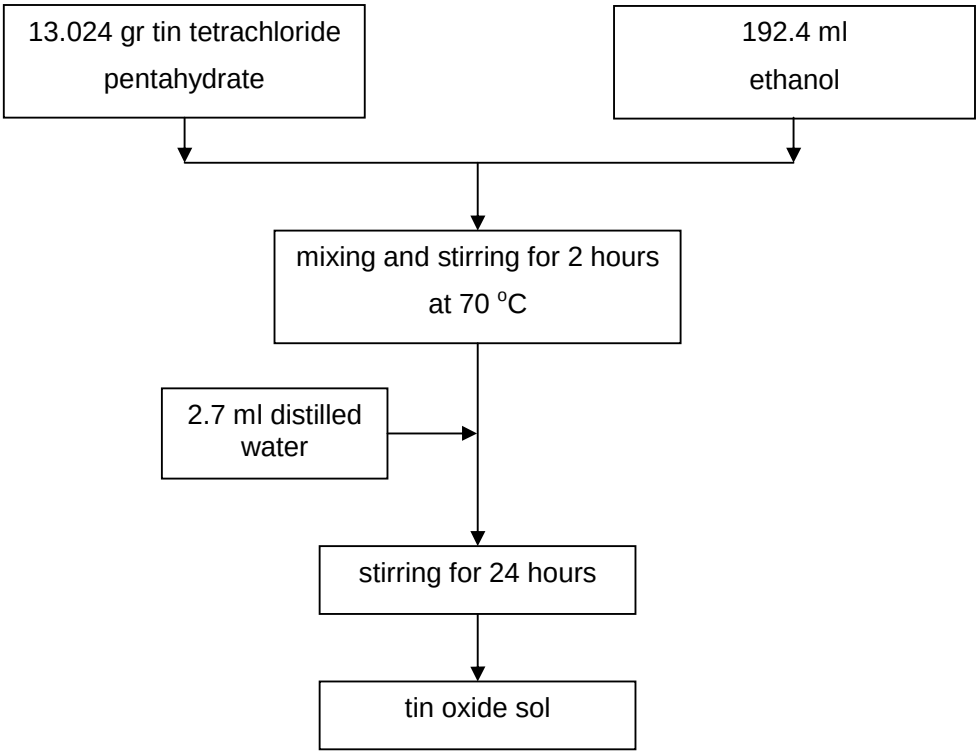

Figure 3.2 Flow chart for the preparation of tin oxide colloidal solution

3.2.3.3 Synthesis of Tin Oxide Doped Titanium Dioxide Colloidal Solutions

Binary mixed oxides of tin oxide and titanium dioxide with different compositions were prepared by using sol-gel technique. For this purpose, titanium dioxide and tin oxide colloidal solutions were prepared by following the procedures explained in sections 3.2.3.1 and 3.2.3.2, respectively. Then, different amounts of colloidal solutions were mixed in order to prepare binary mixed oxide colloidal solutions having different compositions. The compositions of the prepared colloidal solutions are shown in Table 3.1.

Table 3.1 Compositions of TiO_2 and SnO_2 binary mixtures

Volume of SnO_2	Volume of TiO_2	Composition of TiO_2-SnO_2
20 ml	80 ml	20 % SnO_2 + 80 % TiO_2
35 ml	65 ml	35 % SnO_2 + 65 % TiO_2
50 ml	50 ml	50 % SnO_2 + 50 % TiO_2
80 ml	20 ml	80 % SnO_2 + 20 % TiO_2

3.2.3.4 Synthesis of Metal Doped Titanium Dioxide and Tin Oxide Colloidal Solutions

Common metal catalysts were selected in order to improve surface properties and examine their effects on photocatalytic reactions. Praseodymium (Pr), palladium (Pd), silver (Ag) and iron (Fe) were selected as metal dopants. The metals and their precursors used are shown in Table 3.2.

Table 3.2 Metals and their precursors used for the preparation of metal doped colloidal solutions

Metal	Precursor	Amount of precursor used (gr)	
		for TiO_2	for SnO_2
Pr	$Pr(C_5H_7O_2)_3 \cdot xH_2O$	0.01998	0.07530
Pd	$(CH_3CO_2)_2Pd$	0.03659	0.13811
Ag	$AgNO_3$	0.01998	0.07530
Fe	$Fe(NO_3)_3.9H_2O$	0.01998	0.07530

The proper amounts of metal precursors, given in Table 3.2, were added during hydrolysis steps of the procedures described in sections 3.2.3.1 and 3.2.3.2 for the synthesis of TiO_2 and SnO_2 (See Appendix A for the sample calculations to determine the amount of metal doped). 1% (weight:weight) metal doped TiO_2 and SnO_2 colloidal solutions were obtained by the addition of corresponding amounts tabulated in Table 3.2.

3.2.4 Coating of Thin Films

After obtaining colloidal solutions, the pretreated soda-lime glass substrates were coated by using dip coating technique (Figure 3.3). For this purpose, glass substrates were immersed in the solution and withdrawn with a speed of 5 cm/min. The samples were dried in an oven for 20 minutes at 120^{o}C in order to complete single layer. To achieve desired film thickness and continuity, the samples were coated 5 subsequent layers.

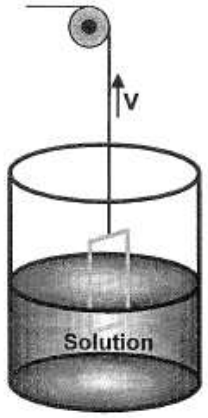

Figure 3.3 Experimental setup for dip coating

3.2.5 Heat Treatment of Thin Films

After the coating step, prepared thin films were calcined in a tube furnace under air flow. The aim of calcination is to achieve the complete removal of organic and inorganic precursor residuals and transform amorphous phase into crystalline phase.

In order to examine the effect of calcination temperature and duration on crystalline structure, the thin films coated with pure titanium dioxide and tin oxide colloidal solutions were treated under different calcination temperatures and durations. Two distinct temperatures were selected for this purpose corresponding to low temperature (250^{o}C) for the complete removal of residuals and high temperature (400^{o}C) to enhance crystallinity but lower temperature than the rutile formation temperature (500^{o}C-550^{o}C). Also, the effect of calcination duration was tested with 15, 30 and 45 minutes.

As explained in section 2.2.3, photocatalytic activity can be increased by increasing surface area, in other words, by obtaining meso porous structure. In literature, changing gelation-drying parameters was reported as a method for having meso porous structure. For that purpose, different gelation-drying periods

were applied to the coated thin films before calcination in order to see the change in surface morphology and photocatalytic activity.

For calcination, samples were inserted in a preheated tube furnace (Protherm 1000W, PTF 12/50/250) which had been adjusted to preset temperature with quartz cuvette.

3.3 Characterization of Thin Films

Thin films were analyzed by using different surface characterization techniques. Surface morphology, porosity, surface area, crystalline structure, photocatalytic activity were the analyzed properties. The surface tophology of the thin films were examined by SEM. For this purpose, the samples were coated with carbon and gold to achieve sufficient conductivity during analysis.

Hydrophilicity of the surface was examined by measuring contact angle of the surface with using CAM while surface area was measured by using Langmuir isotherms.

Absorption edge energy of the coated thin films were measured with UV-Visible Spectrophotometer by scanning the sample in the wavelengths between 190 nm and 800 nm with Thermo Electron Corporation, Nicolet Evolution 100.

Photocatalytic activity of the coated thin films were measured with the degradation of organic materials when subjected to artificial solar light irradiation and with antimicrobial activity tests as counting viable *E.coli* cells after irradiation.

3.3.1 Contact Angle Measurements

Contact angle measurements were performed for the characterization of the hydrophilicity of coated thin films relative to bare glass surface. Also, the effect of heat treatment parameters explained in section 3.2.5 and composition was

examined using contact angle (degree of surface free energy) measurements. Since contact angle strongly depends on surface hydroxyl groups and their concentrations, the coated thin film samples were conditioned at 23.5^{o}C and 65% humidity for 24 hours before measurements. Contact angles were measured by sessile drop method dropping UP (ultra pure) distilled water over the different positions of coated thin films.

3.3.2 Surface Area Measurements

BET (Brunauer Emmett Teller) method is one of the techniques that can be used for surface area measurements. On the other hand, due to the reasons that the amount of coated sol on the glass substrate was very low and the weight of the sample was the combination of glass substrate's and coated sol's weights; desired sensitivity could not be achieved with BET method.

Other method is using Langmuir isotherms for surface area measurements. Adsorption of methylene blue is the widely used method in literature [Adamson, 1982]. This method is based on the principle of measuring the differences between initial and equilibrium concentrations of methylene blue solution. In order to use Langmuir isotherms, it is assumed that methylene blue is adsorbed on the surface with kinetic and equilibrium relations appropriate to Langmuir theory (equation 3.1) [Gregg and Sing, 1982; Inel and Tumsek, 2000; Kipling, 1965]:

$$\frac{C_E}{X/m} = \frac{1}{k\,X_m} + \frac{C_E}{X_m} \qquad (3.1)$$

where

C_E : Equilibrium concentration of methylene blue remaining in the solution

X/m : Quantity of methylene blue adsorbed per unit weight of adsorbent

X_m : Adsorption capacity (solute monolayer capacity), Langmuir constant

k : Bonding energy constant, Langmuir Constant

When straight line is obtained by plotting $\frac{C_E}{X/m}$ versus C_E, it indicates a good fit to the Langmuir monolayer theory. The slope of this line is $1/X_m$ and the intercept is $1/kX_m$.

After accepting Langmuir monolayer theory for methylene blue adsorption, specific surface area (cm^2/cm^2) of the thin film is defined by [Inel and Tumsek, 2000]:

$$S = \frac{X_m A_{MB} L}{N} \tag{3.2}$$

where

X_m : Amount of methylene blue adsorbed at monolayer per gram of adsorbent, mol/cm^2

A_{MB} : Cross-sectional area of methylene blue adsorbed on the surface, cm^2

L : Avogadro's number, 1/mol

N : Coverage factor

For calibration, absorbances of methylene blue solutions having different concentrations varying from 0 ppm to 2 ppm were measured. With these measurements, the corresponding equilibrium concentration of methylene blue was related with absorbance.

In the experimental study, coated thin films having three different areas were immersed in 10 ml methylene blue solution with 2 ppm initial concentration. At constant temperature (5^oC) and in dark medium, they were waited for 72 hours in order to reach equilibrium. After reaching equilibrium, concentrations of methylene blue solutions were measured with UV-Visible Spectrophotometer and surface areas of coated thin films were measured.

3.3.3 Measurement of Photocatalytic Activity with Organic Materials

Photocatalytic activity was analyzed with the degradation of organic materials such as red wine and methylene blue. Qualitative measurement of photocatalytic activity is the visual control of dried spots of known amount of dyestuff over the substrate after specific time and quantitative measurement corresponds to the measurement of concentration change of organic material over the thin film sample with respect to time under controlled irradiation source. However, all experiments must be verified with blank tests under dark conditions and over the bare surface without any metal oxide thin film because of the possible non-catalytic photo assisted decay of organic dyestuff under irradiation. During qualitative measurements, 20 µl red wine (Kayra, Cumartesi) was dropped over the samples for the formation of spots and dried in dark cabinet, at room temperature. Dried spots of red wine were subjected to 300 W/m^2 artificial solar irradiation (Atlas CPS, Xe 1000 W) for 24 hours. Color change of the dried spots was measured qualitatively by comparing with the blank samples kept under dark.

Photocatalytic activity was measured quantitatively with the degradation of methylene blue. In order to have quantitative analysis, the thin films were immersed in the methylene blue solution being 240 mg/lt and waited for one hour to adsorb methylene blue. Then, they were allowed to dry for 2 hours. Before irradiation, absorbances of the thin films were measured and taken as the initial states of the samples. After this application, the films were subjected to 600 W/m^2 artificial solar irradiation and at 654 nm, absorbances were measured with UV-Visible Spectrophotometer after irradiating for 30 minutes.

Absorbance measured before irradiation was taken as 1 for initial concentration and absorbances measured after irradiation was converted to concentration as taking ratio of it with initial state. So, concentration change was analyzed during quantitative measurements.

3.3.4 Measurement of Photocatalytic Activity with Antimicrobial Activity Tests

Another technique used to analyze photocatalytic activity was antimicrobial activity test. For that purpose, *E. coli* was used in this study. The experiments were based on the measurement of the number of living colonies of microorganism with known initial number of colonies under constant irradiation. For verification of the results, the blank experiments were repeated under dark conditions and under irradiation with bare glass samples. In antimicrobial activity test; agar, peptone and LB (Luria-Bertani) broth were prepared for the measurement of the number of living colonies [Erkan, 2005; Erdural et al., 2008].

Preparation of agar: In order to prepare 750 ml agar; 7.5 gr tryptone, 3.75 gr yeast extract, 7.5 gr NaCl and 11.25 gr agar-agar hochrein were mixed. Distilled water was added to the mixture and the final volume was 750 ml. For 30 minutes, the mixture was stirred and heated to prevent hardening.

Preparation of peptone: 0.7 gr peptone was mixed with 700 ml water in order to prepare 700 ml peptone water with 0.1% concentration.

Preparation of LB broth: Although, it was enough to prepare 25 ml LB broth for culturing *E.coli*, 50 ml LB broth was prepared by taking the situation of any problem during culturing into consideration. In order to prepare 50 ml LB broth, 0.5 gr tryptone, 0.25 gr yeast extract and 0.5 gr NaCl were mixed. Distilled water was added to the mixture and the final volume was 50 ml.

Prepared solutions were sterilized in autoclave and agar solution was poured into plates where each plate had almost 20 ml agar solution. In incubator adjusted to 35^{o}C and 195 rpm, *E.coli* was cultured aerobically in 25 ml LB broth overnight (16 hours). For each of the coated thin films, one of the eppendorfs were filled with 2ml LB broth and centrifuged at 10.000 rpm for 5 minutes. After centrifuging, supernatant fluid left at the top was removed and, instead of it, 1 ml peptone water was added. The fluid obtained was poured on the coated thin films and they were subjected to artificial solar irradiation with solar light simulator lamp, Ultra-Vitalux light (Osram), for 1 hour. As a control group, coated thin films having the same properties were waited in dark conditions. After 1

hour, 1 ml fluid was taken from the coated thin film samples and added into the peptone water which was 9 ml in the test tubes. After mixing 10 ml mixture, 1 ml was taken and added to other peptone water, 10^7 dilution was achieved with this process. 200 µl mixture was taken from the sixth test tube and maintained on the agar plate. For control purposes, additional agar plate was prepared with maintaining 200 µl mixture and the coated thin film sample was put on another agar plate. The plates were incubated at 35^oC overnight. Antimicrobial activity was analyzed by counting viable *E.coli* cells.

CHAPTER 4

RESULTS AND DISCUSSION

4.1 Introduction

The thin films of titanium dioxide (TiO_2), tin oxide (SnO_2), binary mixtures (TiO_2-SnO_2) and their metal doped counterparts were synthesized and their surface properties and photocatalytic activities were characterized. Different sol-gel routes and formulations were applied in order to improve the chemical and physical surface properties. For this purpose, the thin film samples were examined by UV-Visible Spectrophotometer, SEM and CAM. The surface area measurements of thin film samples were carried out with methylene blue adsorption by using Langmuir isotherms. The photocatalytic activities of the samples were measured by the degradation of organic materilas and antimicrobial activity against *E.coli*.

Depending on their compositions, the thin films samples produced might be classified as follows:

- Thin films coated with titanium dioxide colloidal solutions
- Thin films coated with tin oxide colloidal solutions
- Thin films coated with tin oxide doped titanium dioxide colloidal solutions
- Thin films coated with metal doped titanium dioxide colloidal solutions
- Thin films coated with metal doped tin oxide colloidal solutions

During this study, in order to improve surface morphology and photocatalytic activity of the thin films, different parameters were applied as follows. Effect of the following parameters on surface structure and photocatalytic activity were examined with the characterization techniques explained above.

- Calcination temperature and duration
- Gelation-drying conditions
- Doping the colloidal solutions with different metals
- Composition of TiO_2-SnO_2 binary mixture

4.2 Effect of Calcination Temperature and Duration on Surface Morphology of Titanium Dioxide Coated Thin Films

Thin films coated with colloidal solutions synthesized by sol-gel method were subjected to different calcination temperatures and durations under air flow in order to see the effect of these parameters on crystalline structure and wetting properties of the surfaces. Calcination temperature is an important parameter that effects crystalline structure of the coated surfaces and determines transformation into anatase phase. The common consent in literature suggests that the anatase structure is the active phase for photocatalytic reactions [Hoffmann, 1995; Kato et al., 1994; Yu et al., 2000; Trapalis et al., 2003]. However, there are studies which report superior activity of rutile phase over anatase phase [Bickley et al., 1991; Yu et al., 2002]. As studied in literature, increasing calcination temperature causes transformation into rutile phase which results in decreased photocatalytic activity [Kim et al., 2002; Rivera, 1993; Deng et al., 2002; Diebold; 2003]. On the other hand, calcination temperature and duration are effective on crystallite size, surface free energy and short range and long range order of the thin films. It is expected that crystal defects and diorderness on the surfaces of the coated thin films will be reduced by increasing calcination temperature and duration because of restructuring and relaxation of the surface during calcination. Besides that, higher calcination temperature and longer calcination duration are important parameters effecting number of hydroxyl (-OH) groups over the surface. The hydroxyl (-OH) sites over the surface act as the hole (h^+) traps and affects the photocatalytic activity [Legrini et al., 1993; Hoffmann et al., 1995]. On the other hand, in case of inadequate calcination duration and low calcination temperature, crystallinity will be affected negatively. In order to investigate the effect of calcination temperature and duration on the hydrophilicity of the surface, thin films coated with titanium dioxide colloidal solution are calcined under low temperature regime (250^oC) for

removal of volatiles only and high temperature (400^{o}C) to increase crystallinity for 15, 30 and 45 minutes.

In order to compare the samples in terms of the surface concentration of hydroxyl (-OH) sites qualitatively, contact angle data of the surfaces are very useful. Before measurements, in order to have surfaces being at equilibrium with hydroxy ions at fixed conditions of temperature and moisture, coated thin films were conditioned at 23.5^{o}C and 65% humidity for 24 hours. Contact angle was measured by dropping UP (ultra pure) distilled water to different positions of coated thin films. The results of the coated thin films films calcined at 250^{o}C and 400^{o}C for three different calcination durations (15, 30 and 45 minutes) are presented in Table 4.1. The results are the averages of measurements at five different spots of the same sample surface from both right and left hand side images of droplet.

Table 4.1 Contact angle measurements of TiO_2 coated thin films calcined at 250^{o}C and 400^{o}C

Not calcined		250^{o}C 15 minutes		250^{o}C 30 minutes		250^{o}C 45 minutes	
Left	Right	Left	Right	Left	Right	Left	Right
81.95	81.45	63.16	64.33	62.50	63.18	63.96	63.64
Not calcined		400^{o}C 15 minutes		400^{o}C 30 minutes		400^{o}C 45 minutes	
Left	Right	Left	Right	Left	Right	Left	Right
81.95	81.45	56.26	57.24	52.96	54.43	54.33	54.24

As indicated above, calcination of the thin films at 250^{o}C causes only removal of volatiles and calcination does not take place at this temperature. On the other hand, calcination takes place at higher temperatures as 400^{o}C for this study. So,

surface structure changes with calcination at 400^{o}C resulting in increased crystallinity while at 250^{o}C, surface structure remains same without any change. From the results tabulated in Table 4.1, it is observed that contact angle decreased with increasing calcination temperature. Since surface becomes hydrophilic when contact angle decreases, surfaces calcined at 400^{o}C had hydrophilic surface properties.

As the mechanism of photocatalysis, electron and hole pairs (e^{-}/h^{+}) are formed with the excitation of electrons from valence band to conduction band having higher energy (equation 2.1). Active hydroxy and super oxygen derivatives are formed after the reaction between formed electron and hole pairs and water and oxygen molecules. With the reactions continuing, hydroxy radicals are formed as products of the reaction between holes and –OH ions present on the surface of titanium dioxide crystallites (equation 4.1); holes and water molecules physically absorbed on the surface (equation 4.2).

$$h^{+} + \text{-OH} \rightarrow \cdot OH_{Ads} \quad (4.1)$$

$$h^{+} + H_2O_{Ads} \rightarrow \cdot OH_{Ads} + H^{+} \quad (4.2)$$

Existence and amount of –OH ions on the surface affect the hydrophilicity of the surface. So, the darkness of the medium is important during contact angle measurements since light irradiation results in increased amount of –OH ions on the surface and hydrophilicity. For this purpose, coated thin films are kept in dark medium during contact angle measurements preventing any light irradiation. When kept in dark medium, contact angle of thin film coated with titanium dioxide (anatase phase) differs between 62^{o} and 68^{o} [Feng et al., 2005; Wu et al., 2006; Fujishima et al., 2000].

Calcination duration has limited effect on the photocatalytic activity of the surface for the coated thin films calcined at 250^{o}C. When average contact angle values are taken into consideration; contact angle is 81^{o} for the uncalcined thin films while it is approximately 63^{o} for the coated thin films calcined at 250^{o}C for 15,30 and 45 minutes. Calcination duration does not cause any change on the hydrophilicity of the surfaces. On the other hand, contact angle decreases considerably when the coated thin films are calcined at 400^{o}C and it becomes

57^{o} after 15 minutes of calcination. Similar with calcination at 250^{o}C, whatever the duration is, contact angle is almost the same for calcination at 400^{o}C. These results show that, calcination temperature has effect on surface energy while calcination duration does not cause any change on surface properties. By increasing calcination temperature, amount of –OH ions on the surface increases and, so, hydrophilicity increases.

Characterization with X-Ray diffractometer can not be possible in order to determine the crystalline properties of the coated thin films since the thicknesses of the coated thin films are not enough for XRD measurements. So, crystalline phases of the coated thin films calcined at two different temperatures and effect of calcination duration on anatase to rutile phase transformation are not known. On the other hand, effect of calcination temperature and duration on band gap might be useful to estimate photocatalytic activities of the coated thin films. The coated thin films calcined under different conditions were scanned between 190 nm and 800 nm by using UV-Visible Spectrophotometer relative to the uncoated glass slide. UV-Visible spectra of the coated thin films calcined at 250^{o}C and 400^{o}C are given in Figure 4.1 and Figure 4.2, respectively. As seen from Figure 4.1, at 250^{o}C calcination is slow and band gap changes significantly between 350 nm and 400 nm. On the other hand, at 400^{o}C, band gap change is less than the change observed for calcination at 250^{o}C since calcination is almost completed after 15 minutes. As given in Figure 4.1 and 4.2, band gaps of the coated thin films are around 360 nm (3.45 eV) which indicates that there is 0.25 eV red shift compared with the literature value which is 3.2 eV [Popielarski, 1998]. The band gap measurements reveal that both calcination temperature and calcination duration were sufficient for the formation of short range semiconductor structure and the band gap corresponding to edge energy (360 nm) is in agreement with literature. However, the difference in surface free energy especially at high temperature (400^{o}C) indicates the crystal relaxation and the change in long range order of the thin films.

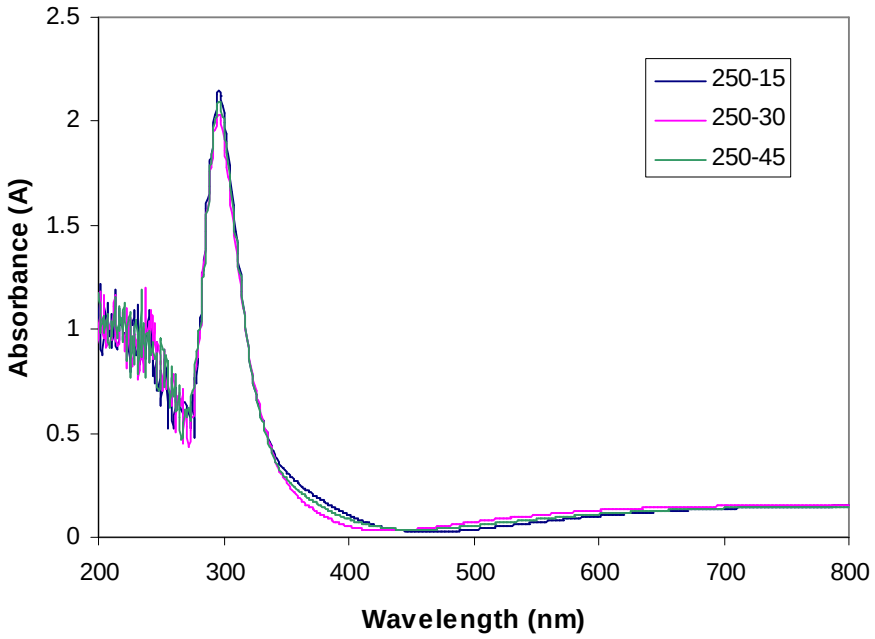

Figure 4.1 UV-Visible spectra of the coated thin films calcined at 250^{o}C for 15, 30 and 45 minutes

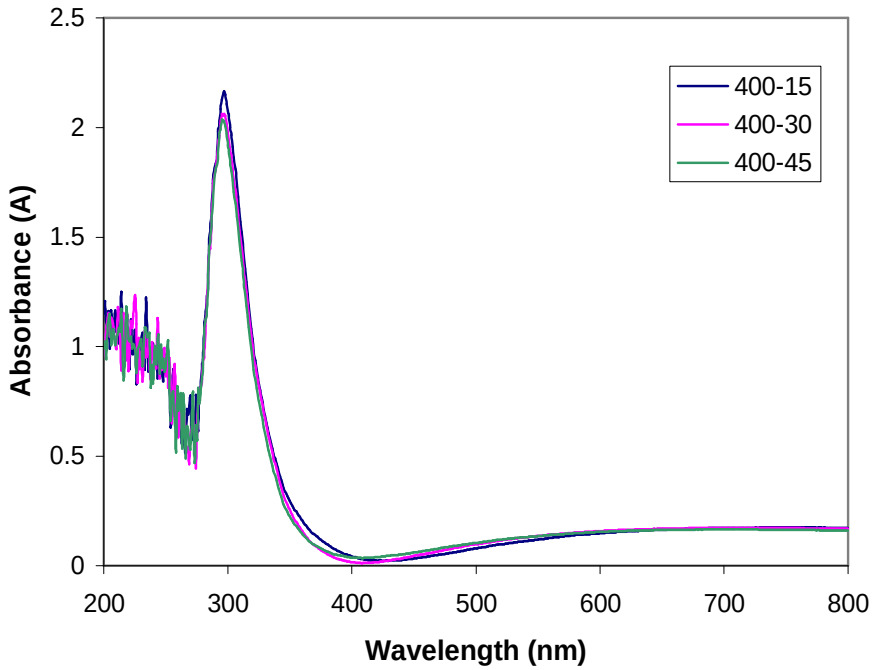

Figure 4.2 UV-Visible spectra of the coated thin films calcined at 400^{o}C for 15, 30 and 45 minutes

4.2.1 Photocatalytic Activity Measurements with Organic Materials

Photocatalytic activities of the coated thin films were characterized by using organic materials. For the coated thin films calcined at 250^{o}C and 400^{o}C for 15, 30 and 45 minutes; photocatalytic activity was measured qualitatively. As an organic material, both red wine and methylene blue were used.

As explained in section 3.3.3, 20 µl red wine was applied over the coated thin film surface and dried in dark cabinet. They were subjected to 300 W/m^2 artificial solar irradiation for 24 hours. Color change of the irradiated samples were followed visually by comparing blank stain which was kept in dark. The scanned images of the samples subjected to 300 W/m^2 artificial solar irradiation for 24 hours, are given in Figure 4.3.

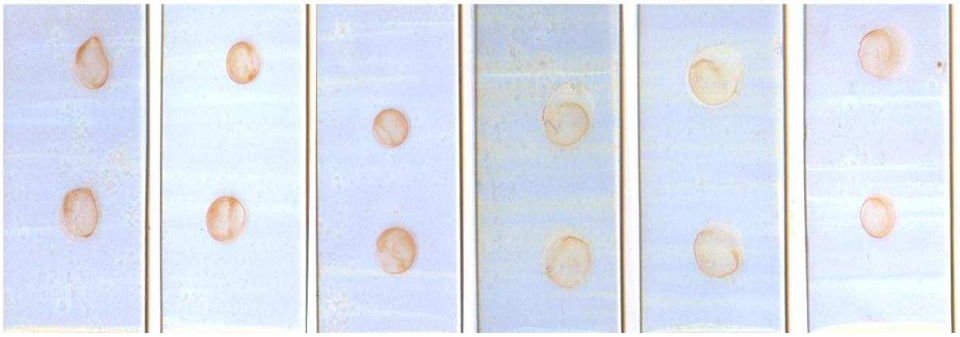

(a) (b) (c) (d) (e) (f)

Figure 4.3 Photocatalytic activity of titanium dioxide coated thin films irradiated for 24 hours calcined at:(a) 250^{o}C for 15 minutes, (b) 250^{o}C for 30 minutes, (c) 250^{o}C for 45 minutes, (d) 400^{o}C for 15 minutes, (e) 400^{o}C for 30 minutes, (f) 400^{o}C for 45 minutes.

As seen from Figure 4.3, the coated thin films calcined at 400^{o}C have better but limited photocatalytic activity than that of the coated thin films calcined at 250^{o}C. For both of the calcination temperatures, calcination duration does not have any effect on photocatalytic activity.

According to these qualitative results, titanium dioxide coated thin films have limited photocatalytic activity which is independent from calcination conditions. As indicated in section 2.2.3, photocatalytic activity could be increased by having micro or meso porous semiconductors having larger surface area. On the other hand, from SEM micrograph of titanium dioxide coated thin film calcined at 400^{o}C for 15 minutes given in Figure 4.4, it is observed that titanium dioxide coated thin films have non porous and dense surface structures. Due to the restructuring and relaxation during thermal treatment of the film, micro cracks appear on the surface of the coated thin film.

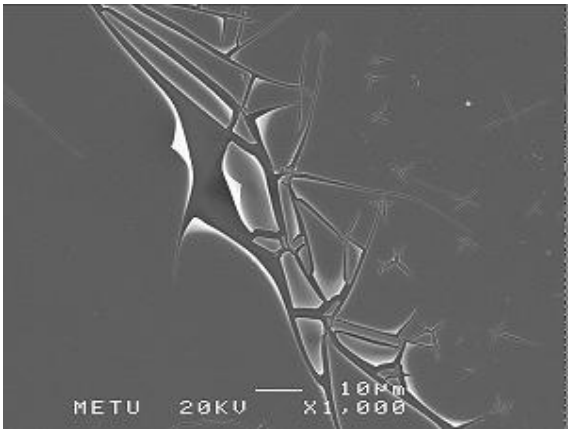

Figure 4.4 SEM micrograph of nonporous and dense titanium dioxide coated thin film, x1,000 magnification

After dip coating process, because of slow drying period during gelation, titanium dioxide coated thin films are dense and they have limited surface area as seen in Figure 4.4. The sol-gel formulations have water and solvent constitutes which evaporates during drying step. As a result of gelation, the evaporation step is mass transfer controlled and it is a slow step at room temperature. Therefore, drying conditions of the coated thin films have to be selected very carefully in order to achieve sufficient porosity and surface area. Thin films having sufficient photocatalytic activity should have larger surface area by having meso porous structure. In order to have meso porous structure, there are several methods in literature as:

- Changing gelation-drying parameters (drying rate of organic residuals)
- Addition of polymeric materials that can be removed from the thin film during calcination (PEG, PVA, etc.)
- Addition of oxides, like silica, to the colloidal solution that can form porous structure

On the other hand, it should be noted that, while preparing thin films having larger surface area, physical properties of the coated thin films like transparency and adhesion strength should not be affected negatively. By considering three

different methods given above, changing gelation-drying conditions is more reasonable choice because of simplicity and purity.

4.3 Effect of Gelation-Drying Conditions on Surface Morphology of Titanium Dioxide Coated Thin Films

While studying the effect of gelation-drying on surface morphology and photocatalytic activity, the glass substrates coated with titanium dioxide colloidal solution were stored at room temperature for 1, 2, 3 and 4 weeks to test prior to the calcination. As a control group, the coated thin films were calcined on the same day after coating. The contact angle measurements are given in Table 4.2

Table 4.2 Effect of gelation-drying period on contact angle measurements of TiO_2 coated thin films calcined at 250^{o}C and 400^{o}C for 15 minutes

Calcined at 250^{o}C after coating		Calcined at 250^{o}C after 1 week		Calcined at 250^{o}C after 2 weeks		Calcined at 250^{o}C after 3 weeks		Calcined at 250^{o}C after 4 weeks	
Left	Right	Left	Right	Left	Right	Left	Right	Left	Right
64.79	64.37	63.63	64.03	66.19	67.08	60.92	60.53	68.68	70.06
Calcined at 400^{o}C after coating		**Calcined at 400^{o}C after 1 week**		**Calcined at 400^{o}C after 2 weeks**		**Calcined at 400^{o}C after 3 weeks**		**Calcined at 400^{o}C after 4 weeks**	
Left	Right	Left	Right	Left	Right	Left	Right	Left	Right
47.30	48.30	40.11	39.98	34.48	33.34	25.46	26.13	19.89	20.52

When the measurements given in Table 4.2 for the samples calcined at 250^{o}C and 400^{o}C are compared, gelation-drying rate does not have any significant

effect on the surface energies of the coated thin films calcined at 250^{o}C. On the other hand, contact angle or surface free energy altered significantly with respect to the duration of gelation-drying period if the thin films are calcined at 400^{o}C. In other words, very hydrophilic surfaces were obtained by increasing the duration of the period and the contact angle can be decreased to 20^{o} for the coated thin films calcined after drying samples for four weeks.

Measurements tabulated in Table 4.2 are summarized in Figure 4.5. As shown in Figure 4.5, hydrophilicity of the surface does not change significantly with the duration of gelation-drying period if the calcination temperature is at lower range, 250^{o}C. On the other hand, for the coated thin films calcined at 400^{o}C, hydrophilicity is considerably enhanced with drying period and longer period results in more hydrophilic surfaces. More hydrophilic surface structure resembles the more porous or more disordered structure with higher surface concentration of hydroxyl (-OH) ions. After calcination at 400^{o}C at the end of 4 weeks of drying period, contact angle is measured as 20^{o} while it is 48^{o} for the coated thin films calcined after coating.

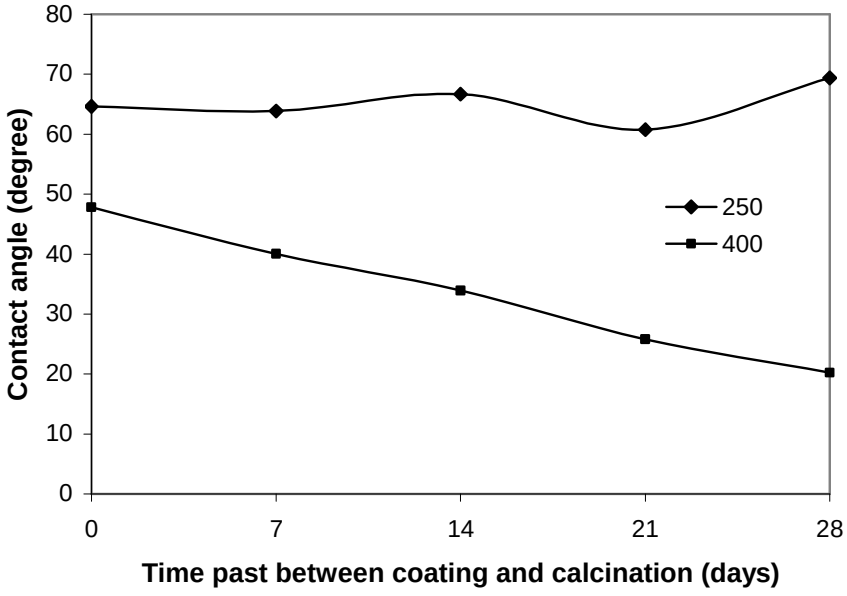

Figure 4.5 Change of contact angle with time past between coating and calcination

The effect of gelation-drying rate on band gap was also analyzed by using UV-Visible Spectrophotometer. UV-Visible spectra of the coated thin films calcined at 250^{o}C and 400^{o}C are given in Figure 4.6 and Figure 4.7, respectively. As seen from the figures, differences occur for the band gap where anatase phase of titanium dioxide occurs which has band gap around 360 nm, in literature [Popielarski, 1998]. Band gap decreases with increasing the duration of gelation-drying period. UV-Vis spectra of the coated thin films calcined at 250^{o}C and 400^{o}C are given in Figure 4.8 for the wavelengths between 300 nm and 400 nm. As seen from the Figure 4.8 (a) and Figure 4.8 (b), when drying time is increased to 4 weeks, band gap decreases to 330 nm.

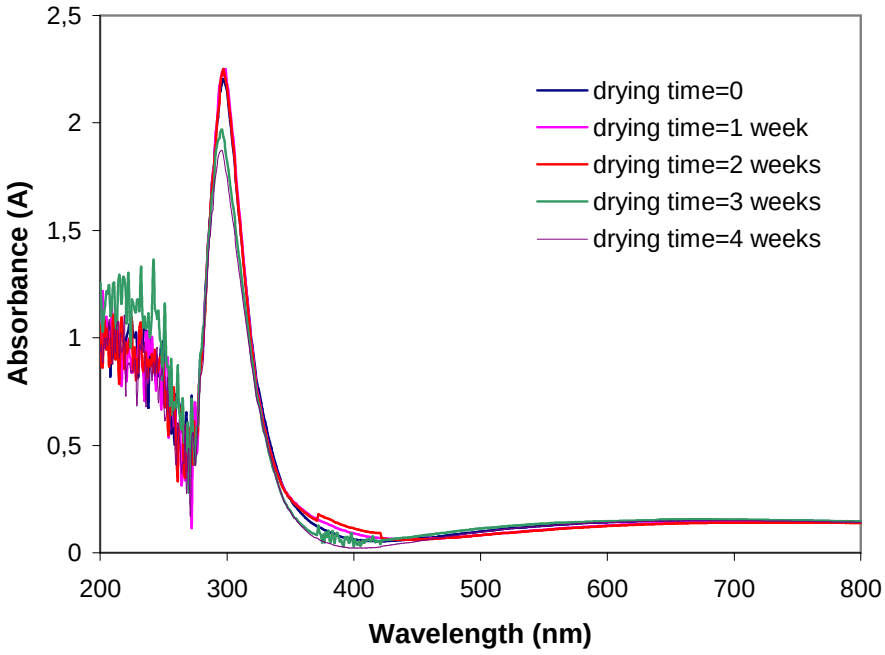

Figure 4.6 Effect of gelation-drying period on UV-Visible spectra of the coated thin films calcined at 250^{o}C for 15 minutes

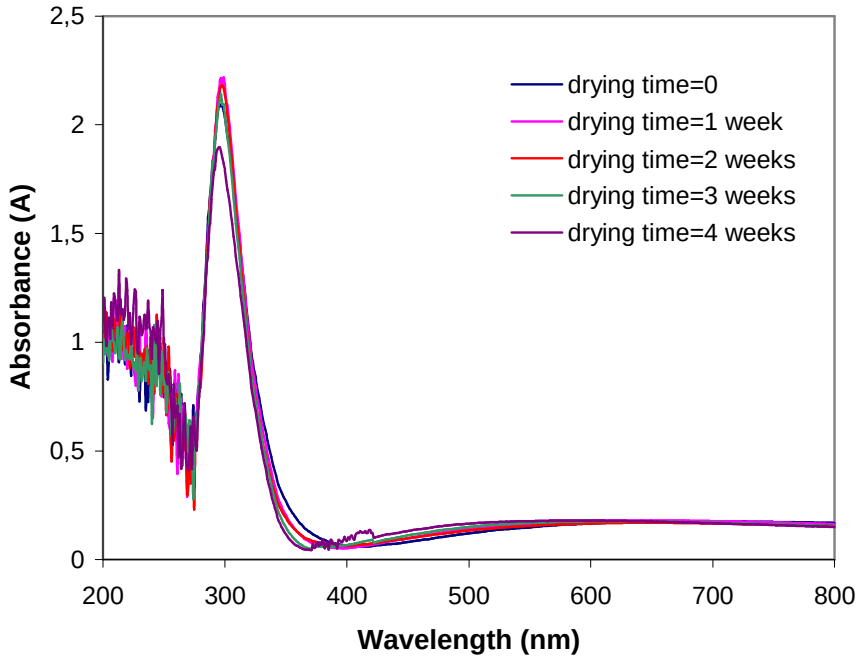

Figure 4.7 Effect of gelation-drying period on UV-Visible spectra of the coated thin films calcined at 400^{o}C for 15 minutes

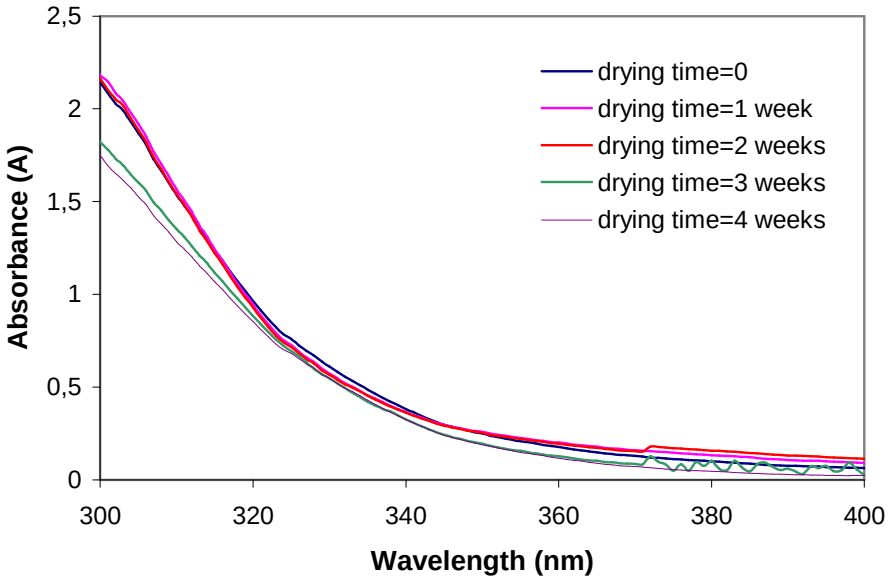

(a)

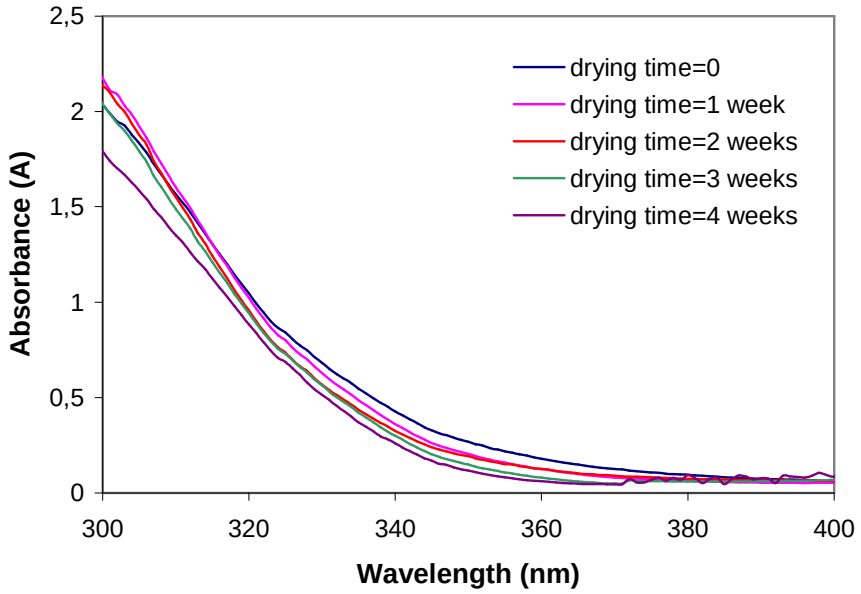

(b)

Figure 4.8 UV-Visible spectra between 300 nm and 400 nm for the coated thin films calcined at (a): 250^{o}C and (b): 400^{o}C for 15 minutes

UV-Visible spectrum for two different calcination temperatures are given in order to show the effect of calcination temperature on the band gap of the coated thin films that were calcined after being dried for 1 week. As shown in Figure 4.9, high calcination temperature and duration of gelation-drying period have similar effect on the band gap. In other words, band gap decreases with increasing calcination temperature.

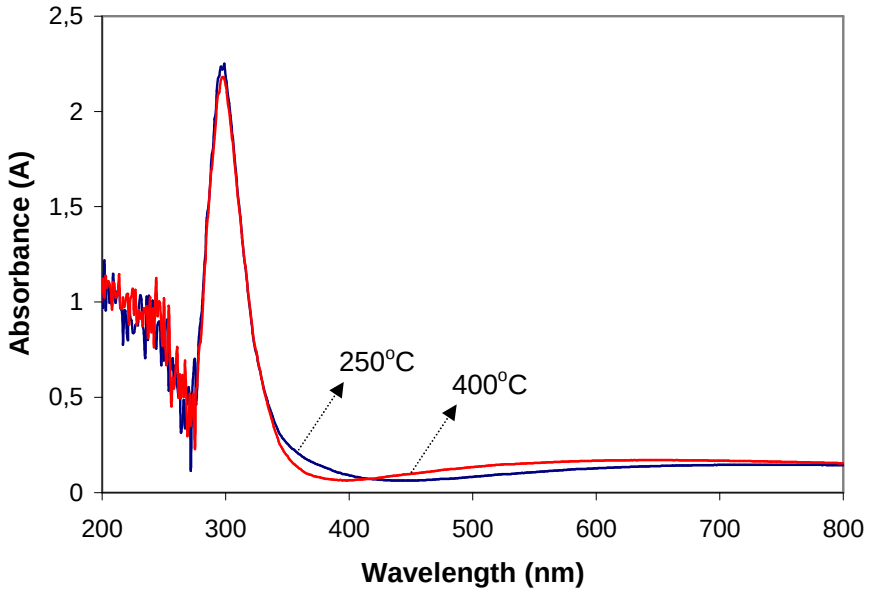

Figure 4.9 UV-Visible spectra of TiO_2 coated thin films calcined at 250°C and 400°C for 15 minutes after being dried for 1 week

4.3.1 Photocatalytic Activity Measurements with Organic Materials

Effect of gelation-drying period before calcination on photocatalytic activities of the coated thin films were also characterized by using the degradation tests for red wine stain as mentioned in previous section. Following the same procedure explained in section 3.3.3, the sample surface was stained by 20 µl red wine and after drying in dark medium, they were subjected to 300 W/m^2 artificial solar irradiation for 24 hours. For better comparison, another sample was tested in dark cabinet as blank experiment. The scanned images of the samples subjected to 300 W/m^2 artificial solar irradiation and kept in dark medium for 24 hours are presented in Figure 4.10, Figure 4.11, Figure 4.12, Figure 4.13 and Figure 4.14 according to the duration of gelation-drying period as calcination after coating, drying for 1 week, drying for 2 weeks, drying for 3 weeks and drying for 4 weeks, respectively.

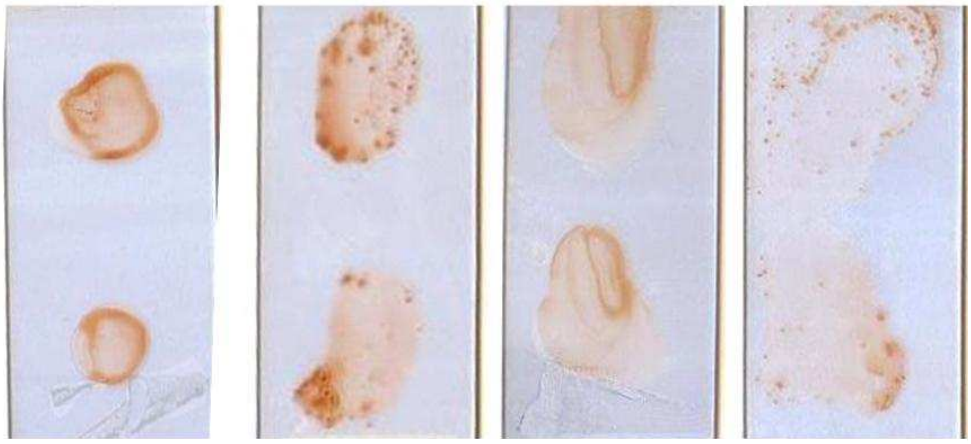

(a) (b) (c) (d)

Figure 4.10 Photocatalytic activity of TiO_2 coated thin films: calcined at 250^{o}C for 15 minutes after coating (a) irradiated, (b) kept in dark; calcined at 400^{o}C for 15 minutes after coating (c) irradiated, (d) kept in dark for 24 hours

(a) (b) (c) (d)

Figure 4.11 Photocatalytic activity of TiO_2 coated thin films: calcined at 250^{o}C for 15 minutes after drying for 1 week (a) irradiated, (b) kept in dark; calcined at 400^{o}C for 15 minutes after drying for 1 week (c) irradiated, (d) kept in dark for 24 hours

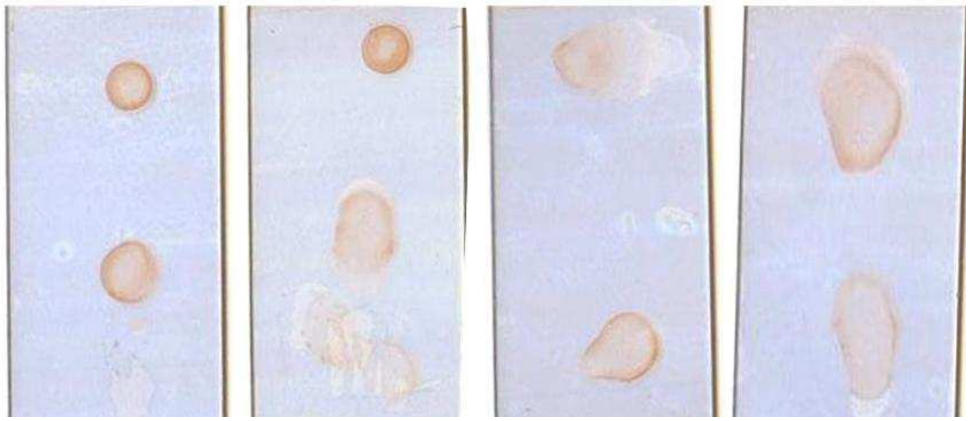

(a) (b) (c) (d)

Figure 4.12 Photocatalytic activity of TiO_2 coated thin films: calcined at 250^{o}C for 15 minutes after drying for 2 weeks (a) irradiated, (b) kept in dark; calcined at 400^{o}C for 15 minutes after drying for 2 weeks (c) irradiated, (d) kept in dark for 24 hours

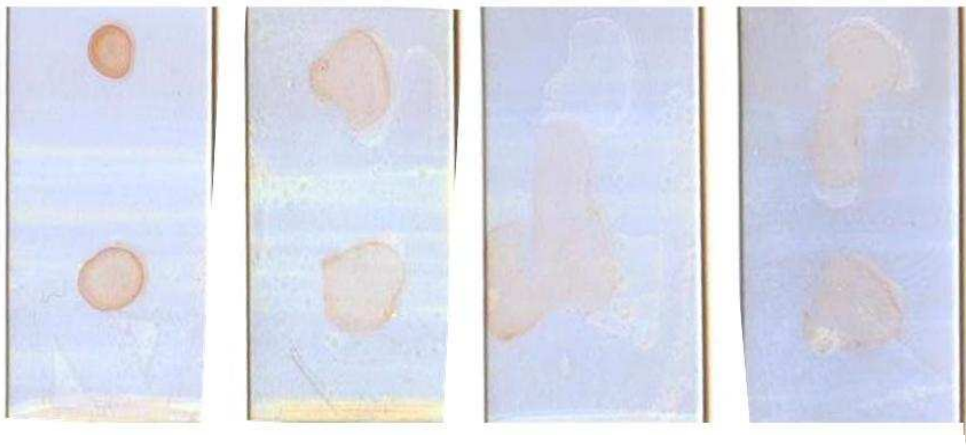

(a) (b) (c) (d)

Figure 4.13 Photocatalytic activity of TiO_2 coated thin films: calcined at 250^{o}C for 15 minutes after drying for 3 weeks (a) irradiated, (b) kept in dark; calcined at 400^{o}C for 15 minutes after drying for 3 weeks (c) irradiated, (d) kept in dark for 24 hours

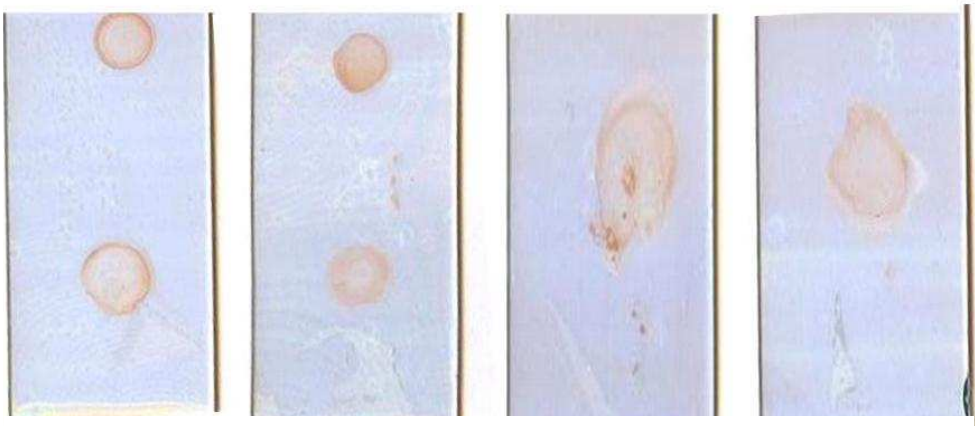

(a) (b) (c) (d)

Figure 4.14 Photocatalytic activity of TiO_2 coated thin films: calcined at 250^oC for 15 minutes after drying for 4 weeks (a) irradiated, (b) kept in dark; calcined at 400^oC for 15 minutes after drying for 4 weeks (c) irradiated, (d) kept in dark for 24 hours

As seen from the figures given above, better photocatalytic activities were observed on the samples calcined at 400^oC than the samples calcined at 250^oC. Furthermore, wine spots dispersed to a larger surface area as a result of more hydrophilic structure of the samples calcined at 400^oC.

The coated thin films calcined at 400^oC and kept in dark medium had photocatalytic activities resulting in the degradation of organic material. This activity is caused by the hydrophilic surface properties as an oxidation between protons and hydroxy radicals on the surface without any existence of photon (equation 4.3 and equation 4.4). On the other hand, activity in dark medium can not be sustained for a long time because of the limited amount of hydroxyl species over the surface. By irradiating the surface, reaction given in equation 4.3 replenishes the surface species. Besides that, there is a parallel reaction mechanism where oxidation takes place between atmospheric oxygen and hydrogen peroxide.

$$-OH + H^+ \rightarrow .OH_{ads} \qquad (4.3)$$

$$.OH_{ads} + .OH_{ads} \rightarrow H_2O_2 \quad (4.4)$$

As observed from Figure 4.10, Figure 4.11, Figure 4.12, Figure 4.13 and Figure 4.14, photocatalytic activity of the coated thin films calcined at 250^{o}C, was very limited and no dependency on gelation-drying time was observed.

4.3.2 Photocatalytic Activity Measurements with Antimicrobial Activity Tests

Another method used in order to characterize photocatalytic activity was the characterization of antimicrobial property. For this purpose, *E.coli* culture was employed. The experiments were based on the quantitative results of viable *E.coli* cells count with respect to irradiation time based on the initial amount of *E.coli* culture applied to the surface of samples. Since better activity was observed with wine spot degradation tests, the antimicrobial activity of the films calcined at 400^{o}C for 15 minutes were measured.

During the antimicrobial activity tests, solution containing *E.coli* cell was spread over the surfaces of the samples which were pretreated glass substrates as blank and titanium dioxide coated thin films calcined after different gelation-drying periods (calcination after coating, drying for 1 week, drying for 2 weeks, drying for 3 weeks and drying for 4 weeks). The samples were subjected to artificial solar irradiation with solar light simulator lamp for 1 hour. For control experiments, same samples were prepared and kept in dark medium. After 1 hour, viable *E.coli* cells were counted by following the procedure given in section 3.3.4. Results of viable *E.coli* cell counting are tabulated in Table 4.3 for the pretreated glass substrates as blank and titanium dioxide coated thin films calcined after different gelation-drying periods irradiated and kept in dark medium.

Table 4.3 Number of viable *E.coli* cells for the pretreated glass subtrates and titanium dioxide coated thin films irradiated and kept in dark medium for 1 hour

Pretreated glass substrate	Under irradiation	351	Calcined after drying for 2 weeks	Under irradiation	253
	In dark	552		In dark	469
Calcined after coating	Under irradiation	267	Calcined after drying for 3 weeks	Under irradiation	262
	In dark	460		In dark	487
Calcined after drying for 1 week	Under irradiation	289	Calcined after drying for 4 weeks	Under irradiation	273
	In dark	495		In dark	479

When the results tabulated in Table 4.3 are compared, the number of viable *E.coli* cells on the coated thin films show 15% decrease with respect to the number of viable *E.coli* cells on the pretreated glass substrates. Furthermore, when the samples irradiated and kept in dark medium are compared, for the irradiated samples, 40% decrease in the number of viable *E.coli* cells is achieved. On the other hand, duration of gelation-drying period does not have significant effect on the antimicrobial activity. These results are in good agreement with the results of wine spot tests. Similar to the results of degradation tests, photocatalytic activity was observed for the samples waited in dark medium since reactive oxygen species can be formed without the existence of light source (photon) and these reactive oxygen species damages *E.coli* cells.

4.4 Metal - Titanium Dioxide Coated Thin Films

Doping the colloidal solutions with metals having catalytic properties is a common method to improve the photocatalytic activities of metal oxide semiconductors [Sharma et al., 2006; Erkan, 2006; Luca et al., 2006; Chang et al., 2008; Sawunyama et al., 1998]. 50% increase in photocatalytic activity was achieved with palladium doped titanium dioxide coated thin films [Erkan, 2006]. In this study, effect of metals like palladium (Pd), silver (Ag), iron (Fe) and praseodymium (Pr) on the photocatalytic activity of sol-gel synthesized TiO_2 was also examined.

From the metals listed above, praseodymium is known with its fluorescent properties in literature [Yan et al., 2006; Jouini et al., 2003]. This property is caused by the behaviour of light in nonlinear media which can be described with non-linear optics and fluorescence of praseodymium results in the formation of photons at the end of serial reactions which are started with the stimulation of orbital having different energy levels by photons. There are two possible ways as down conversion and up conversion which are thermodynamically possible Down conversion is leaving two photons having low energy free with the absorption of photon having high energy while up conversion is the formation of photon having high energy with the absorption of two photons having low energy. When the band gaps of titanium dioxide and tin oxide are compared, band gap energy of titanium dioxide is 3.2 eV (388 nm) and it can be stimulated by photons having wavelength closer to visible region while tin oxide's band gap energy is 3.6 eV (345 nm) and it can be stimulated with photons having higher energy in UV region. Up-conversion is a promising way to utilize solar energy with wide band gap metal oxides as a result of harvesting more photons from visible region. In literature, there are limited studies about the optical properties of metal doped semiconductors and effect of praseodymium on up conversion is newly started to be studied [Sun et al., 2006; Amlouk et al., 2008; Sua et al., 2008].

Other metals (Ag, Fe and Pd) used in this study are well known catalytic metals with their unique oxygen transfer properties [Schmidt et al., 2003; Erkan, 2006].

In this study, glass substrates were coated with metal doped titanium dioxide (1%metal/TiO_2) colloidal solutions which were prepared according to the procedure explained in section 3.2.3.4. Metal precursors were dissolved in ethanol and, then colloidal solution was prepared. After coating process, the coated thin films were calcined at 500^oC for 15 minutes.

Contact angle of the surfaces were measured after conditioning the coated thin films at the same conditions as 23.5^oC and 65% humidity for 24 hours before the measurements. Contact angle measurements for the thin films coated with pure titanium dioxide and metal doped titanium dioxide are tabulated in Table 4.4.

Table 4.4 Contact angle measurements of pure titanium dioxide and metal doped titanium dioxide coated thin films calcined at 500^oC for 15 minutes

Pure TiO_2		1%Pd/TiO_2		1%Pr/TiO_2		1%Ag/TiO_2		1%Fe/TiO_2	
Left	Right	Left	Right	Left	Right	Left	Right	Left	Right
64.19	64.23	29.05	29.10	24.64	25.28	10.23	10.30	21.53	20.75

When the results in Table 4.4 are compared, metal doping has an improving effect on the hydrophilicity of the coated thin films. Especially, the sample doped with Ag performs super-hydrophilic structure.

Band gaps of the thin films coated with metal doped titanium dioxide colloidal solutions are given in Figure 4.15. As observed from the UV-Visible spectra, metal doped titanium dioxide has band gap between 300 nm and 350 nm. Almost in all metal doped samples, the band gap shift to the visible region were observed.

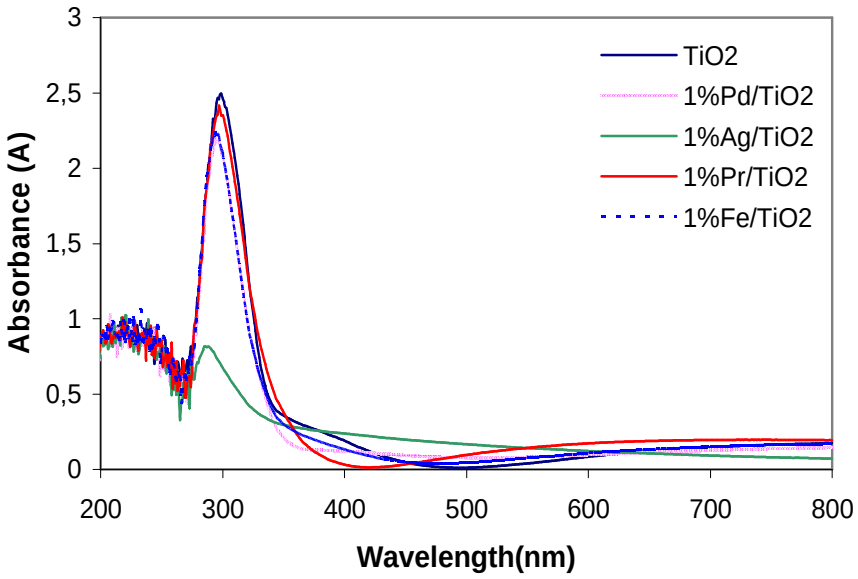

Figure 4.15 UV-Visible spectra of metal doped titanium dioxide coated thin films calcined at 500^{o}C for 15 minutes

Optical properties of the metal doped titanium dioxide coated thin films show differences when compared with the films coated with pure titanium dioxide colloidal solution. For instance, silver doped samples have gray tint while palladium doped samples have brown tint. As seen from the UV-Visible spectra given in Figure 4.15, light transmittance decreases for the silver doped samples. For all samples, the effect of surface plasmons appears in the region 500 nm-800 nm and no isolated metal particles are detected in 500 nm-600 nm range which indicated ionic dispersion of metal sites in TiO_2 matrix. Band gap is largest for praseodymium doped TiO_2 coated thin films and red shift occurs for the band gap. This shows the success of doping process for improving photocatalytic activity and it was observed that, after irradiating for 24 hours with 600 W/m^2 artificial solar irradiation, concentration of methylene blue became zero for praseodymium doped samples.

4.4.1 Photocatalytic Activity Measurements with Organic Materials

Photocatalytic activities of the coated thin films were measured quantitatively by following the procedure explained in section 3.3.3. The coated thin films were immersed into methylene blue solution having 240 mg/lt concentration and they were waited in this solution for 1 hour. Then, the coated thin films were allowed to dry for 2 hours and the absorbance was measured before irradiation in order to define the initial concentration C_0. After measuring initial absorbance values, they were subjected to 600 W/m^2 artificial solar irradiation for 30 minutes of time intervals. On the other hand, it was waited for 90 minutes after each solar light irradiation in order to prevent formation of leuco form and reconvert reduced methylene blue of the leuco form (LMB) into its initial state [Miyauchi et al, 2002]. By waiting in dark medium for 90 minutes, absorbance value changes would show only the concentration of methylene blue as a result of the decomposition from the oxidation reaction [Mills and Wang, 1999]. After waiting, photocatalytic activity was examined quantitatively by measuring the absorbance values at 654 nm wavelength.

Concentration change of methylene blue solution is shown in Figure 4.16 (Data of concentration change is given in Appendix B). C_0 is the initial concentration corresponding to the measured absorbance value before irradiation. As observed in Figure 4.16, effect of palladium on photocatalytic activity is very high. On the other hand, iron doping has declining effect on photocatalytic activity. The reason for this situation can be deformation of crystalline structure of titanium dioxide by Fe^{+2} ions [Sawunyama et al., 1998]. As a result of the photocatalytic activity measurements, highest activity is achieved with palladium and silver is in the second rank for increasing photocatalytic activity. Even if it was not shown in Figure 4.16, concentration of methylene blue was zero for 1%Pr/TiO_2 coated samples after being subjected to 600 W/m^2 artificial solar irradiation for 24 hours.

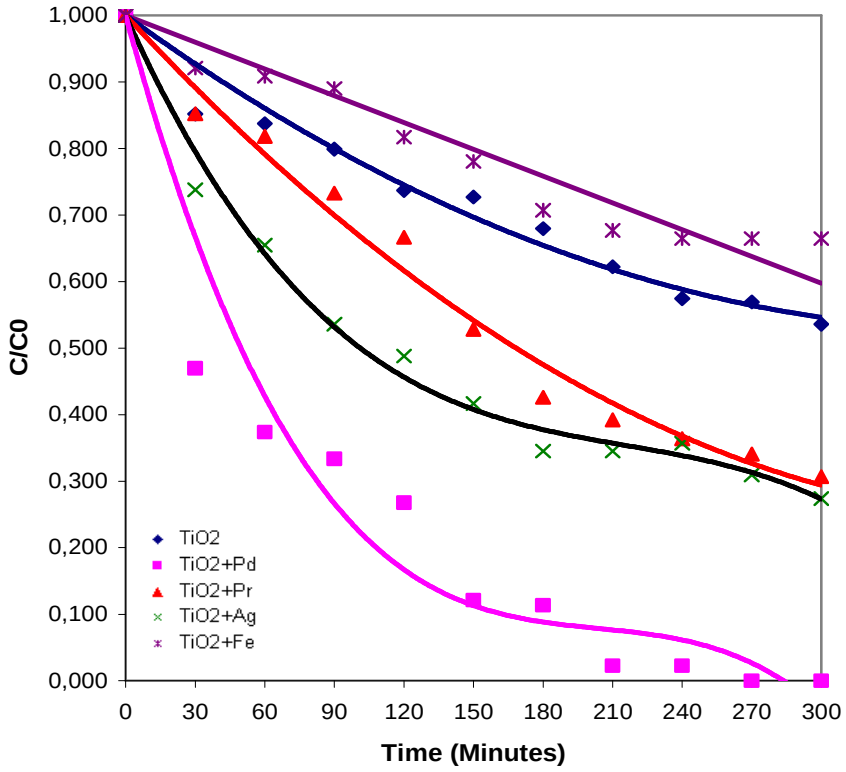

Figure 4.16 Concentration change of methylene blue solution for the metal doped titanium dioxide coated thin films subjected to 600 W/m^2 artificial solar irradiation

4.4.2 SEM Analysis

Surface iamges of the coated thin films were characterized by SEM. At this stage, titanium dioxide and metal doped titanium dioxide coated thin films were coated with carbon and gold in order to achieve sufficient conductivity for characterization. SEM micrographs of surfaces of the coated thin films are given in Figure 4.17. As seen from the micrographs, nonporous and dense titanium dioxide film structure was obtained.

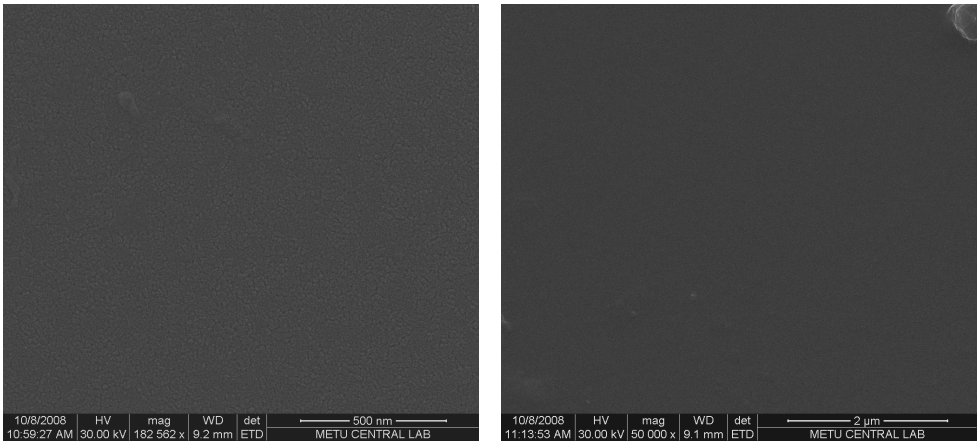

(a) (b)

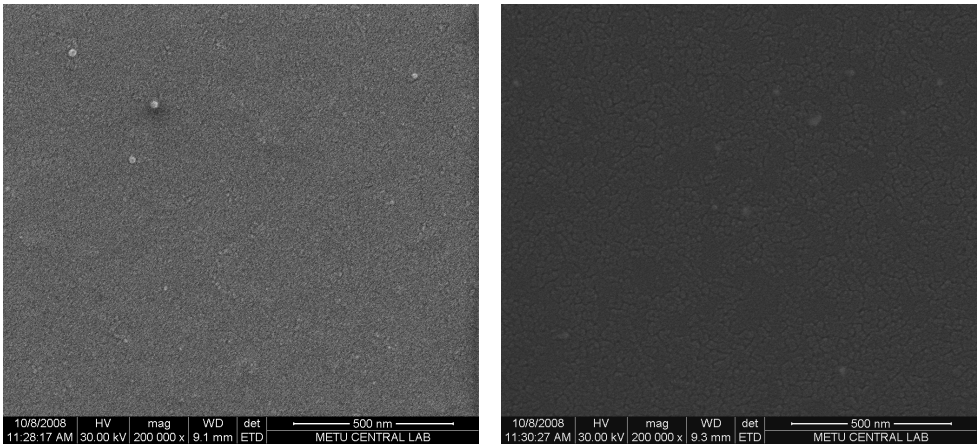

(c) (d)

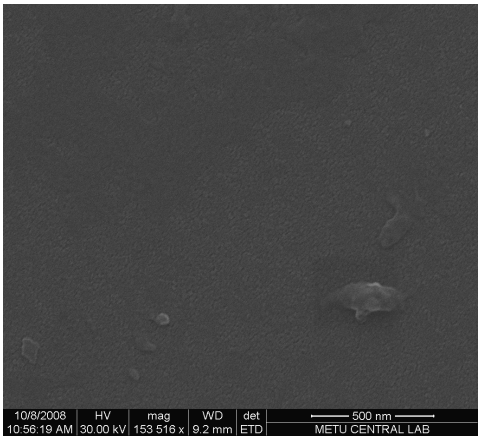

(e)

Figure 4.17 SEM micrographs of surfaces coated with; (a): TiO_2, (b): 1%Pd/TiO_2, (c): 1%Ag/TiO_2, (d): 1%Pr/TiO_2, (e): 1%Fe/TiO_2

4.5 Metal - Tin Oxide Coated Thin Films

Tin oxide is an n-type semiconductor having wide band gap with a band gap energy around 3.6 eV corresponding to 345 nm [Benedix et al., 2000; Batzill et al., 2005]. So it is the most widely used metal oxide after titanium dioxide.

In this study, glass substrates were coated with metal doped tin oxide colloidal solutions which were prepared according to the procedure explained in section 3.2.3.4. Metal precursors were dissolved in ethanol and, then colloidal solution was prepared. After coating process, the coated thin films were calcined at 500^{o}C for 15 minutes.

Contact angle measurements for the thin films coated with pure tin oxide and metal doped tin oxide colloidal solutions are given in Table 4.5

Table 4.5 Contact angle measurements of pure tin oxide and metal doped tin oxide coated thin films calcined at 500^{o}C for 15 minutes

Pure SnO_2		1%Pd/SnO_2		1%Pr/SnO_2		1%Ag/SnO_2		1%Fe/SnO_2	
Left	Right	Left	Right	Left	Right	Left	Right	Left	Right
17.17	17.22	7.65	7.42	7.92	7.37	7.73	7.48	13.04	12.71

When the results in Table 4.5 are compared, metal doping has an improving effect on the hydrophilicity of the coated thin films. Contact angle of the coated thin film decreases down to 7^{o} for metal doped tin oxide coated surfaces. More hydrophilic surfaces were obtained with metal doped SnO_2 coated surfaces compared to metal doped TiO_2 coated surfaces. Even though, hydrophilicty is directly related with the number of hydroxyl ions on the surface, it does not only depend on the number of hydroxyl ions for this case. It also depends on the surface morphology thus SnO_2 coated surfaces are more porous than TiO_2

coated surfaces and hydrophilicity is improved with having micro or meso porous coatings having smaller particles and air-filled pores.

Band gaps were measured by using UV-Visible spectrophotometer (Figure 4.18). As shown in Figure 4.18, metal doped tin oxide has absorbance between 200 nm and 300 nm. For pure tin oxide, band gap is around 280 nm corresponding to the band gap energy as 4.4 eV which represents less conductivity than the literature value since band gap energy is 3.6 eV (345 nm) [Benedix et al., 2000; Batzill et al., 2005].

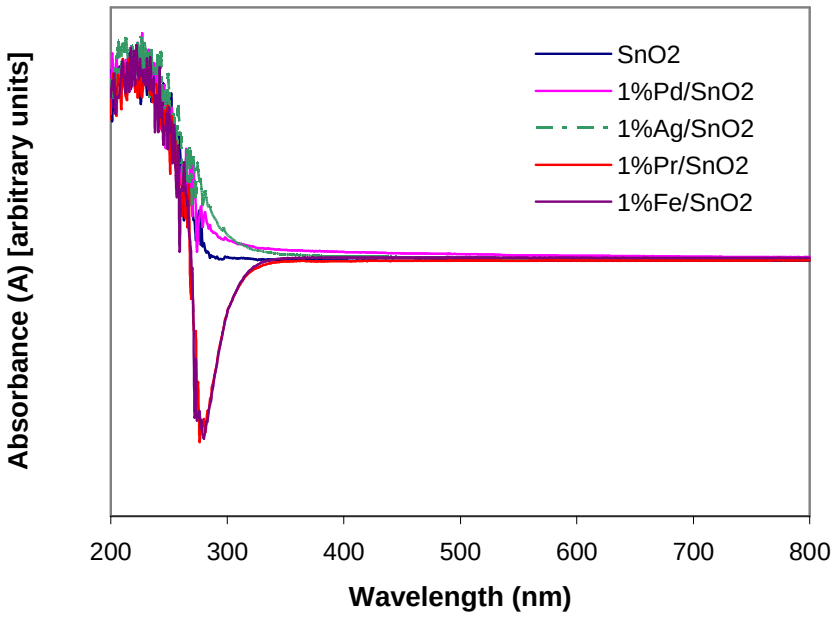

Figure 4.18 UV-Visible spectra of metal doped tin oxide coated thin films calcined at 500^{o}C for 15 minutes

4.5.1 Photocatalytic Activity Measurements with Organic Materials

For quantitative measurements of photocatalytic activity with organic materials, procedure explained in section 3.3.3 was followed. Samples were subjected to

600W/m^2 artificial solar irradiation. Concentration change of methylene blue solution is shown in Figure 4.19.

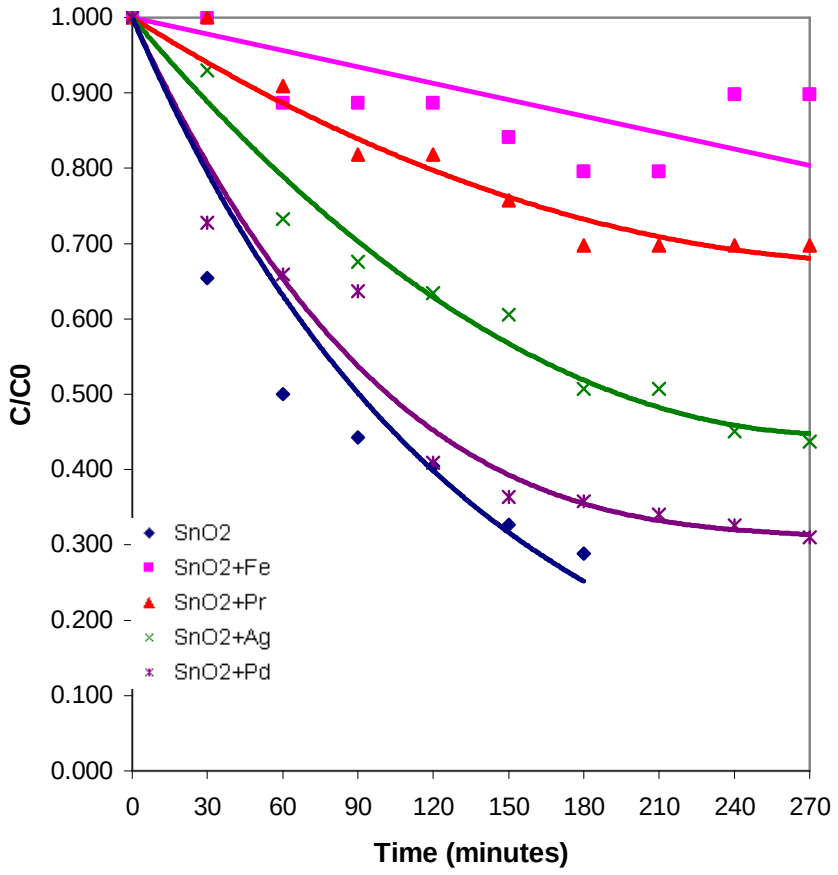

Figure 4.19 Concentration change of methylene blue solution for the metal doped tin oxide coated thin films subjected to 600 W/m^2 artificial solar irradiation

As observed from Figure 4.19, metal doping has declining effect on photocatalytic activity since pure SnO_2 coated thin films have higher photocatalytic activity. On the other hand, for TiO_2 colloidal solution, metal doping has an increasing effect on the activity. When the activities of pure TiO_2 (Figure 4.16) and pure SnO_2 (Figure 4.19) are compared, pure SnO_2 has higher activity as decreasing the concentration of methylene blue by 61.2% (C/C_0=0.288) by irradiation for 180 minutes. On the other hand, TiO_2 decreases

the concentration of methylene blue by 22.1% (C/C_0=0.679) after 180 minutes of irradiation. Despite the fact that band gap of SnO_2 (280 nm) was smaller than the band gap of TiO_2 (360 nm), photocatalytic activity of tin oxide was greater than the activity of titanium dioxide. Even though, photons having higher wavelength is preferred in order to increase reaction turnover for photocatalysts, surface morphology has considerable effect on photocatalytic activity. So, more porous surfaces have greater photocatalytic activity and since tin oxide has more porous structure, it has greater photocatalytic activity.

4.5.2 SEM Analysis

Figure 4.20 shows SEM micrographs of pure tin oxide coated thin films. As seen from the figure, tin oxide particles are distributed to the surface homogeneously. From SEM micrographs given below, characteristic dimension of the analyzed sample is around 50 nm. Characteristic dimension is defined as particle diameter for porous films while it is film thickness for dense and nonporous films. With particles having diameter around 50 nm, surface area of tin oxide coated thin films is higher than the area of titanium dioxide coated thin films because of being porous.

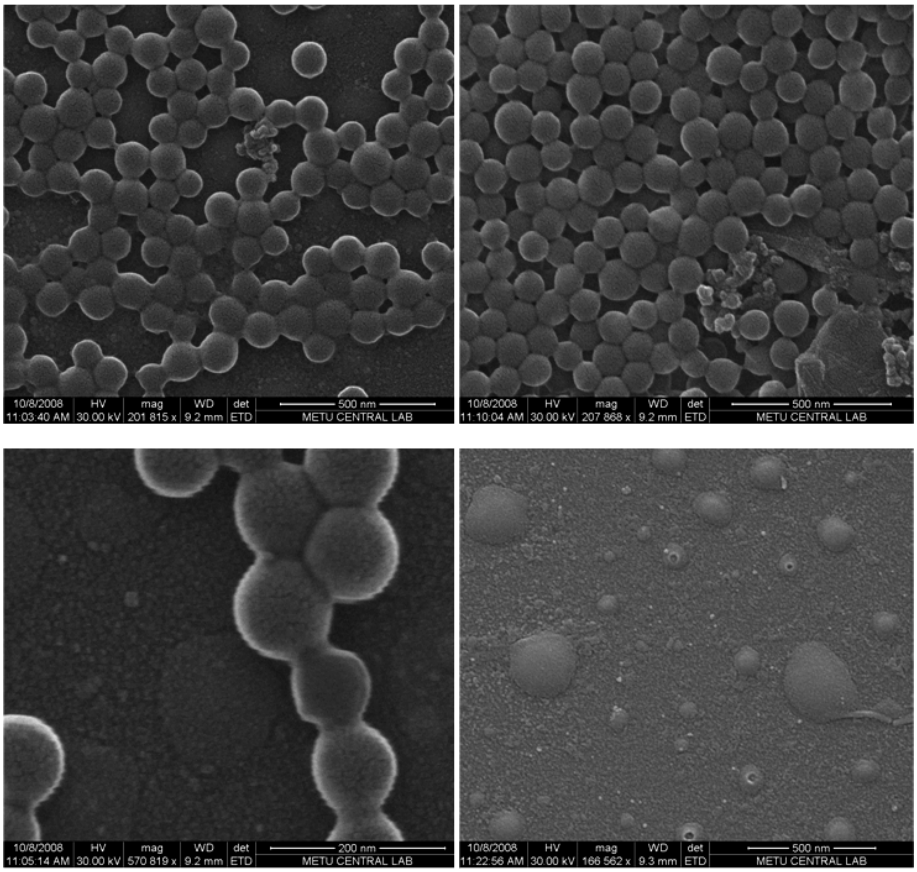

Figure 4.20 SEM micrographs of surfaces coated with pure tin oxide colloidal solution

In section 4.5.1, it is stated that, metal doping has declining effect on photocatalytic activity. When SEM micrographs of metal doped tin oxide coated thin films are observed (Figure 4.21 and Figure 4.22), metal doping affects the porosity of the surface and causes sintering of the particles on the surface resulting in decreased porosity and, so decreased surface area. By taking this situation into consideration, metal doping decreases the sintering temperature resulting in the decreased photocatalytic activity.

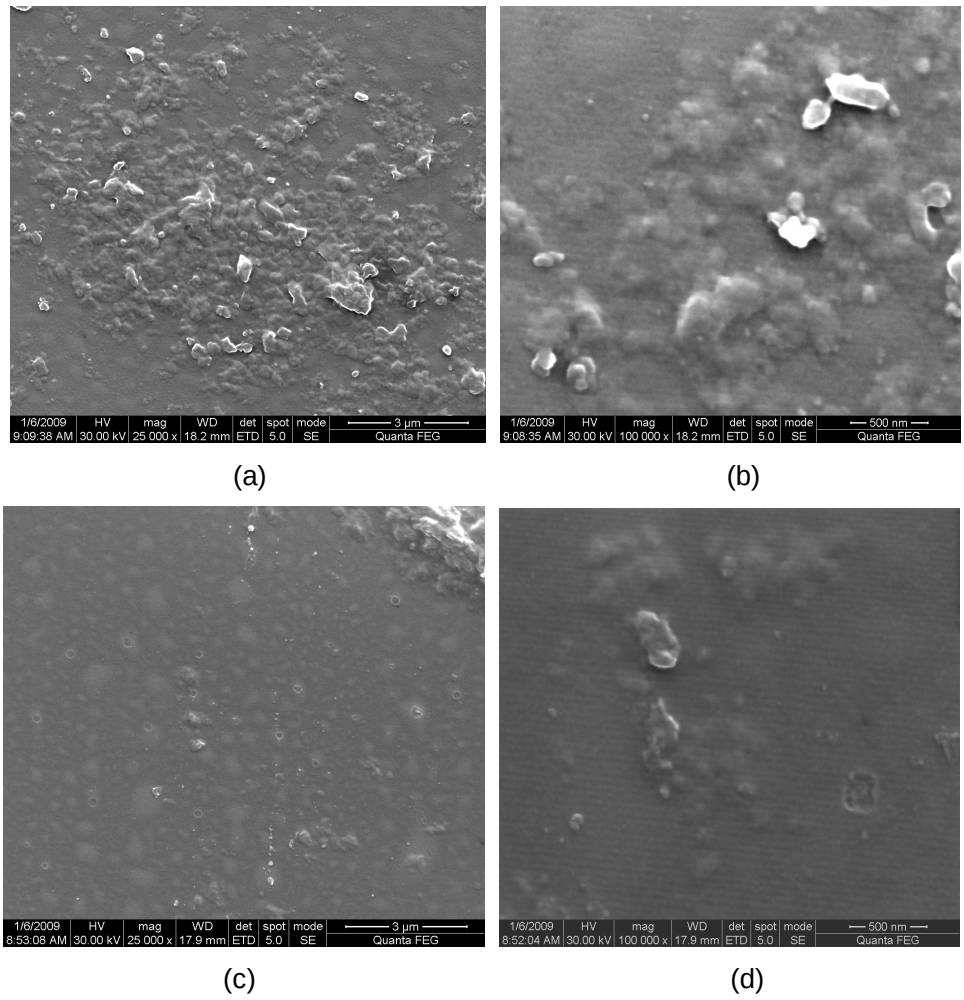

Figure 4.21 SEM micrographs of surfaces coated with; (a): 1%Pd/SnO_2 with x25,000 magnification, (b): 1%Pd/SnO_2 with x100,000 magnification, (c): 1%Ag/SnO_2 with x25,000 magnification, (d): 1&Ag/SnO_2 with x100,000 magnification

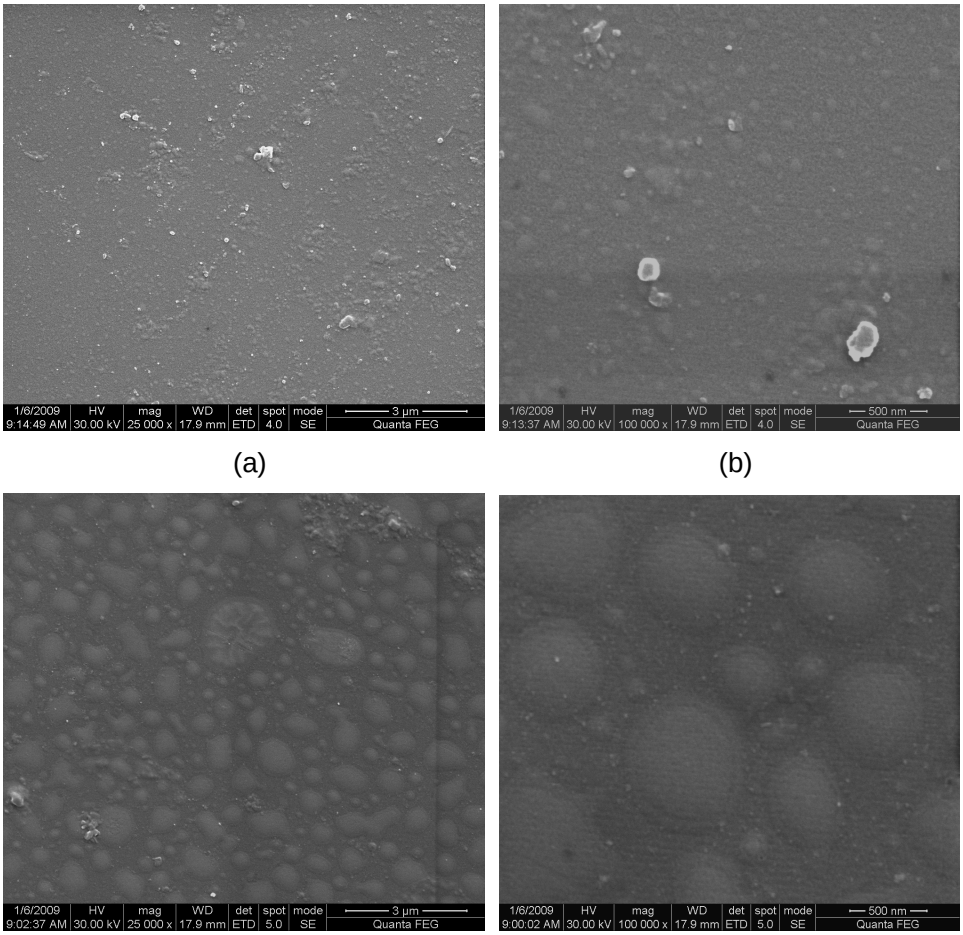

Figure 4.22 SEM micrographs of surfaces coated with; (a): 1%Pr/SnO_2 with x25,000 magnification, (b): 1%Pr/SnO_2 with x100,000 magnification, (c): 1%Fe/SnO_2 with x25,000 magnification, (d): 1%Fe/SnO_2 with x100,000 magnification

4.6 Tin Oxide Doped Titanium Dioxide Coated Thin Films

In literature, it is observed that tin promotes anatase to rutile phase transformation and forms a complete solid solution with rutile phase of titanium dioxide [Mahanty et al., 2003]. In this study, mixtures with different compositions of tin oxide and titanium dioxide were synthesized to increase photocatalytic activity by obtaining lattice parameter mismatch and using the advantage of

hydroxyl radicals on the surfaces of different crystalline structures. For this purpose, 4 different colloidal solutions with different compositions are synthesized as:

- 20 % SnO_2 + 80 % TiO_2
- 35 % SnO_2 + 65 % TiO_2
- 50 % SnO_2 + 50 % TiO_2
- 80 % SnO_2 + 20 % TiO_2

Titanium dioxide and tin oxide colloidal solutions were synthesized by following the procedures given in sections 3.2.3.1 and 3.2.3.2, respectively. Then, they were mixed with respect to the ratios given above and the glass substrates were coated with these solutions in order to form 5 layers. The coated thin films were calcined at 500^{o}C for 15 minutes.

Contact angle of the surfaces were measured in order to make comment on the amount of -OH ions on the surface. The coated thin films were conditioned at the same conditions as 23.5^{o}C and 65% humidity for 24 hours before the measurements. In Table 4.6, measurements are given for the tin oxide doped titanium dioxide coated thin films.

Table 4.6 Contact angle measurements of tin oxide doped titanium dioxide coated thin films calcined at 500^{o}C for 15 minutes

TiO_2		20 % SnO_2 + 80 % TiO_2		35 % SnO_2 + 65 % TiO_2	
Left	Right	Left	Right	Left	Right
64.19	64.23	56.19	56.67	38.67	39.06
50 % SnO_2 + 50 % TiO_2		80 % SnO_2 + 20 % TiO_2		SnO_2	
Left	Right	Left	Right	Left	Right
24.27	23.93	19.57	20.87	17.17	17.22

When the measurements tabulated Table 4.6 are compared, it is observed that by increasing the amount of tin oxide in titanium dioxide colloidal solution, hydrophilicity of the surface, coated with the corresponding colloidal solution, also increases. The reason of this situation is the amount of –OH ions of different crystalline structures as tin oxide has greater amount of –OH ions. Besides that, more hydrophilic surfaces can be achieved by having micro or meso porous metal oxide coatings having smaller particles and air-filled pores. With the addition of tin oxide to titanium dioxide, more porous structure was achieved since tin oxide has smaller particles resulting in more porosity than that of titanium dioxide (Figure 4.20).

Band gap was analyzed by using UV-Visible spectrophotometer (Figure 4.24). As seen from the spectra, SnO_2 present on the surface has absorbance between 200 nm and 260 nm while absorbance of TiO_2 is between 300 nm and 360 nm and the spectra show the existence of a mixture.

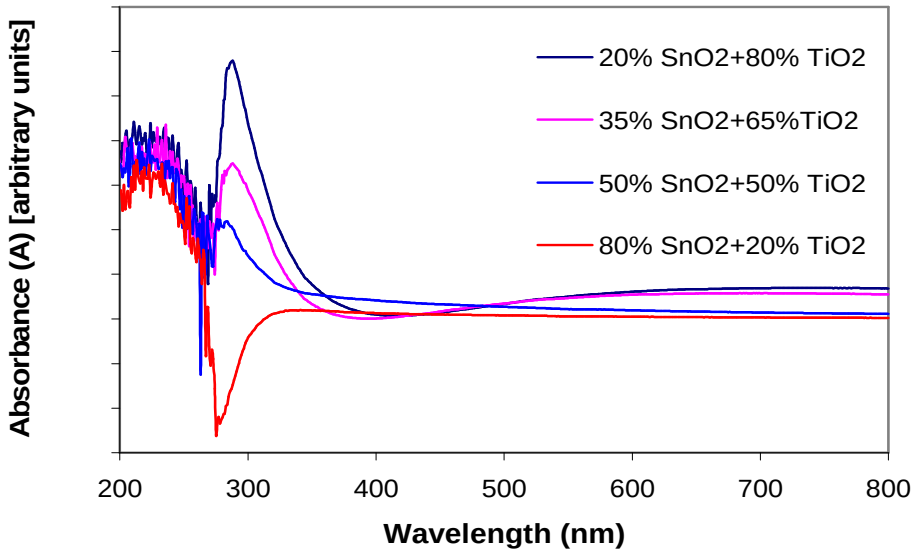

Figure 4.24 UV-Visible spectra of tin oxide doped titanium dioxide coated thin films

4.6.1 Photocatalytic Activity Measurements with Organic Materials

Concentration change of methylene blue solution is shown in Figure 4.25. As observed from Figure 4.25, by increasing the amount of tin oxide in titanium dioxide colloidal solution, photocatalytic activity increases. On the other hand, pure tin oxide coated thin films have higher photocatalytic activity than the films coated with tin oxide doped titanium dioxide.

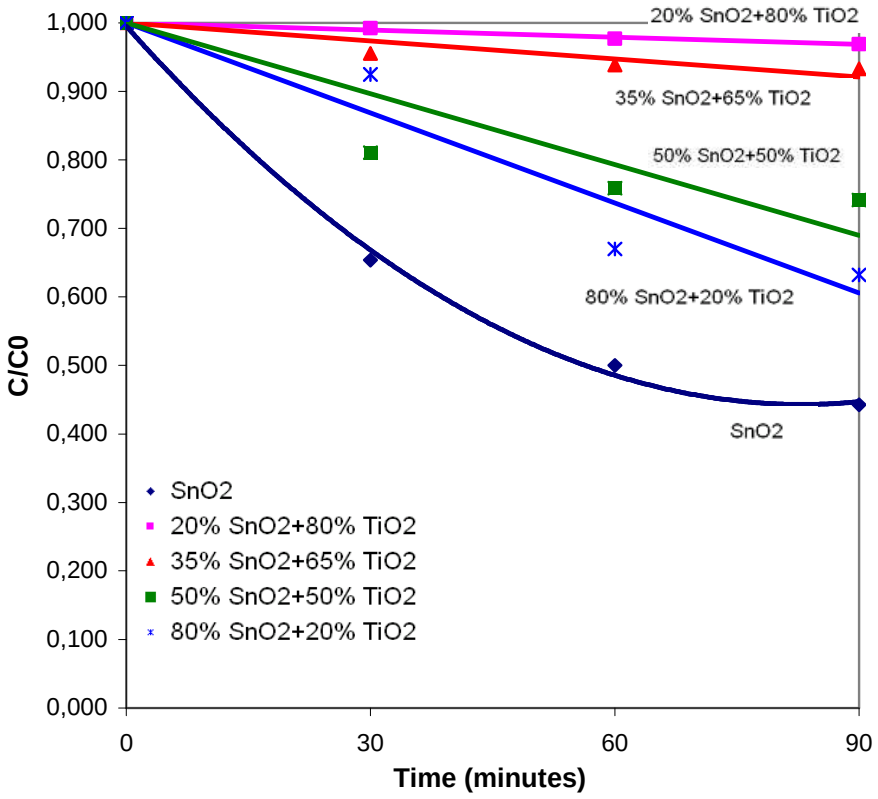

Figure 4.25 Concentration change of methylene blue solution for titanium dioxide-tin oxide coated thin films subjected to 600 W/m^2 artificial solar irradiation

4.6.2 Surface Area Measurements

Surface areas of the coated thin films were measured with the adsorption of methylene blue by using Langmuir isotherms. Procedure explained in section 3.3.2 was followed for the surface area measurement of thin films coated with pure titanium dioxide, pure tin oxide and their binary mixtures. During measurements, for each coated thin film, three samples having different areas were immersed into 10 ml methylene blue solution having 2 ppm concentration. After waiting for 72 hours to reach equilibrium concentration, by determining concentrations, surface areas were measured by using Langmuir isotherms. Straight lines were fitted to the data points (3 data points were present for each sample) where the slope of the regression line was $1/X_m$ and the intercept is

$1/k.X_m$. Langmuir isotherms and Langmuir constants are given in Appendix C. During measurements, cross-sectional area of methylene blue adsorbed on the surface (A_{MB}) was taken as 1.2 nm^2 while coverage factor (N) was taken as 1 [Inel and Tumsek, 2000]. Surface area measurement results are tabulated in Table 4.7.

Table 4.7 Surface area of the coated thin films with different colloidal solutions

	Surface Area (cm^2/cm^2)
TiO_2	6.42
20%SnO_2 + 80%TiO_2	6.52
35%SnO_2 + 65%TiO_2	6.89
50%SnO_2 + 50%TiO_2	7.09
80%SnO_2 + 20%TiO_2	8.88
SnO_2	9.81

From Table 4.7, it is observed that; with the addition of tin oxide into titanium dioxide, surface area increases and it is maximum for pure tin oxide coated thin film as 9.81 cm^2/cm^2. As indicated in previous parts, surface area has effect on photocatalytic activity and larger surface area results in the increased photocatalytic activity. From these measurements, tin oxide coated thin film has the largest surface area which confirms the results of photocatalytic activity measurements as pure tin oxide has greater photocatalytic activity when compared with photocatalytic activities of tin oxide doped titanium dioxide coated thin films (Figure 4.25).

CHAPTER 5

CONCLUSIONS

Within the scope of present study; titanium dioxide, tin oxide, tin oxide doped titanium dioxide, metal doped titanium dioxide and metal doped tin oxide colloidal solutions are synthesized by using sol-gel method and they are applied to the surface of the pretreated glass substrates. As metal catalysts, praseodymium (Pr), palladium (Pd), silver (Ag) and iron (Fe) precursors are used. Different parameters like effect of calcination temperature, calcination duration and duration of gelation-drying period, are studied in order to see surface morphology change with respect to these parameters. The coated thin films are characterized withSEM, UV-Visible Spectrophotometer and CAM. Furthermore, surface area measurements are done by using Langmuir isotherms. The following conclusions are drawn from the data gathered:

- Increase of calcination temperature results in the increased hydrophilicity. On the other hand, calcination duration does not have any effect on the amount of –OH ions on the surface.
- Independent from calcination duration, the coated thin films calcined at 400^{o}C have higher photocatalytic activity when compared with the films calcined at 250^{o}C.
- Duration of gelation-drying period does not have any significant effect on the surface energies of the coated thin films calcined at 250^{o}C. On the other hand, for 400^{o}C, hydrophilic surfaces are achieved by increasing the duration of the period with contact angle decreased down to 20^{o}.
- Increase in the duration of gelation-drying period and increase in the calcination temperature decrease band gap.

- Photocatalytic activity does not depend on the duration of gelation-drying period strongly which is also relevant for antimicrobial activity.
- Pure titanium dioxide coated thin films have limited photocatalytic activity since surface is nonporous, dense and it has amorphous structure.
- For titanium dioxide and tin oxide colloidal solution, metal doping has an improving effect on hydrophilicity.
- Pd, Ag and Pr doped titanium dioxide coated thin films have increased photocatalytic activity while Fe doping has declining effect on it since Fe^{+2} ions present in the precursor cause deformation on the crystalline structure of titanium dioxide.
- Surface area of tin oxide coated thin films is higher than the area of titanium dioxide coated thin films with particles having diameter around 50 nm causing porosity on the surface.
- Pure tin oxide coated thin films have higher photocatalytic activity, so metal doping has declining effect on photocatalytic activity.
- Since tin oxide has greater amount of –OH ions on the surface, hydrophilicity of the surface increases by increasing the amount of tin oxide addition to titanium dioxide colloidal solution. With tin oxide addition, porosity of the surface increases.
- Increase in the amount of tin oxide in titanium dioxide colloidal solution results in the increased photocatalytic activity. On the other, pure tin oxide coated thin films have higher photocatalytic activity when compared with the photocatalytic activity of the films coated with tin oxide doped titanium dioxide.
- Surface area is increased with tin oxide addition to titanium dioxide and pure tin oxide has the largest surface area resulting in highest photocatalytic activity.

CHAPTER 6

RECOMMENDATIONS

- Polymeric materials like PEG with different molecular weights can be added to the colloidal solutions in order to have meso porous structure with larger surface area.

- Surface area increasing methods should be further investigated. One way is the addition of oxides, like silica, to the colloidal solution in order to obtain porous structure.

- Antimicrobial activity tests should be repeated for the metal doped colloidal solutions and titanium dioxide-tin oxide binary mixtures in order to have idea about antimicrobial properties in addition to the photocatalytic properties depending on the degradation of organic materials.

- Surfaces other than glass substrates can be the focus of future studies. For this purpose, ceramic can be used.

- A detailed study about surface area measurement techniques is recommended in order to achieve better results for modeling and fitting the parameters to the corresponding method of measurement.

REFERENCES

Adamson A.W., *Physical Chemistry of Surfaces*, 4th edition, Wiley-Interscience, New York, (1982).

Amlouk A., Mir L., Kraiem S., Saadoun M., Alaya S. And Pierre A.C., *Luminescence of TiO_2:Pr Nanoparticles Incorporated in Silica Aerogel*, Materials Science and Engineering: B, 146(1-3), 74-79, (2008).

Bard A.J., *Photoelectrochemistry and heterogeneous photocatalysis at semiconductors,* Journal of Photochemistry, 10, 59-75, (1979).

Batzill M. and Diebold U., *The Surface and Materials Science of Tin Oxide*, Progress in Surface Science, 79, 47, (2005).

Beganskiene A., Raudonis R., Jokhadar S.Z., Batista U. and Kareiva A., *Modified Sol-gel Coatings for Biotechnological Applications, Functional Materials and Nanotechnologies*, Journal of Physics: Conference Series, 93, 012050, 1-6, (2007).

Benedix R., Dehn F., Quaas J. and Orgass M., *Application of Titanium Dioxide Photocatalysis to Create Self-Cleaning Building Materials*, LACER, 5, 157-167, (2000).

Bickley R., Gonzalez-Carreno T., Lees J., Palmisano L. and Tille R., *A Structural Investigation of Titanium Dioxide Photocatalysts*, Journal of Solid State Chemistry, 92, 178-190, (1991).

Bornside D.E., Macosko C.W. and Scriven L.E., *Method for compensating film height modulations in spin coating of a resist film layer*, Journal of Imaging Technology, 13, 122-130, (1987).

Brinker C.J. and Scherer G.W., *Sol-Gel Science: The Physics and Chemistry of Sol-Gel Processing,* Academic Press, New York, (1990).

Brinker C.J., Hurd A.J., Schunk P.R., Frye G.C. and Ashley C. S., *Review of Sol-Gel Thin Film Formation*, Journal of Non-Crystalline Solids, 147-48, 424-436, (1992).

Carp O., Huisman C.L. and Reler A., *Photoinduced Reactivity of Titanium Dioxide*, Progress in Solid State Chemistry, 32(1), 331-177, (2004).

Carraway E.R., Hoffman A.J. and Hoffmann M.R., *Photocatalytic Oxidation of Organic Acids on Quantum-Sized Semiconductor Colloids*, Environmental Science and Technology, 28(5), 786-793, (1994).

Chang C., Chen J., Hsu T., Lin C. and Chan C., *Photocatalytic Properties of Porous TiO_2/Ag Thin Films,* Thin Solid Films, 516, 1743-1747, (2008).

Chanon M., *Homogeneous Photocatalysis*, Volume 2, John Wiley & Sons, England, (1997).

Cho C.H., Han M.H., Kim D.H. and Kim D.K., *Morphology Evolution of Anatase TiO_2 Nanocrystals Under a Hydrothermal Condition (pH = 9.5) and Their Ultra-High Photo-Catalytic Activity*, Materials Chemistry and Physics, 92, 104-111, (2005).

Cunningham J., Tobin J.P.J. and Meriaudeau P., *Oxygen Migration and Isotope Exchange During Photoassisted Splittıng of Water-Vapor on TiO_2-Carbon Mixtures*, Surface Science, 108(3), L465-L469, (1981).

Deng, X., Yue Y. and Gao Z., *Gas-Phase Photo-Oxidation of Organic Compounds over Nanosized TiO_2 Photocatalysts by Various Preparations*, Applied Catalysis B: Environmental, 39(2), 135-147, (2002).

Diebold U., *The Surface Science of Titanium Dioxide*, Surface Science Reports, 48, 53-229, (2003).

Erdural B.K., Yurum A., Bakir U. and Karakas G., *Hydrothermal Synthesis of Nanostructured TiO_2 Particles and Characterization of Their Photocatalytic Antimicrobial Activity*, Journal of Nanoscience and Nanotechnology, 8(2), 878-886, (2008).

Erkan A., *Investigation of thin semiconductor coatings and their antimicrobial properties*, MSc Thesis, METU, Ankara, (2005).

Erkan A., Bakir U. and Karakas G., *Photocatalytic Microbial Inactivation over Pd Doped SnO_2 and TiO_2 Thin Films*, Journal of Photochemistry And Photobiology A: Chemistry, 184(3), 313-321, (2006).

Euvananont C., Junin C., Inpor K., Limthongkul P. and Thanachayanont C., *TiO_2 Optical Coating Layers for Self-Cleaning Applications*, Ceramics International, 34(4), 1067-1071, (2008).

Evans P. and Sheel D.W., *Photoactive and Antibacterial TiO_2 Thin Ffilms on Stainless Steel*, Surface & Coatings Technology, 201, 9319–9324, (2007).

Feng X., Zhai J. and Jiang L., *The Fabrication and Switchable Superhydrophobicity of TiO_2 Nanorod Films*, *Angewandte Chemie*, 44(32), 5115 – 5118, (2005).

Fujishima A., Rao T.N. and Try D.A., *Titanium Dioxide Photocatalysis*, Journal of Photochemistry and Photobiology C: Photochemistry Reviews 1, 1-21, (2000).

Garcia J.C. and Takashima K., *Photocatalytic Degradation of Imazaquin in an Aqueous Suspension of Titanium Dioxide*, Journal of Photochemistry and Photobiology A: Chemistry, 155(1-3), 215-222, (2003).

Gärtner M., Dremov V., Müller P. and Kisch H., *Bandgap Widening of Titania Through Semiconductor Support Interactions*, Chemphyschem, 6(4):714-718, (2005).

Goh G.K.L, Donthu S.K. and Pallathadka P.K., *Cracking and Orientation of Solution-Deposited Rutile TiO_2 Films*, Chemistry of Materials, 16(15), 2857-2861, (2004).

Goh G.K.L., Han X.Q., Liew C.P.K. and Tay C.S.S., *Crystallinity and Orientation of Solution Deposited Anatase TiO_2 Films*, Journal of The Electrochemical Society, 152(8), 532-536, (2005).

Grätzel M., *Energy Resources through Photochemistry and Catalysis*, Academic Press, New York, (1983).

Gregg S. J. and Sing K. S. W., *Adsorption, Surface Area and Porosity*, 2nd edition, Academic Press, London, (1982).

Grela M.A., Coronel M.E.J. and Colussi A.J., *Quantitative Spin-Trapping Studies of Weakly Illuminated Titanium Dioxide Solutions: Implications for the Mechanism of Photocatalysis*, Journal of Physical Chemistry, 100(42), 16940-16946, (1996).

Grove A.S., *Physics and Technology of Semiconductor Devices*, John Wiley & Sons, New York, (1967).

Guan K.H., *Relationship Between Photocatalytic Activity, Hydrophilicity and Self-cleaning Effect of TiO_2/SiO_2 Films*, Surface & Coatings Technology, 191(2-3), 155-160, (2005).

Guo B., Liu Z., Hong L. and Jiang H., *Sol Gel Derived Photocatalytic Porous TiO_2 Thin Films*, Surface & Coatings Technology, 198, 24-29, (2005).

Harbour J.R. and Hair M.L., *Transient radicals in heterogeneous systems: detection by spin trapping*, Advances in Colloid and Interfaces Science, 24, 103–141, (1986).

Hoffmann M.R., Martin S.T., Choi W. and Bahnemann D.W., *Environmental Applications of Semiconductor Photocatalysis*, Chemistry Reviews, 95(1), 69-96, (1995).

Hong Y.C., Bang U.C., Shin D.H. and Uhm H.S., *Band Gap Narrowing of TiO_2 by Nitrogen Doping in Atmospheric Microwave Plasma*, Chemical Physics Letters, 413(4-6), 454-457, (2005).

Hsiunga T.L., Wanga H.P. and Wang H.C., *XANES Studies of Photocatalytic Active Species in Nano TiO_2–SiO_2*, Radiation Physics and Chemistry, 75, 2042-2045, (2006).

Inel O. and Tumsek F., *The Measurement of Surface Areas of Some Silicates by Solution Adsorption*, Turkish Journal of Chemistry, 24, 9-20, (2000).

Jaeger, C.D., Bard, A.J., *Spin Trapping and Electron Spin Resonance Detection of Radical Intermediates in the Photo Decomposition of Water at TiO_2 Rarticulate Systems*, Journal of Physical Chemistry, 83, 3146–3152, (1979).

Jiang D.L., Zhao H.J., Zhang S.Q. and John R., *Kinetic Study of Photocatalytic Oxidation of Adsorbed Carboxylic Acids at TiO_2 Porous Films by Photoelectrolysis*, Journal of Catalysis, 223(1), 212-220, (2004).

Jouini A., Gâcon J.C., Ferid M. and Trabelsi-Ayadi M., *Luminescence and scintillation properties of praseodymium poly and diphosphates,* Optical Materials, 24(1-2), 175-180, (2003).

Kamat P.V., *Photoinduced Transformations in Semiconductor-Metal Nanocomposite Assemblies*, Pure and Applied Chemistry, 74(9), 1693-1706, (2002).

Kato K., Tsuzuki A., Taoda H., Torii Y. and Butsugan Y., *Crystal Structures of TiO_2 Thin Coatings Prepared from the Alkoxide Solution via the Dip-coating Technique Affecting the Photocatalytic Decomposition of Aqueous Acetic Acid,* Journal of Materials Science, 29, 5911-5915, (1994).

Kaya O, Characterization of Titanium Dioxide Thin Films Prepared by Sol-Gel Processing, MSc Thesis, METU, Ankara, (2002).

Kim D.J., Hahn S.H., Oh S.H. and Kim E.J., *Influence of Calcination Temperature on Structural and Optical Properties of TiO_2 Thin Films Prepared by Sol-gel Dip Coating*, Materials Letters, 57, 335, (2002).

Kipling J. J., *Adsorption from Solutions of Non-electrolytes*, Academic Press, London, (1965).

Kumar P.M., Badrinarayanan S. and Sastry M., *Nanocrystalline TiO_2 Studied by Optical, FTIR and X-ray Photoelectron Spectroscopy: Correlation to Presence of Surface States*, Thin Solid Films, 358, 122-130, (2000).

Landau L.D. and Levich B.G., *Dragging of a Liquid by a Moving Plate*, Acta Physicochim. U.R.S.S., 17, 42-54, (1942).

Lasa H., Serrano B. and Salaices M., *Photocatalytic Reaction Engineering,* Springer, United States of America, (2005).

Lawn B.R. and Wilshaw T.R., *Fracture of Brittle Solids*, Cambridge University Press, Cambridge, England, (1975).

Lee K., Lee N.H., Shin S.H., Lee H.G. and Kima S.J., *Hydrothermal Synthesis and Photocatalytic Characterizations of Transition Metals Doped Nano TiO_2 Sols*, Materials Science and Engineering B, 129, 109–115, (2006).

Legrini, O., Oliveros E. and Braun A.M., *Photochemical Processes for Water Treatment*, Chemical Reviews, 93(2), 671-698, (1993).

Lin H., Kozuka H. and Yoko T., *Preparation of TiO_2 Films on Self- Assembled Monolayers by Sol-Gel Method*, Thin Solid Films, 315, 111-117, (1998).

Linsebigler A.L., Lu G. and Yates J.T., *Photocatalysis on TiO_2 Surface: Principles, Mechanism, and Selected Results*, Chemical Reviews, 95(3), 735-758, (1995).

Liu Q., Wu X., Wang B. and Liu Q., *Preparation and Super-hydrophilic Properties of TiO_2/SnO_2 Composite Thin Films*, Materials Research Bulletin, 37, 2255-2262, (2002).

Luca D., Mardare D., Iacomi F. and Teodorescu C.M., *Increasing Surface Hydrophilicity of Titania Thin Films by Doping,* Applied Surface Science, 252, 6122-6126, (2006).

Ma B., Goh G.K.L. and Ma J., *Crystallinity and Photocatalytic Activity of Liquid Phase Deposited TiO_2 Films*, Journal of Electroceramics, 16, 441-445, (2006).

Mahanty S., Roy S. and Sen S., *Effect of Sn doping on the Structural and Optical Properties of Sol-gel TiO_2 thin fil*ms, Journal of Crystal Growth, 261, 77-81, (2004).

Mellott N.P., Durucan C. and Pantano C.G., *Commercial and Laboratory Prepared Titanium Dioxide Thin Films for Self-Cleaning Glasses: Photocatalytic Performance and Chemical Durability*, Thin Solid Films, 502 (1-2), 112-120, (2006).

Mennig M., Kalleder A., Koch T., Mohr S., Fink-Straube C., Heusing S., Munro B., Zapp P. and Schmidt H., *proc. 2nd ICCG*, *Saarbrücken 06. - 10. 09. 98*, to be published in Thin Solid Films, (1998).

Mills A. and Wang J., *Photobleaching of Methylene Blue sensitised by TiO_2: an Ambiguous System?*, Journal of Photochemistry and Photobiology A: Chemistry, 1*27*, 123-134, (1999).

Mirkelamoglu B., *Investigation of Carbon Monoxide Oxidation Over Tin Dioxide Based Catalysts By Dynamic Methods*, MSc Thesis, METU, Ankara, (2002).

Miyauchi M., Nakajima A., Watanabe T. and Hashimoto K., *Photocatalysis and Photoinduced Hydrophilicity of Various Metal Oxide Thin Films*, Chemistry Materials, 14, 2812-2816, (2002).

Nam W. and Han G.Y., *Preparation and Characterization of Anodized Pt-TiO_2 Nanotube Arrays for Water Splitting*, Journal of Chemical Engineering of Japan, 40(3), 266-269, (2007).

Negishi N. and Tageuchi K., *Structural Changes of Transparent TiO Thin Films with Heat Treatment*, Materials Letters, 38, 150-153, (1999).

Ohno T., Sarukawa K., Tokieda K. and Matsumura M., *Morphology of a TiO_2 Photocatalyst (Degussa, P-25) Consisting of Anatase and Rutile Crystalline Phases*, Journal of Catalysis, 203(1), 82-86, (2001).

Ohno T., Tagawa S., Itoh H., Suzuki H. and Matsuda T., *Size Effect of TiO_2–SiO_2 Nano-Hybrid Particle,* Materials Chemistry and Physics, 113, 119-123, (2009).

Ostomel T.A. and Stucky G.D., *Free-standing Mesoporous Titania Films with Anatase Nanocrystallites Synthesized at 80℃*, Chemical Communications, 1016-1017, (2004).

Ozmen M., *Titanyum Dioksit (TiO_2) İnce Filmi Üzerine Çeşitli Organik Bileşiklerin İmmobilizasyonu ve Uygulamaları*, MSc Thesis, Selcuk University, Konya, (2006).

Pascual J., Camassel J. and Mathieu H., *Fine Structure in the Intrinsic Absorption Edge of TiO_2*, Physical Review B, 18, 5606, (1978).

Pierre A.C., *Introduction to Sol-Gel Processing*, Kluwer Academic Publishers, London, (1998).

Popielarski S., *Photocatalysis on Nano-Sized Semiconductors*, Chemical Reviews, 95, 735, (1998).

Prairie M.R., Evans L.R., Stange B.M., Martinez S.L., *An Investigation of TiO_2 Photocatalysis for the Treatment of Water Contaminated with Metals and Organic Chemicals*, Environmental Science and Technololgy, 27(9),1776-1782, (1993).

Rao M.V., Rajeshwar K., Verneker V.R.P. and DuBow J., *Photosynthetic Production of Hydrogen and Hydrogen Peroxide on Semiconducting Oxide Grains in Aqueous Solutions*, Journal of Physical Chemistry, 84(15), 1987-1991, (1980).

Reddya K.M., Manorama S.V. and Reddy A.R., *Bandgap Studies on Anatase Titanium Dioxide Nanoparticles*, Materials Chemistry and Physics, 78(1), 239-245, (2002).

Rivera A.P., Tanaka K. and Hisanaga T., *Photocatalytic Degradation of Pollutant over TiO_2 in Different Crystal Structure*, Applied Catalysis B: Environmental, 3(1), 37-44, (1993).

Sakthivel S., Shankar M.V., Palanichamy M., Arabindoo B., Bahnemanna D.W. and Murugesan V., *Enhancement of Photocatalytic Activity by Metal Deposition: Characterisation and Photonic Efficiency of Pt, Au and Pd Deposited on TiO_2 Catalyst*, Water Research, 38, 3001–3008, (2004).

Sawunyama P., Yasumori O. and Okada K., *The Nature Of Multilayered TiO_2-based Photocatalytic Films Prepared by a Sol-gel Process,* Materials Research Bulletin, 33 (5), 795-801, (1998).

Schmidt M., Masson A. and Bréchignac C., *Oxygen and Silver Clusters: Transition from Chemisorption to Oxidation,* Physics Revised Letters, 91(24), 243401, (2003).

Schwartz J., Contescu C. and Contescu A., *Methods for Preparation of Catalytic Materials*, Chemical Reviews, 95, 477-510, (1995).

Scriven L.E., Brinker C.J., Clark D.E. and Ulrich D.R., *Better Ceramics Through Chemistry III: Symposium (Materials Research Society Symposium Proceedings)*, Materials Research Society, San Francisco, United States of America, 111, 717-729, (1988).

Serpone N., Terzian R., Lawless D., Kennepohl P. and Sauve G., *On the Usage of Turnover Numbers and Quantum Yields in Heterogeneous Photocatalysis*, Journal of Photocemistry and Photobiology A: Chemistry, 11(6), 73, (1993).

Serpone N., *Is the Band Gap of Pristine TiO_2 Narrowed by Anion- and Cation-Doping of Titanium Dioxide in Second-Generation Photocatalysts?*, Physical Chemistry B: Chemistry, 110 (48), 24287 -24293, (2006).

Sharma S.D., Singh D., Saini K.K., Kant C., Sharma V., Jain S.C. and Sharma C.P., *Sol–Gel Derived Super-Hydrophilic Nickel Doped TiO_2 Film as Active Photo-Catalyst*, Applied Catalysis A: General, 314, 40–46, (2006).

Sivakumar T. and Shanthi K., *Kinetic Studies on the Photo Decolourisation of Textile Dyes (reactive) Using ZnO Catalyst*, Indian Journal of Chemical Technology, 7(3), 121-126, (2000).

Sonawane R.S. and Dongare M.K., *Sol–gel synthesis of Au/TiO_2 thin films for Photocatalytic Degradation of Phenol in Sunlight*, Journal of Molecular Catalysis A: Chemical 243, 68–76, (2006).

Sopyan I., *Kinetic Analysis on Photocatalytic Degradation of Gaseous Acetaldehyde, Ammonia and Hydrogen Sulfide on Nanosized Porous TiO_2 Films*, Science and Technology of Advanced Materials, 8(1-2), 33-39, (2007).

Su C., Hong B.Y. and Tseng C.M., *Sol–gel Preparation and Photocatalysis of Titanium Dioxide*, Catalysis Today, 96, 119–126, (2004).

Sua W., Chen J., Wu L., Wang X., Wang X. and Fu X., *Visible Light Photocatalysis on Ppraseodymium(III)-Nitrate-Modified TiO_2 Prepared by an*

Ultrasound Method, Applied Catalysis B: Environmental, 77(3-4), 264-271, (2008).

Sun L. and Bolton J.R., *Determination of the Quantum Yield for the Photochemical Generation of Hydroxyl Radicals in TiO_2 Suspensions,* Journal of Physical Chemistry,100(10), 4127-4134, (1996).

Sun B., Vorontsov A.V. and Smirniotis P.G., *Role of Platinum Deposited on TiO_2 in Phenol Photocatalytic Oxidation*, *Langmuir*, 19(8), 3151-3156, (2003).

Sun C.L., Li J.F., Hu C.H., Jiang H.M. and Jiang Z.K., *Ultraviolet Upconversion in Pr :YSiO Crystal by Ar Laser (488 nm) Excitation*, Europian Physics Journal:D, 39, 303-306, (2006).

Tahiri H., Serpone N. and Mao R.L., *Application of Concept of Relative Photonic Efficiencies and Surface Characterization of a New Titania Photocatalyst Designed for Environmental Remediation*, Journal of Photochemistry and Photobiology A: Chemistry, 93(2-3), 199-203, (1996).

Tanaka K., Luesaiwong W. and Hisanaga T., *Photocatalytic Degradation of Mono-, Di- and Trinitrophenol in Aqueous TiO_2 Suspension*, Journal of Molecular Catalysis A: Chemical, 122(1), 67-74, (1997).

Trapalis C.C., Keivanidis P., Kordas G., Zaharescu M., Crisan M., Szatvanyi A. and Gärtner M., T*iO (Fe^{3+}) Nanostructured Thin Films with Antibacterial Properties*, Thin Solid Films, 433, 186–190, (2003).

Tsai S.J. and Cheng S., *Effect of TiO_2 Crystalline Structure in Photocatalytic Degradation of Phenolic Contaminants*, Catalyis Today, 33(1-3), 227-237, (1997).

Tseng, J.M. and Huang C.P., *Removal of Chlorophenols from Water by Photocatalytic Oxidation*, *Water Science and Technology*, 23(1-3), 377-387, (1991).

Tsuge Y., Kim J., Sone Y., Kuwaki O. and Shiratori S., *Fabrication of Transparent TiO_2 film with High Adhesion by Using Self-Assembly Methods: Application to Super-Hydrophilic Film*, Thin Solid Films, 516(9), 2463-2468, (2008).

Turhan I., *TiO_2 ve Katkılı TiO_2 İnce Filmlerinin Hazırlanması ve Karakterizasyonu,* MSc Thesis, ITU, Istanbul, (2000).

Uhlmann D.R., Suratwala T.., Davidson K., Boulton J.M. and Teowee G., *Sol-gel Derived Coatings on Glass*, Journal of Non-crystalline Solids, 218, 113-122, (1997).

Wang C.Y., Tang H.J. and Pang S.H., *Enhancing Sunlight Photocatalytic Efficiency of Self-Cleaning Glass by Coating $ZnFe_2O_4$-TiO_2 Film*, Rare Metal Materials and Engineering, 37, 548-551, (2008).

Wu K.R., Wang J.J., Liu W.C., Chen Z.S. and Wu J.K., *Deposition of Graded TiO_2 Films Featured Both Hydrophobic and Photo-Induced Hydrophilic Properties*, Applied Surface Science*,* 252, 5829–5838, (2006).

Yan B., Wang W. and Song Y., *Double Fluorescence Conversion in Ultraviolet and Visible Region for Some Praseodymium Complexes of Aromatic Carboxyates,* Journal of Fluoroscence, 16(4), 495-500, (2006).

Yang H., Guo L., Yan W. and H. Liu, *A Novel Composite Photocatalyst for Water Splitting Hydrogen Production*, Journal of Power Sources, 159(2), 1305-1309, (2006).

Yu J., Zhao X., Du J. and Chen W., Preparation, *Microstructure and Photocatalytic Activity of the Porous TiO_2 Anatase Coating by Sol-Gel Processing*, Journal of Sol-gel Science and Technology, 17, 163-171, (2000).

Yu J., Yu J., Ho W. and Jiang Z., *Effects of Calcination Temperature on the Photocatalytic Activity and Photo-induced Super-hydrophilicity of Mesoporous TiO_2 Thin Films,* New Journal of Chemistry, 26, 607-613, (2002).

Yu J., Su Y., Cheng B. and Zhou M., *Effects of pH on the Microstructures and Photocatalytic Activity of Mesoporous Nanocrystalline Titania Powders Prepared via Hydrothermal Method*, Journal of Molecular Catalysis A: Chemical , 258, 104–112, (2006).

Zhang F., Zhao J., Shen T., Hidaka H., Pelizzetti E. and Serpone N., *TiO_2-Assisted Photodegradation of Dye Pollutants II. Adsorption and Degradation Kinetics of Eosin in TiO_2 Dispersions Under Visible Light Irradiation*, Applied Catalysis B: Environmental,15(1-2), 147-156, (1998).

Zhang X., Fujishima A., Jin M., Emeline A.V. and Murakami T., *Double-Layered TiO_2-SiO_2 Nanostructured Films with Self-Cleaning and Antireflective Poperties*, Journal of Physical Chemistry B, 110, 25142-25148, (2006).

Zheng Y., Shi E., Chen Z., Li W. and Hu X., *Influence of Solution Concentration on the Hydrothermal Preparation of Titania Crystallites,* Journal of Materials Chemistry, 11, 1547-1551, (2001).

APPENDIX A

SAMPLE CALCULATIONS FOR THE SYNTHESIS OF METAL DOPED COLLOIDAL SOLUTIONS

A.1 Praseodymium Doping

- **Titanium Dioxide Colloidal Solution**

According to the procedure given in part 3.4.1, 8.6 ml titanium n-butoxide ($(C_4H_9O)_4Ti$) was used for sol-gel synthesis.

Density of titanium n-butoxide is:

$$\rho_{(C_4H_9O)_4Ti} = 0.990 \quad gr/ml$$

Mass of titanium n-butoxide added is:

$$Mass \quad of \quad (C_4H_9O)_4Ti = 8.6 \quad ml \quad x \quad 0.990 \quad \frac{gr}{ml} = 8.514 \quad gr$$

Since molecular weight of titanium n-butoxide is 340. 35 gr /mol,

$$8.514 \quad gr \quad x \quad \frac{1}{340.35} \quad \frac{mol}{gr} = 0.025015 \quad mol \quad Ti$$

$$\Downarrow$$

$$0.025015 \quad mol \quad TiO_2$$

Since molecular weight of titanium dioxide is 79.87 gr /mol,

$$Mass\ \ of\ \ TiO_2 = 79.87\ \frac{gr}{mol}\ \ x\ \ 0.025015\ \ mol\ \ TiO_2 = 1.998\ \ gr\ \ TiO_2$$

So, 0.01998 gr Pr would be added. For praseodymium doped titanium dioxide colloidal solution, 0.01998 gr praseodymium(III) acetyl-acetone hydrate was added.

- **Tin Oxide Colloidal Solution**

According to the procedure given in part 3.4.2, 13.024 gr tin tetrachloride pentahydrate ($SnCl_4.5H_2O$) was used for sol-gel synthesis.

Since molecular weight of tin tetrachloride is 260.502 gr /mol,

$$13.024\ \ gr\ \ x\ \ \frac{1}{260.502}\ \ \frac{mol}{gr} = 0.049996\ \ mol\ \ Sn$$

$$\Downarrow$$

$$0.049996\ \ mol\ \ SnO_2$$

Since molecular weight of tin oxide is 150.71 gr /mol,

$$Mass\ \ of\ \ SnO_2 = 150.71\ \frac{gr}{mol}\ \ x\ \ 0.04996\ \ mol\ \ SnO_2 = 7.523\ \ gr\ \ SnO_2$$

So, 0.07530 gr Pr would be added. For praseodymium doped tin oxide colloidal solution, 0.07530 gr praseodymium(III) acetyl-acetone hydrate was added.

A.2 Palladium Doping

- **Titanium Dioxide Colloidal Solution**

According to the procedure given in part 3.4.1, 8.6 ml titanium n-butoxide ($(C_4H_9O)_4Ti$) was used for sol-gel synthesis.

Density of titanium n-butoxide is:

$$\rho_{(C_4H_9O)_4Ti} = 0.990 \quad gr/ml$$

Mass of titanium n-butoxide added is:

$$Mass \quad of \quad (C_4H_9O)_4Ti = 8.6 \quad ml \quad x \quad 0.990 \quad \frac{gr}{ml} = 8.514 \quad gr$$

Since molecular weight of titanium n-butoxide is 340. 35 gr /mol,

$$8.514 \quad gr \quad x \quad \frac{1}{340.35} \quad \frac{mol}{gr} = 0.025015 \quad mol \quad Ti$$

$$\Downarrow$$

$$0.025015 \quad mol \quad TiO_2$$

Since molecular weight of titanium dioxide is 79.87 gr /mol,

$$Mass \quad of \quad TiO_2 = 79.87 \quad \frac{gr}{mol} \quad x \quad 0.025015 \quad mol \quad TiO_2 = 1.998 \quad gr \quad TiO_2$$

So, 0.01998 gr PdO would be added and molecular weight of PdO is 122.4 gr/mol.

$$0.01998 \quad gr \quad x \quad \frac{1}{122.4} \quad \frac{mol}{gr} = 0.000163 \quad mol \quad Pd$$

As palladium precursor, palladium acetate is used. So, 0.000163 mol palladium acetate is added and its molecular weight is 224.5 gr/mol.

$$0.000163 \ \ mol \ \ x \ \ 224.5 \ \ \frac{gr}{mol} = 0{,}03659 \ \ gr \ \ palladium \ \ acetate$$

For palladium doped titanium dioxide colloidal solution, 0.03659 gr palladium(II) acetate was added.

- **Tin Oxide Colloidal Solution**

According to the procedure given in part 3.4.2, 13.024 gr tin tetrachloride pentahydrate ($SnCl_4.5H_2O$) was used for sol-gel synthesis.

Since molecular weight of tin tetrachloride is 260.502 gr /mol,

$$13.024 \ \ gr \ \ x \ \ \frac{1}{260.502} \ \ \frac{mol}{gr} = 0.049996 \ \ mol \ \ Sn$$

$$\Downarrow$$

$$0.049996 \ \ mol \ \ SnO_2$$

Since molecular weight of tin oxide is 150.71 gr /mol,

$$Mass \ \ of \ \ SnO_2 = 150.71 \ \ \frac{gr}{mol} \ \ x \ \ 0.04996 \ \ mol \ \ SnO_2 = 7.523 \ \ gr \ \ SnO_2$$

So, 0.07530 gr PdO would be added and molecular weight of PdO is 122.4 gr/mol.

$$0.07530 \ \ gr \ \ x \ \ \frac{1}{122.4} \ \ \frac{mol}{gr} = 0.000615 \ \ mol \ \ Pd$$

As palladium precursor, palladium acetate is used. So, 0.000615 mol palladium acetate is added and its molecular weight is 224.5 gr/mol.

$$0.000615 \ \ mol \ \ x \ \ 224.5 \ \ \frac{gr}{mol} = 0{,}13811 \ \ gr \ \ palladium \ \ acetate$$

For palladium doped tin oxide colloidal solution, 0.13811 gr palladium(II) acetate was added.

A.3 Silver Doping

- **Titanium Dioxide Colloidal Solution**

According to the procedure given in part 3.4.1, 8.6 ml titanium n-butoxide ($(C_4H_9O)_4Ti$) was used for sol-gel synthesis.

Density of titanium n-butoxide is:

$$\rho_{(C_4H_9O)_4Ti} = 0.990 \ \ gr/ml$$

Mass of titanium n-butoxide added is:

$$Mass \ \ of \ \ (C_4H_9O)_4Ti = 8.6 \ \ ml \ \ x \ \ 0.990 \ \ \frac{gr}{ml} = 8.514 \ \ gr$$

Since molecular weight of titanium n-butoxide is 340. 35 gr /mol,

$$8.514 \ \ gr \ \ x \ \ \frac{1}{340.35} \ \ \frac{mol}{gr} = 0.025015 \ \ mol \ \ Ti$$

$$\Downarrow$$

$$0.025015 \ \ mol \ \ TiO_2$$

Since molecular weight of titanium dioxide is 79.87 gr /mol,

$$Mass\ \ of\ \ TiO_2 = 79.87\ \frac{gr}{mol}\ \ x\ \ 0.025015\ \ mol\ \ TiO_2 = 1.998\ \ gr\ \ TiO_2$$

So, 0.01998 gr Ag would be added. For silver doped titanium dioxide colloidal solution, 0.01998 gr silver nitrate was added.

- **Tin Oxide Colloidal Solution**

According to the procedure given in part 3.4.2, 13.024 gr tin tetrachloride pentahydrate ($SnCl_4.5H_2O$) was used for sol-gel synthesis.

Since molecular weight of tin tetrachloride is 260.502 gr /mol,

$$13.024\ \ gr\ \ x\ \ \frac{1}{260.502}\ \ \frac{mol}{gr} = 0.049996\ \ mol\ \ Sn$$

$$\Downarrow$$

$$0.049996\ \ mol\ \ SnO_2$$

Since molecular weight of tin oxide is 150.71 gr /mol,

$$Mass\ \ of\ \ SnO_2 = 150.71\ \frac{gr}{mol}\ \ x\ \ 0.04996\ \ mol\ \ SnO_2 = 7.523\ \ gr\ \ SnO_2$$

So, 0.07530 gr Ag would be added. For silver doped tin oxide colloidal solution, 0.07530 gr silver nitrate was added.

A.4 Iron Doping

- **Titanium Dioxide Colloidal Solution**

According to the procedure given in part 3.4.1, 8.6 ml titanium n-butoxide ($(C_4H_9O)_4Ti$) was used for sol-gel synthesis.

Density of titanium n-butoxide is:

$$\rho_{(C_4H_9O)_4Ti} = 0.990 \quad gr/ml$$

Mass of titanium n-butoxide added is:

$$Mass \quad of \quad (C_4H_9O)_4Ti = 8.6 \quad ml \quad x \quad 0.990 \quad \frac{gr}{ml} = 8.514 \quad gr$$

Since molecular weight of titanium n-butoxide is 340. 35 gr /mol,

$$8.514 \quad gr \quad x \quad \frac{1}{340.35} \quad \frac{mol}{gr} = 0.025015 \quad mol \quad Ti$$

$$\Downarrow$$

$$0.025015 \quad mol \quad TiO_2$$

Since molecular weight of titanium dioxide is 79.87 gr /mol,

$$Mass \quad of \quad TiO_2 = 79.87 \quad \frac{gr}{mol} \quad x \quad 0.025015 \quad mol \quad TiO_2 = 1.998 \quad gr \quad TiO_2$$

So, 0.01998 gr Fe would be added. For iron doped titanium dioxide colloidal solution, 0.01998 gr iron(III) nitrate nonahydrate was added.

- **Tin Oxide Colloidal Solution**

According to the procedure given in part 3.4.2, 13.024 gr tin tetrachloride pentahydrate ($SnCl_4.5H_2O$) was used for sol-gel synthesis.

Since molecular weight of tin tetrachloride is 260.502 gr /mol,

$$13.024\ gr\ \ x\ \ \frac{1}{260.502}\ \ \frac{mol}{gr} = 0.049996\ \ mol\ \ Sn$$

$$\Downarrow$$

$$0.049996\ \ mol\ \ SnO_2$$

Since molecular weight of tin oxide is 150.71 gr /mol,

$$Mass\ \ of\ \ SnO_2 = 150.71\ \frac{gr}{mol}\ \ x\ \ 0.04996\ \ mol\ \ SnO_2 = 7.523\ \ gr\ \ SnO_2$$

So, 0.07530 gr Fe would be added. For iron doped tin oxide colloidal solution, 0.07530 gr iron(III) nitrate nonahydrate was added.

APPENDIX B

DATA OF PHOTOCATALYTIC ACTIVITY MEASUREMENTS

Table B.1 Data of Figure 4.16, Concentration change of methylene blue solution for the metal doped titanium dioxide coated thin films subjected to 600 W/m^2 artificial solar irradiation

Irradiation Time	C/C_0 TiO_2	C/C_0 1%Pd/TiO_2	C/C_0 1%Pr/TiO_2	C/C_0 1%Ag/TiO_2	C/C_0 1%Fe/TiO_2
0	1.000	1.000	1.000	1.000	1.000
30	0.852	0.470	0.852	0.738	0.921
60	0.837	0.374	0.818	0.655	0.909
90	0.799	0.333	0.733	0.536	0.890
120	0.737	0.268	0.667	0.488	0.817
150	0.727	0.121	0.528	0.417	0.780
180	0.679	0.114	0.426	0.345	0.707
210	0.622	0.023	0.392	0.345	0.677
240	0.574	0.023	0.364	0.357	0.665
270	0.569	0.000	0.341	0.310	0.665
300	0.536	0.000	0.307	0.274	0.665

Table B.2 Data of Figure 4.19, Concentration change of methylene blue solution for the metal doped tin oxide coated thin films subjected to 600 W/m^2 artificial solar irradiation

Irradiation Time	C/C_0 SnO_2	C/C_0 1%Pd/SnO_2	C/C_0 1%Pr/SnO_2	C/C_0 1%Ag/SnO_2	C/C_0 1%Fe/SnO_2
0	1.000	1.000	1.000	1.000	1.000
30	0.654	0.727	1.000	0.930	1.000
60	0.500	0.659	0.909	0.732	0.886
90	0.442	0.636	0.818	0.676	0.886
120	0.404	0.409	0.818	0.634	0.886
150	0.327	0.364	0.758	0.606	0.841
180	0.288	0.358	0.697	0.507	0.795
210	0.288	0.340	0.697	0.507	0.795
240	0.288	0.326	0.697	0.451	0.897
270	0.288	0.310	0.697	0.437	0.897

Table B.3 Data of Figure 4.19, Concentration change of methylene blue solution for the titanium dioxide-tin oxide coated thin films subjected to 600 W/m^2 artificial solar irradiation

Irradiation Time	**C/C_0 SnO_2**	**C/C_0 $20\%SnO_2+80\%TiO_2$**	**C/C_0 $35\%SnO_2+65\%TiO_2$**
0	1.000	1.000	1.000
30	0.654	0.992	0.969
60	0.500	0.977	0.886
90	0.442	0.969	0.729

Irradiation Time	**C/C_0 $50\%SnO_2+50\%TiO_2$**	**C/C_0 $80\%SnO_2+20\%TiO_2$**
0	1.000	1.000
30	0.810	0.925
60	0.759	0.670
90	0.741	0.632

APPENDIX C

CALCULATIONS FOR SURFACE AREA MEASUREMENTS

Methylene blue solution with 2 ppm concentration was prepeared for surface area measurements. For calibration, solution having different concentrations were prepared and their corresponding absorbance values were measured at 654 nm with UV-Visible Spectrophotometer. Calibration curve obtained at the end of measurements are given in Figure C.1 and Table C.1 tabulates the data points of Figure C.1.

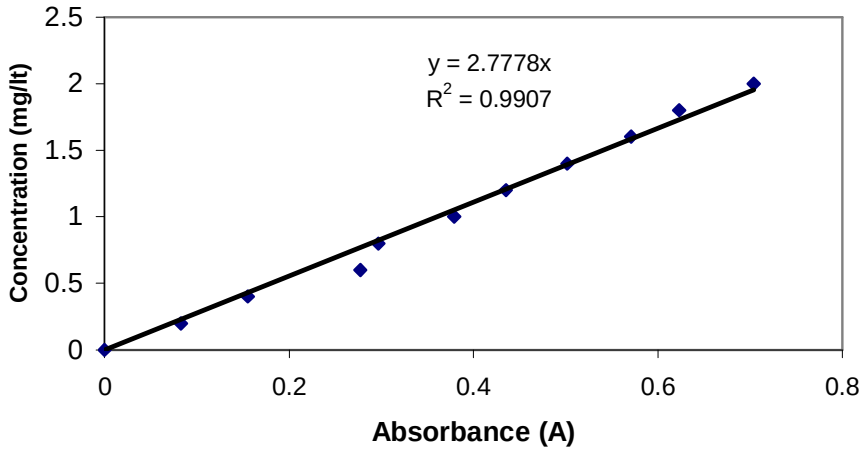

Figure C.1 Calibration curve for methylene blue concentration between 0-2 ppm

Table C.1 Data of Figure C.1

Concentration (ppm, mg/lt)	Absorbance (A)
0	0
0.2	0.083
0.4	0.155
0.6	0.277
0.8	0.297
1	0.379
1.2	0.435
1.4	0.502
1.6	0.571
1.8	0.623
2	0.704

After calibration, for TiO_2 coated thin films, three samples with different areas were immersed into 10 ml methylene blue solution having initial concentration 2 ppm. Areas were multiplied by 2 in order to have the area coated since both sides of the glass substrate were coated. Areas of the samples were: 5.32 cm^2, 4.5 cm^2 and 3.96 cm^2 .

At the end of 72 hours, absorbances of methylene blue were measuredand corresponding concentration values were calculated as:

- C_E= 1.75557 mg/lt for 3.96 cm^2 with 0.632 A
- C_E= 1.4528 mg/lt for 4.5 cm^2 with 0.523 A
- C_E= 1.1528 mg/lt for 5.32 cm^2 with 0.415 A

Adsorbed methylene blue on the surface was measured by using concentration of the solution and knowing the initial solute amount solved in water.

Initial solute solved in 10 ml water was:

$$2 \ \ mg \ \ x \ \ \frac{10 \ \ ml}{1000 \ \ ml} = 0.02 \ \ mg \ \ methylene \ \ blue$$

Adsorbed methylene blue on the surface;

$$For \ \ 3.96 \ \ cm^2 \Rightarrow 0.02 - (1.75557 \ \ \frac{mg}{1000ml} \ \ x \ \ 10 \ \ ml) = 0.002444304 \ \ mg$$

With the same procedure, adsorbed methylene blue was found to be:

3.96 cm^2	0.002444304 mg
4.5 cm^2	0.005472106 mg
5.32 cm^2	0.00847213 mg

X/m (Quantity of methylene blue adsorbed per unit volume of adsorbent) was calculated by dividing adsorbed amount of methylene blue to the coated area of the sample. With respect to the equation given below:

$$\frac{C_E}{X/m} = \frac{1}{k \ X_m} + \frac{C_E}{X_m} \qquad (3.1)$$

$\frac{C_E}{X/m}$ versus C_E was plotted and a straight line was obtained where slope of the line was $1/X_m$ and the intercept was $1/kX_m$.

Then specific surface area (cm^2/cm^2) was calculated according to equation 3.1:

$$S = \frac{X_m A_{MB} L}{N} \qquad (3.2)$$

where A_{MB} (cross-sectional area of methylene blue adsorbed on the surface) and N (coverage factor) were taken as 1.2 nm^2 and 1, respectively.

Surface areas of the samples, amounts of adsorbed methylene blue, regression coefficients for each sample are tabulated below and curves for fitting parameters to Langmuir isotherms are shown in the figures belowe.

Table C.2 Surface area measurement for TiO_2 samples

Area of the sample (cm^2)	Absorbance (A)	C_E (mg/lt)	X/m (mg/cm^2)	$1/X_m$	$1/k.X_m$
5.32	0.415	1.152787	0.001592506		
3.96	0.632	1.7555696	0.000617248	3520.5	-3530.2
4.5	0.523	1.4527894	0.001216024		

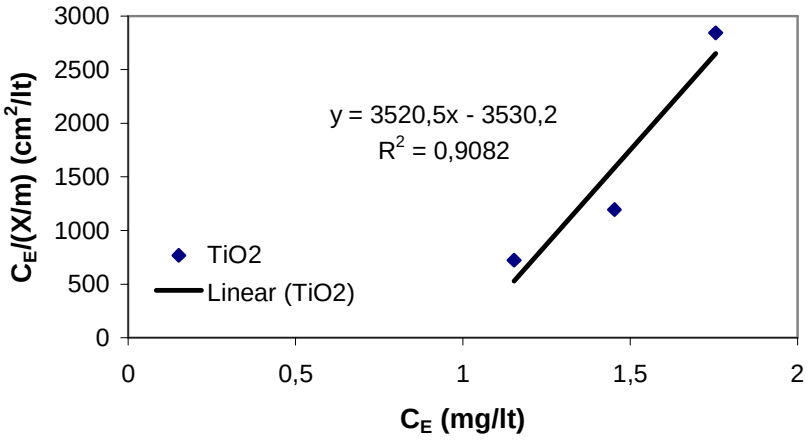

Figure C.2 Adsorption isotherm for TiO_2 samples

Table C.3 Surface area measurement for 20%SnO_2 + 80%TiO_2 samples

Area of the sample (cm^2)	Absorbance (A)	C_E (mg/lt)	X/m (mg/cm^2)	$1/X_m$	$1/k.X_m$
5.46	0.541	1.5027898	0.000910641		
2.16	0.667	1.8527926	0.000681516	3464.9	-3710
4.4	0.548	1.5222344	0.001085831		

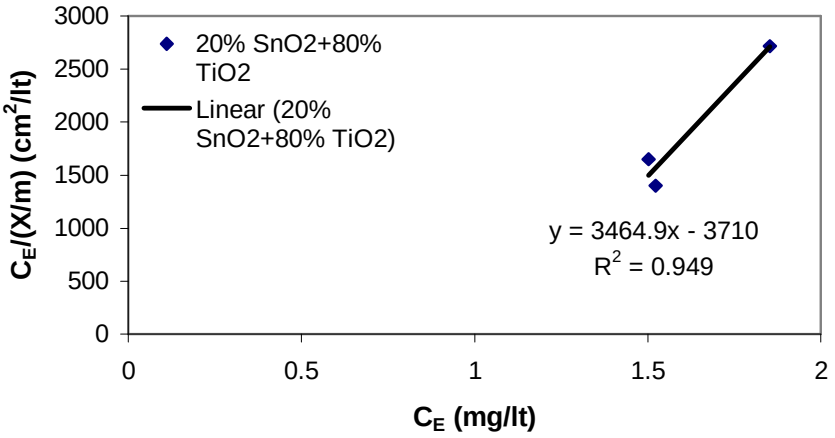

Figure C.3 Adsorption isotherm for 20%SnO_2 + 80%TiO_2 samples

Table C.4 Surface area measurement for 35%SnO_2 + 65%TiO_2 samples

Area of the sample (cm^2)	Absorbance (A)	C_E (mg/lt)	X/m (mg/cm^2)	$1/X_m$	$1/k.X_m$
3.08	0.614	1.7055692	0.000955944		
3.12	0.625	1.736125	0.000845753	3278.8	-3714.1
3.92	0.572	1.5889016	0.00104872		

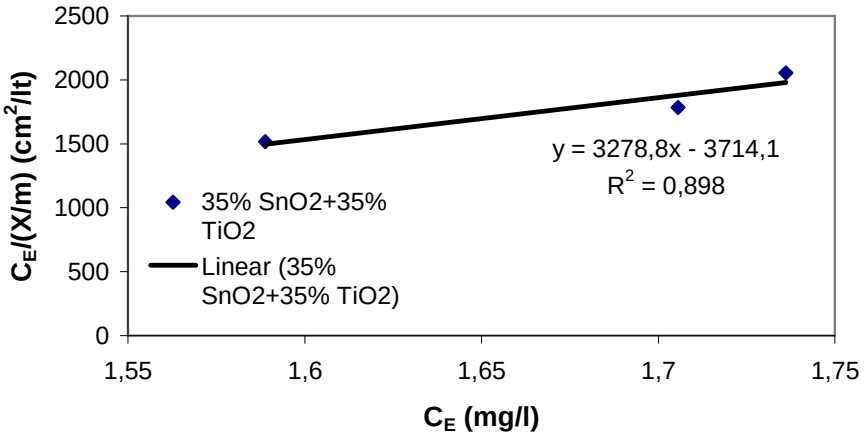

Figure C.4 Adsorption isotherm for 35%SnO_2 + 65%TiO_2 samples

Table C.5 Surface area measurement for 50%SnO_2 + 50%TiO_2 samples

Area of the sample (cm^2)	Absorbance (A)	C_E (mg/lt)	X/m (mg/cm^2)	$1/X_m$	$1/k.X_m$
1.44	0.675	1.875015	0.000867951	3185.8	-3808.7
3.12	0.535	1.486123	0.001647042		
3.36	0.557	1.5472346	0.001347516		

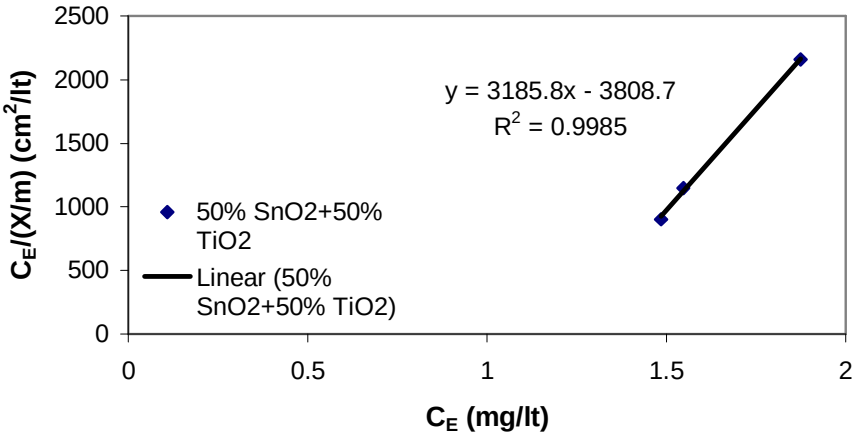

Figure C.5 Adsorption isotherm for 50%SnO_2 + 50%TiO_2 samples

Table C.6 Surface area measurement for 80%SnO_2 + 20%TiO_2 samples

Area of the sample (cm^2)	Absorbance (A)	C_E (mg/lt)	X/m (mg/cm^2)	$1/X_m$	$1/k.X_m$
3.6	0.595	1.652791	0.000964469		
4	0.562	1.5611236	0.001097191	2542	-2501.5
4.4	0.547	1.5194566	0.001092144		

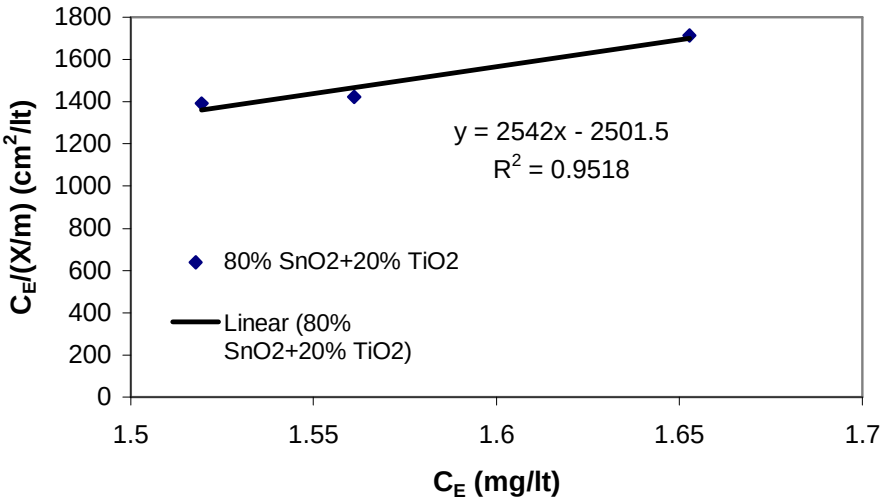

Figure C.6 Adsorption isotherm for 80%SnO_2 + 20%TiO_2 samples

Table C.7 Surface area measurement for SnO_2 samples

Area of the sample (cm^2)	Absorbance (A)	C_E (mg/lt)	X/m (mg/cm^2)	$1/X_m$	$1/k.X_m$
3.74	0.595	1.652791	0.000928366		
4.5	0.554	1.5389012	0.001024664	2301.9	-2014.9
4.48	0.565	1.569457	0.000961033		

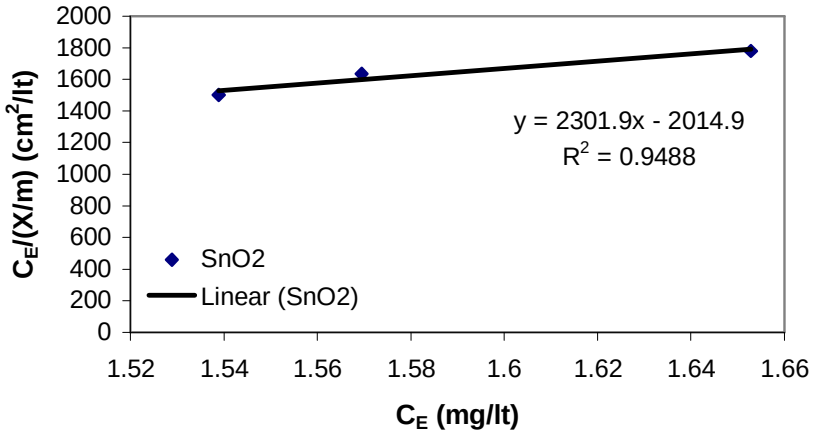

Figure C.7 Adsorption isotherm for SnO_2 samples

Using Langmuir isotherms, surface areas were found as:

Table C.8 Surface areas of the coated thin films

	Surface Area (cm^2/cm^2)
TiO_2	6.42
$20\%SnO_2 + 80\%TiO_2$	6.52
$35\%SnO_2 + 65\%TiO_2$	6.89
$50\%SnO_2 + 50\%TiO_2$	7.09
$80\%SnO_2 + 20\%TiO_2$	8.88
SnO_2	9.81